

AD-A101 316

CLEMSON UNIV S C DEPT OF ELECTRICAL AND COMPUTER EN--ETC F/6 10/2
DYNAMIC SIMULATION OF AIRBORNE HIGH POWER SYSTEMS. (U)

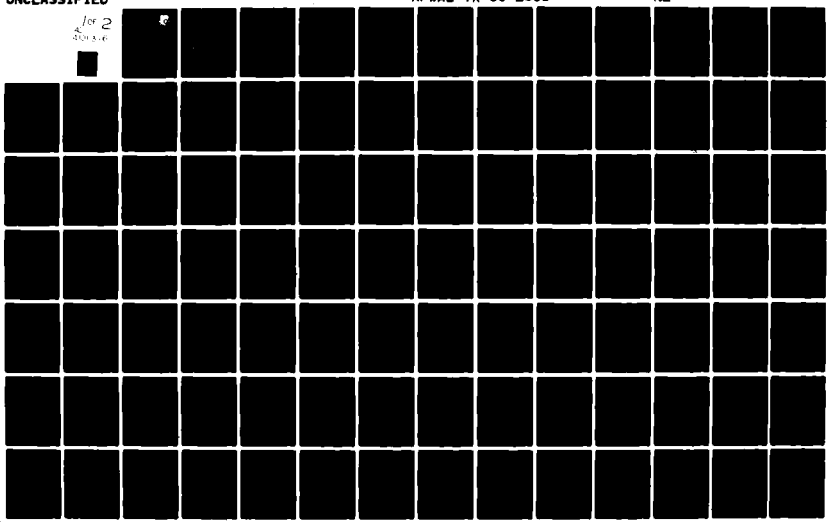
MAR 81 R W GILCHRIST, H ALMAULA F33615-79-C-2047

AFWAL-TR-80-2115

NL

UNCLASSIFIED

for 2
50915-6



ADA101316

AFWAL-TR-80-2115

LEVEL 4
2



DYNAMIC SIMULATION OF AIRBORNE HIGH POWER SYSTEMS

Gilchrist, Et al

R. University
Clem South Carolina 29631
Clem

March 1

TECHNICAL REPORT AFWAL-TR-80-2115
Interim Report for Period August 1979 - August 1980

Approved for public release; distribution unlimited,

BUFILE COPY

AERO PROPULSION LABORATORY
AIR FORCE WRIGHT AERONAUTICAL LABORATORIES
AIR FORCE SYSTEMS COMMAND
WRIGHT-PATTERSON AIR FORCE BASE, OHIO 45433

JUL 14 1981

A

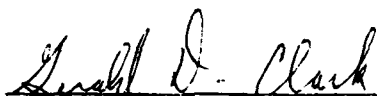
81713310

NOTICE

When Government drawings, specifications, or other data are used for any purpose other than in connection with a definitely related Government procurement operation, the United States Government thereby incurs no responsibility nor any obligation whatsoever; and the fact that the government may have formulated, furnished, or in any way supplied the said drawings, specifications, or other data, is not to be regarded by implication or otherwise as in any manner licensing the holder or any other person or corporation, or conveying any rights or permission to manufacture use, or sell any patented invention that may in any way be related thereto.

This report has been reviewed by the Office of Public Affairs (ASD/PA) and is releasable to the National Technical Information Service (NTIS). At NTIS, it will be available to the general public, including foreign nations.

This technical report has been reviewed and is approved for publication.



GERALD D. CLARK, CAPT, USAF
Project Engineer
Power Systems Branch
Aerospace Power Division



PAUL R. BERTHEAUD, Tech Area Manager
Power Systems Branch
Aerospace Power Division
Aero Propulsion Laboratory

FOR THE COMMANDER



JAMES D. REAMS
Chief, Aerospace Power Division
Aero Propulsion Laboratory

If your address has changed, if you wish to be removed from our mailing list, or if the addressee is no longer employed by your organization please notify AFWAL/POCS-2 W-PAFB, OH 45433 to help us maintain a current mailing list.

Copies of this report should not be returned unless return is required by security considerations, contractual obligations, or notice on a specific document.

SECURITY CLASSIFICATION OF THIS PAGE (When Data Entered)

(19) REPORT DOCUMENTATION PAGE		READ INSTRUCTIONS BEFORE COMPLETING FORM
1. REPORT NUMBER 18 AFWAL-TR-80-2115	2. GOVT ACCESSION NO. AD-A101 316	3. RECIPIENT'S CATALOG NUMBER
4. TITLE (and Subtitle) Dynamic Simulation of Airborne High Power Systems.	5. TYPE OF REPORT & PERIOD COVERED Interim Report Aug 79 - Sept 80	
6. AUTHOR(s) Fred G.W. Bell, R. Ramanathan R. W. Gilchrist, D.C. Lee R.A. Almala, R.L. Avant P. J. Alajaiian, D.Y. Chen	7. CONTRACT OR GRANT NUMBER(s) 15 F33615-79-C-2047	
8. PERFORMING ORGANIZATION NAME AND ADDRESS Electrical and Computer & Electrical Engr. Dept. Engr. Department VPI & SU Clemson University Blacksburg, VA 24061 Clemson, SC 29631	9. PROGRAM ELEMENT, PROJECT, TASK AREA & WORK UNIT NUMBERS 16) 3145 /	
10. CONTROLLING OFFICE NAME AND ADDRESS Air Force Aero Propulsion Laboratory 1 AFWAL/POOS Wright Patterson Air Force Base, Ohio 45433	11. REPORT DATE 11 March 1981	
12. NUMBER OF PAGES 15) 443	13. SECURITY CLASS. (of this report) Unclassified	
14. MONITORING AGENCY NAME & ADDRESS (if different from Controlling Office) 9) Interim technical rept. 15 Aug 79-30 Aug 80.	15a. DECLASSIFICATION/DOWNGRADING SCHEDULE	
16. DISTRIBUTION STATEMENT (of this Report) Approved for public release; distribution unlimited.	17. DISTRIBUTION STATEMENT (of the abstract entered in Block 20, if different from Report)	
18. SUPPLEMENTARY NOTES		
19. KEY WORDS (Continue on reverse side if necessary and identify by block number) Generator Modeling including saturation Direct phase variables Transformer modeling SCR modeling Resonant Charging		
20. ABSTRACT (Continue on reverse side if necessary and identify by block number) This interim report describes the progress in model development for three phase ac generator, three phase transformers, SCR's and resonant charging circuits. The generator and transformer models include nonlinear effects due to magnetic field saturation. The SCR's and the resonant charging circuit are modeled in sufficient detail to include switching transients during turn-on and turn-off intervals. The component models are to be assembled into a system to simulate ac and dc resonant charging applications. Use of SCEPTRF is elected as the		

DD FORM 1 JAN 73 1473 EDITION OF 1 NOV 65 IS OBSOLETE

SECURITY CLASSIFICATION OF THIS PAGE (When Data Entered) *405932*

SECURITY CLASSIFICATION OF THIS PAGE(When Data Entered)

- ✓ method for solving the problem of assembling the components into a system model and for solving the problems arising from the "stiff" differential equations of the composite systems.

SECURITY CLASSIFICATION OF THIS PAGE(When Data Enters)

Foreword

This interim report was submitted by Clemson University, Clemson, S. C. 29631 under contract F33615-79-2047. The effort was sponsored by the Air Force Aero Propulsion Laboratory, Air Force Wright Aeronautical Laboratories, Air Force Systems Command, Wright Patterson AFB, Ohio 45433 under Project 3145. Capt. Fred Brockhurst was the Project Engineer at the beginning of the project. Capt. Jerry Clark is currently the Project Engineer. The time period covered by the report is August 15, 1979 through August 30, 1980.

Dr. R. W. Gilchrist (Principal Investigator), Dr. Haren Almaula, Dr. Charles J. Alajajian and G. Frank Bell performed the part of the work done at Clemson. The work subcontracted to VPI and SU was performed by Dr. Fred C. Lee (Principal Investigator), Dr. G. Y. Chen, R. L. Avant and R. Ramanathan.

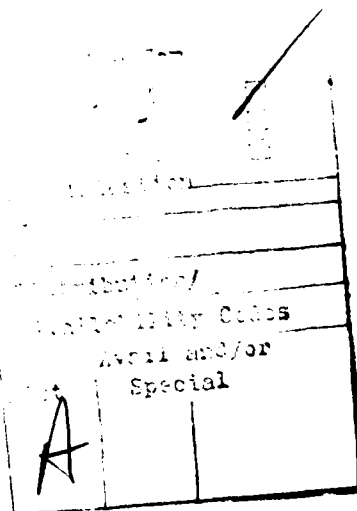


TABLE OF CONTENTS

SECTION	PAGE
I INTRODUCTION	1
II THE GENERATOR MODEL	2
2.1 OBJECTIVE	2
2.2 GENERATOR MATHEMATICAL MODEL	2
2.3 CHOICE OF GENERATOR VARIABLES	3
2.4 FORMULATION FOR NON-LINEAR INDUCTANCE	4
2.5 SCEPTRE EQUIVALENT CIRCUIT	10
2.6 INCLUSION OF PRIME-MOVER AND EXCITATION CONTROL MODEL	12
III THE TRANSFORMER MODEL	13
3.1 OBJECTIVE	13
3.2 THE TRANSFORMER EQUIVALENT CIRCUIT	13
3.3 THE MAGNETIC CORE DATA	16
3.4 A SIMPLIFYING APPROXIMATION	18
3.5 DETERMINING THE OPERATING POINT	20
IV THE AC RESONANT CHARGING CIRCUIT	22
4.1 OBJECTIVE	22
4.2 SCR MODEL SELECTION	22
4.3 SCR MODEL IN AC RESONANT CHARGING	24
V CHOICE OF VARIABLES	34
5.1 OBJECTIVE	34
5.2 CHOICE OF VARIABLES	34
5.3 SCEPTRE VARIABLES	38
VI NUMERICAL METHODS FOR STIFF DIFFERENTIAL EQUATIONS	39
6.1 INTRODUCTION	39

TABLE OF CONTENTS (Continued)

SECTION	PAGE
6.2 INTEGRATION METHODS	39
6.3 INTEGRATION METHODS OF SCEPTRE	41
VII SYSTEM INTEGRATION	42
VIII GENERATOR MODEL RESULTS	44
8.1 INTRODUCTION	44
8.2 DISCUSSION OF RESULTS	44
APPENDIX A THE GENERATOR MODEL	54
A.1 EQUIVALENT CIRCUIT EQUATIONS	
A.2 SATURATION EFFECTS	57
A.3 THE TORQUE EQUATION	61
APPENDIX B SATURATED GENERATOR MODEL	63
B.1 SATURATED GENERATOR EQUATIONS	63
APPENDIX C GENERATOR DATA USED	70
C.1 UNSATURATED GENERATOR DATA	70
C.2 SATURATION DATA	71
C.3 MEASUREMENT OF THE UNSATURATED INDUCTANCES	72
APPENDIX D THE SCEPTRE GENERATOR PROGRAM	77
D.1 INTRODUCTION	
APPENDIX E SCR MODELS FOR SPICE 2, AND SCEPTRE	81
E.1 THE BIPOLAR JUNCTION TRANSISTOR MODEL	84
E.2 LIST OF PARAMETERS	84
E.3 CIRCUIT SIMPLIFICATION	87
E.4 THE SCR MODEL IN SPICE 2	88
E.5 THE SCR MODEL IN SCEPTRE	96
REFERENCES	100

LIST OF ILLUSTRATION

FIGURE	PAGE
1. VARIATION OF L_{aa} WITH i_x	6
2. EQUIVALENT CIRCUIT FOR PHASE "a" OF SYNCHRONOUS MACHINE	11
3. CURVES COMPUTED BY EQUATION (30)	17
4. DATA FOR INCREMENTAL INDUCTANCE	19
5. THE TWO BIPOLAR JUNCTION TRANSISTOR MODEL OF THE SCR	25
6. SPICE CIRCUIT DIAGRAM FOR THE SINGLE LOOP AC RESONANT CHARGING SYSTEM	26
7. SPICE 2 SIMULATION OF THE AC RESONANT CHARGING CIRCUIT OF FIGURE 6	27
7a. SPICE 2 PROGRAM LISTING FOR CIRCUIT OF FIGURE 6 WITH SNUBBER	28
8. SPICE 2 SIMULATION OF SINGLE LOOP AC RESONANT CIRCUIT WITH SNUBBER	29
9. SINGLE LOOP CIRCUIT WITH SNUBBER	30
10. SPICE 2 CIRCUIT DIAGRAM FOR THE TWO BRACH AC RESONANT CHARGING SYSTEM WITH SNUBBER	32
11. SPICE 2 TWO LOOP AC RESONANT CHARGING SYSTEM INPUT DECK FOR FIGURE 10.	33
12. CALAHAN'S EXAMPLE CIRCUIT	37
13. SATURATION MULTIPLIER, C_{aa} VERSUS i_x	46
14. SATURATION MULTIPLIER, C_{ff} VERSUS i_x	47
15. PHASE "a" CURRENT	49
16. FIELD CURRENT I_F	50
17. DIRECT AXIS DAMPER CURRENT	51
18. QUADRATURE AXIS DAMPER CURRENT	52
19. ROTOR SPEED	53
20. THREE-PHASE	55

LIST OF ILLUSTRATIONS (Cont'd)

FIGURE	PAGE
21. CONVENTION FOR DEFINING ROTOR POSITION	58
22. VARIATION OF INDUCTANCE WITH θ	60
23. MODIFIED EBERS-MOLL BJT MODEL (INJECTION)	85
24. MODIFIED EBERS-MOLL BJT MODEL (TRANSPORT)	89
25. MODIFIED EVERE-MOLL BJT MODEL	90
26. SPICE 2 MODIFIED EBERS-MOLL BJT MODEL	91
27. A SPICE 2 SCR MODEL BASED ON THE TWO BJT MODEL	92
28. THE SPICE 2 SCR MODEL EQUIVALENT CKT	94
29. SCEPTRE TWO BJT SCR MODEL.	97

LIST OF TABLES

TABLE	PAGE
1. REGRESSION DATA	21
2. SATURATION COEFFICIENT	73
3. CONVERSION OF SPICE 2 TO SCEPTRE	99

AFWAL-TR-80-2115

Dynamic Simulation of Airborne High Power Systems

R.W. Gilchrist
H. Almaula
C.J. Alajajian
G.F. Bell

Department of Electrical and Computer Engineering
Clemson University
Clemson, S.C. 29631

F.C. Lee
D.Y. Chen
R.L. Avant
R. Ramanathan

Electrical Engineering Department
Virginia Polytechnic Institute and State University
Blacksburg, Virginia 24061

March, 1981

Technical Report AFWAL-TR-80-2115
Interim Report for the Period August 15, 1979
through August 30, 1980

Air Force Aero Propulsion Laboratory
Air Force Wright Aeronautical Laboratories
Air Force Systems Command
Wright Patterson Air Force Base, Ohio 45433

SECTION I

INTRODUCTION

This is the interim report for work on the project Dynamic Simulation of Airborne High Power Systems for the period of August 15, 1979 through August 30, 1980.

The work has included modeling of a three phase ac generator including effects of speed variation and field saturation in sufficient detail to accurately simulate start up and severe faults. Data are included for a specific machine and results are included for simulation of a severe fault condition.

Preliminary work on modeling a three phase three-leg core type transformer is included here. Circuit equations, magnetic core characteristics and the electric circuit relation to magnetic core characteristics under saturation conditions are developed.

The subcontractors work on the modeling of the ac resonant charging circuit is reported in Section IV. This work consists mainly of determining an SCR model which adequately represents turn-on and turn-off phenomena in a high power resonant circuit application.

The period's work also addresses the problems of system variables in nonlinear simulation, stiff differential equations, and system simulation using SPICE 2 and SCEPTRE. The subcontractor shares responsibility and work in this area.

The sections of the report correspond to the tasks outlined in the project work statement. Detailed development and data are included in the appendices.

The results of a generator simulation run are included in Section VII. The results of the ac charging simulations are included in the Section IV.

In the ac charging circuit simulation a single loop charging and a double loop charging were simulated using SPICE 2. A turn-off problem was corrected using a snubber circuit, a premature turn-on problem is being investigated. The SCR model is being converted to SCEPTRE.

The subcontractor is Virginia Polytechnic Institute and State University with Dr. Fred C. Lee as Principal Investigator.

SECTION II

THE GENERATOR MODEL

2.1 OBJECTIVE

This part of the project was to develop a mathematical and computer model of a three phase ac generator. The model is to be adequate for including effects of unbalanced transient loads, startup transient, speed variation, field excitation variation and saturation of the field.

Most of the models existing in the literature (References 1,5,6) were developed for representing generators in power system stability studies. In power system applications the generator is usually connected to a large system and the generator is constrained to operation in a narrow range or it is removed from the system by protective devices. In the airborne high power system one has a single generator supplying an isolated load and the machine may be subject to more severe transients of a wider range.

Further, in a power system the concerns of the modeling for stability studies are sustained overload currents and the synchronising of the generator with the system. In this airborne high power system the operation is asynchronous and there is need to consider short duration transient pulses that may affect the operation of the electronics in the associated load.

In order to have a model sensitive to these concerns, more detail is included than is usual in power system stability studies. The model used has these additional features: direct and quadrature damping effects; variable speed; saturation effects including both variation in inductance and variation in $\partial L/\partial i$; more accurate developed torque formulation; formulation in a form such that the prime mover model and the field control model may be added if these become available at some later time.

2.2 GENERATOR MATHEMATICAL MODEL

Appendix A shows the generator equivalent circuit and establishes the notation and time and space references used in the modeling.

In vector and matrix form the equation for the circuit model is given either by Equation (43) or (46) and repeated here as Equations (1) or (2).

$$V = RI + \frac{d\lambda}{dt} \quad (1)$$

$$V = RI + \frac{d}{dt} (LI) \quad (2)$$

The torque equations relating electrical to mechanical variables is given by Equations (55) and (56) and here as Equations (3), (4), and (5).

$$\frac{d^2\theta}{dt^2} = \frac{1}{J} [T_m - T_e - B \frac{d\theta}{dt}] \quad (3)$$

where the T_e terms represents the so called electrical torque and corresponds to the power converted from mechanical form to electrical form, P_e

$$P_e = T_e \frac{d\theta}{dt} \quad (4)$$

Concordia (Reference 7) shows that the T_e is defined by

$$T_e = \frac{1}{2} [I]^T \left[\frac{\partial L}{\partial \theta} \right] [I] \quad (5)$$

Equations (1) through (5) basically define the generator model. These equations are standard forms in the literature (References [1,3,5,6,7]). The model used in this work differs from others in the choice of system variables and in the details of defining the inductance coefficients. These points are discussed in Appendix A and in subsequent sections of this report.

2.3 CHOICE OF GENERATOR VARIABLES

Choices of generator state variables were made in two areas. First, the direct phase variables were chosen over the more traditional direct and quadrature axis variables. Secondly, the current variables were chosen over the flux linkage variables.

The direct phase variables were chosen over the traditional direct and quadrature variables for three reasons. First, while Parks (Reference 1) transformation does significantly simplify the generator model equations and hence aid in their solution, it is necessary at each numerical integration step to transform the variables back to direct-phase variables for compatibility

with the external load made up of electronic components and resonant charging elements. Any expected gain would be greatly diminished by this transformation.

Secondly, additional logic would need developing to represent the effect of direct-phase open and short circuits on d-q variables.

Thirdly, the application of Parks transformation and the resulting simplified equations depend on certain simplifying assumptions which don't really apply if saturation effects and $\partial L/\partial i$ effects are significant.

The choice of the current variables over the flux linkage variables was dictated not by generator model considerations but by limitations imposed by models of the electronic components of the load (resonant charging circuit).

The developments in Section V and VI of this report indicate that for appropriate numerical integration methods, use of the λ variable gives less propagated error for non-linear inductances. Further, Nakra (Reference 8) and Manly (Reference 9) cite inaccuracies that may arise due to noise in the $\partial L/\partial i$ terms which appear in the current variable formulation.

However, available data and existing models for diodes, transistors and SCR's are given in terms of current and voltage variables instead of flux linkages and charge variables. This and the need to use a program such as SPICE or SCEPTRE for the electronic component modeling dictated the use of current variables for modeling the generator. SCEPTRE normally requires that currents be the state variables in inductor elements.

2.4 FORMULATION FOR NON-LINEAR INDUCTANCE

Saturation effects cause the inductance coefficients to be non-linear functions of the machine currents. The circuit model equations for direct-phase current formulation with saturation effects are now developed. The terms arising due to dependence of inductance on the currents are illustrated.

The generator circuit model equations for direct-phase current formulation and inductance as a function of current are

$$V = RI + L \frac{dI}{dt} + \left(\frac{dL}{dt} \right) (I) \quad (6)$$

In the second term on the right-hand side of the equation the inductances are those defined in the appendix by Equation (50) except that the L and M coefficients are modified by saturation. The third term involving dL/dt will be treated subsequently.

The assumptions made on the effect of saturation on the inductance terms are discussed in Appendix A. Equation (53), repeated here, illustrates how one of the inductance terms is affected by saturation.

$$\begin{aligned} L_{aas} &= C_{aa} L_s + C_{aa} L_m \cos 2\theta \\ &= C_{aa} L_{aa} \end{aligned} \quad (53)$$

Implied here is that the shape of the inductance curve as a function of rotor position is not changed by saturation, (the validity of this assumption is discussed in Appendix A). This form further implies that saturated inductance measurements can be made on the direct axis as a function of net excitation contributed by the various currents. The net excitation current in terms of equivalent main field current is

$$\begin{aligned} i_x &= i_F + N_{FD} i_D + N_{Fa} [i_a \cos(\theta) + i_b \cos(\theta - \frac{2\pi}{3}) \\ &\quad + i_c \cos(\theta + \frac{2\pi}{3})] \end{aligned} \quad (7)$$

To determine the C_{aa} , the rotor is aligned with the "a" phase axis and L_{aa} is measured as i_x is varied over an appropriate range giving a curve as shown in Figure 1.

The equation for L_{aa} as a function of i_x is obtained by appropriate polynomial curve matching techniques and results in the following form.

$$\begin{aligned} L_{aas} &= L_{ao}(1 + a_1 i_x + a_2 i_x^2 + a_3 i_x^3 + \dots) \\ &= L_{ao} C_{aa} \end{aligned} \quad (8)$$

Thus C_{aa} is the normalized polynomial of the variation of the inductance L_{aas} with i_x .

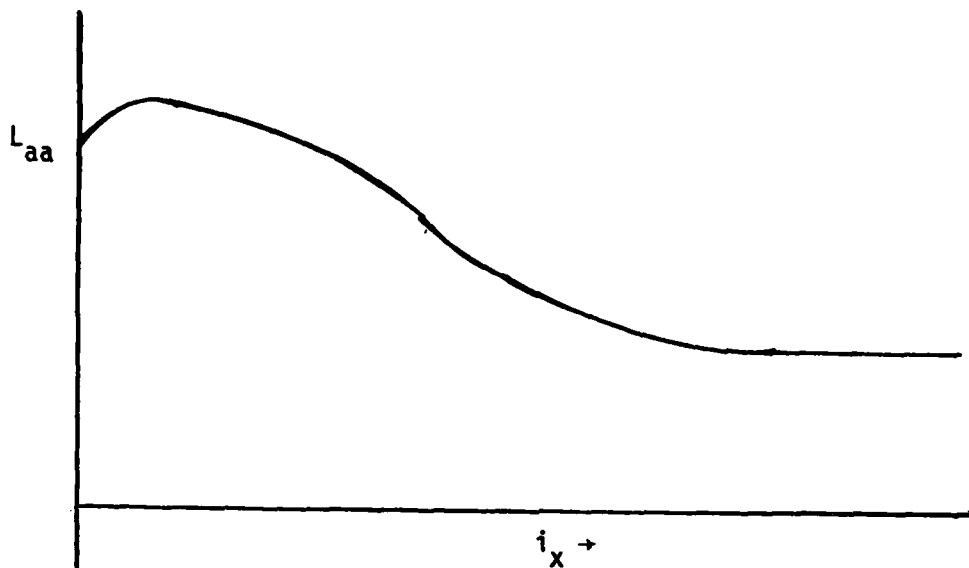


FIGURE 1. VARIATION OF L_{aa} WITH i_x (SATURATION EFFECTS)

C terms are required for each of the equations listed in Equation (50). Measurements are needed to determine the following C polynomials: C_{aa} , C_{aF} , C_{aD} , C_{aQ} , C_{FF} , C_{FD} , C_{DD} . These requirements are listed in more detail in a later section.

These saturation coefficients are associated with the inductance terms as shown below in Equation (9) where the s subscript is dropped

$$L_{aa} = C_{aa} (L_s + C_m \cos(2\theta))$$

$$L_{ab} = C_{aa} \left(-M_s + L_m \cos(2\theta - \frac{2\theta}{3})\right) = L_{ba}$$

$$L_{ac} = C_{aa} \left(-M_s + L_m \cos(2\theta + \frac{2\theta}{3})\right) = L_{ca}$$

$$L_{aF} = C_{aF} (M_{aF} \cos(\theta)) = L_{Fa}$$

$$L_{aD} = C_{aD} (M_{aD} \cos(\theta)) = L_{Da}$$

$$L_{aQ} = C_{aQ}(M_{aQ} \sin(\theta)) = L_{Qa}$$

$$L_{bb} = C_{aa}(L_s + L_m \cos(2\theta + \frac{2\pi}{3}))$$

$$L_{bc} = C_{aa}(-M_s + L_m \cos(2\theta)) = L_{cb}$$

$$L_{bF} = C_{aF}(M_{aF} \cos(\theta - \frac{2\pi}{3})) = L_{Fc}$$

$$L_{bD} = C_{aD}(M_{aD} \cos(\theta - \frac{2\pi}{3})) = L_{Dc}$$

$$L_{bQ} = C_{aQ}(M_{aQ} \sin(\theta - \frac{2\pi}{3})) = L_{Qb}$$

$$L_{cc} = C_{aa}(L_s + L_m \cos(2\theta - \frac{2\pi}{3}))$$

$$L_{cF} = C_{aF}(M_{aF} \cos(\theta + \frac{2\pi}{3})) = L_{Fc}$$

$$L_{cD} = C_{aD}(M_{aD} \cos(\theta + \frac{2\pi}{3})) = L_{Dc}$$

$$L_{cQ} = C_{aQ}(M_{aQ} \sin(\theta + \frac{2\pi}{3})) = L_{Qc}$$

$$L_{FF} = C_{FF}L_F$$

$$L_{FD} = C_{FD}M_R = L_{DF}$$

$$L_{FQ} = 0 = L_{QF}$$

$$L_{DD} = C_{DD}L_D$$

$$L_{DQ} = 0 = L_{QD} \quad (9)$$

$$L_{QQ} = L_Q$$

Next consider the third term on the right hand side of Equation (6), $(dL/dt)(I)$.

Consider, for example, the first row of the matrix product $(dL/dt)(I)$.

$$\begin{aligned} & \left(\frac{d}{dt} L_{aa} \right) i_a + \left(\frac{d}{dt} L_{ab} \right) i_b + \left(\frac{d}{dt} L_{ac} \right) i_c + \left(\frac{d}{dt} L_{aF} \right) i_F \\ & + \left(\frac{d}{dt} L_{aD} \right) i_D + \left(\frac{d}{dt} L_{aQ} \right) i_Q \end{aligned} \quad (10)$$

now noting that the inductances are functions of the net excitation, i_x , and i_x is given by Equation (7), the derivative in the first term of Equation (10) expanded becomes.

$$\begin{aligned} \frac{d}{dt} L_{aa} &= \frac{\partial L_{aa}}{\partial i_x} \frac{\partial i_x}{\partial t} + \frac{\partial L_{aa}}{\partial \theta} \frac{\partial \theta}{\partial t} \\ &= \frac{\partial L_{aa}}{\partial i_x} \left[\frac{\partial i_F}{\partial t} + N_{FD} \frac{\partial i_D}{\partial t} + N_{Fa} \left(\frac{\partial i_a}{\partial t} \right) \cos(\theta) - N_{Fa} i_a \sin(\theta) \frac{\partial \theta}{\partial t} \right. \\ &\quad + N_{Fa} \left(\frac{\partial i_b}{\partial t} \right) \cos(\theta - \frac{2\pi}{3}) - N_{Fa} i_b \sin(\theta - \frac{2\pi}{3}) \frac{\partial \theta}{\partial t} \\ &\quad \left. + N_{Fa} \left(\frac{\partial i_c}{\partial t} \right) \cos(\theta + \frac{2\pi}{3}) - N_{Fa} \sin(\theta + \frac{2\pi}{3}) \frac{\partial \theta}{\partial t} \right] + \frac{\partial L_{aa}}{\partial \theta} \frac{\partial \theta}{\partial t} \end{aligned} \quad (12)$$

The expressions for the other terms after expanding the derivative terms of Equation (10):

$$\frac{d}{dt} L_{ab}; \frac{d}{dt} L_{ac}; \frac{d}{dt} L_{aF}; \frac{d}{dt} L_{aD}; \frac{d}{dt} L_{aQ};$$

will be the same as Equation (12) except for the quantities outside the square brackets where the inductance in question will appear. When these terms are all expanded and terms are collected, the first row of the $L \frac{dI}{dt} + \left(\frac{dL}{dt} \right) I$ matrix becomes

$$\begin{aligned}
\frac{d\lambda_a}{dt} = & [A_a N_{Fa} \cos(\theta) + L_s C_{aa} + L_m C_{aa} \cos(2\theta)] \frac{di_a}{dt} \\
& + [A_a N_{Fa} \cos(\theta - \frac{2\pi}{3}) - M_s C_{aa} + L_m C_{aa} \cos(2\theta - \frac{2\pi}{3})] \frac{di_b}{dt} \\
& + [A_a N_{Fa} \cos(\theta + \frac{2\pi}{3}) - M_s C_{aa} + L_m C_{aa} \cos(2\theta + \frac{2\pi}{3})] \frac{di_c}{dt} \\
& + [A_a + C_{aF} M_{aF} \cos(\theta)] \frac{di_F}{dt} \\
& + [A_a N_{FD} + C_{aD} M_{aD} \cos(\theta)] \frac{di_D}{dt} \\
& + [C_{aQ} M_{aQ} \sin(\theta)] \frac{di_Q}{dt} \\
& - [A_a B + 2C_{aa} C_a L_m + (C_{aF} M_{aF} i_F + C_{aD} i_D) \sin(\theta) - C_{aQ} M_{aQ} i_Q \cos(\theta)] \frac{d\theta}{dt}
\end{aligned} \tag{13}$$

where

$$\begin{aligned}
A_a = & i_a \frac{\partial L_{aa}}{\partial i_x} + i_b \frac{\partial L_{ab}}{\partial i_x} + i_c \frac{\partial L_{ab}}{\partial i_x} + i_F \frac{\partial L_{aF}}{\partial i_x} + i_F \frac{\partial L_{aF}}{\partial i_x} + i_D \frac{\partial L_{aD}}{\partial i_x} + i_Q \frac{\partial L_{aQ}}{\partial i_x} \\
B = & N_{Fa} [i_a \sin(\theta) + i_b \sin(\theta - \frac{2\pi}{3}) + i_c \sin(\theta + \frac{2\pi}{3})] \\
C_a = & i_a \sin(2\theta) + i_b \sin(2\theta - \frac{2\pi}{3}) + i_c \sin(2\theta + \frac{2\pi}{3})
\end{aligned}$$

Similar expansions are required for each of the rows of the matrix terms corresponding to the terms

$$\frac{\partial \lambda_b}{\partial t}, \frac{\partial \lambda_c}{\partial t}, \frac{\partial \lambda_F}{\partial t}, \frac{\partial \lambda_D}{\partial t}, \text{ and } \frac{\partial \lambda_Q}{\partial t}.$$

The complete listing of these terms is included in Appendix B.

Further, one must note and include the saturation effects on the $\frac{\partial L}{\partial i_x}$ terms. Again using phase "a" terms as example

$$L_{aa} = C_{aa}(L_s + L_m \cos(2\theta)) \tag{14}$$

and noting from Equation (8)

$$C_{aa} = 1 + a_1 i_x + a_2 i_x^2 + a_3 i_x^3 + \dots \quad (15)$$

$$\frac{\partial L_{aa}}{\partial i_x} = (L_s + L_m \cos(2\theta))(a_1 + 2a_2 i_x + 3a_3 i_x^2 + \dots) \quad (16)$$

Again the derivative of the other inductance terms with respect to i_x may be written in a similar fashion.

Finally the derivatives of the inductance terms with respect to θ are obtained. The "a" phase terms are listed

$$\begin{aligned} \frac{\partial L_{aa}}{\partial \theta} &= -2 C_{aa} L_m \sin(2\theta) \\ \frac{\partial L_{ab}}{\partial \theta} &= -2 C_{ao} L_m \sin(2\theta - \frac{2\pi}{3}) \\ \frac{\partial L_{ac}}{\partial \theta} &= -2 C_{aa} L_m \sin(2\theta + \frac{2\pi}{3}) \\ \frac{\partial L_{aF}}{\partial \theta} &= -C_{aF} M_{aF} \sin(\theta) \\ \frac{\partial L_{aD}}{\partial \theta} &= -C_{aD} M_{aD} \sin(\theta) \\ \frac{\partial L_{aQ}}{\partial \theta} &= -C_{aQ} M_{aQ} \cos(\theta) . \end{aligned} \quad (17)$$

2.5 SCEPTRE EQUIVALENT CIRCUIT

The circuit model equations developed in previous sections are now in a form from which the equivalent circuit may be readily discerned. An equivalent phase "a" circuit that is easily analyzed by the SCEPTRE program is shown in Figure 2. Equations for the other circuits of Figure 20 are developed in a similar manner and equivalent circuits built for them. A program in SCEPTRE can then be written. Such a program is listed in Appendix C.

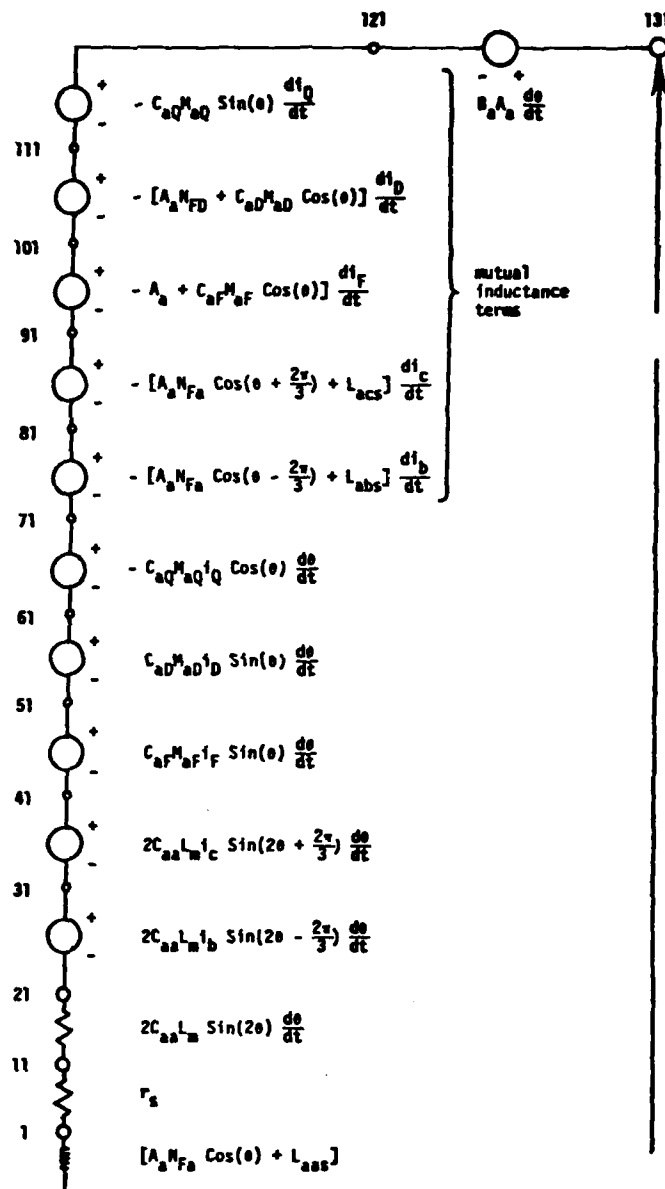


FIGURE 2. EQUIVALENT CIRCUIT FOR PHASE "a" OF SYNCHRONOUS MACHINE.

2.6 INCLUSION OF PRIME-MOVER AND EXCITATION CONTROL MODEL

While SCEPTRE was primarily developed to facilitate network analysis, it can be used to analyse other dynamic systems. Particularly, it has the ability to analyze systems for which transfer functions are available. SCEPTRE requires that the transfer function be converted to state equations and the state equations entered into the program. (The details of this conversion procedure are given in the manual (Reference 2).) This capability of SCEPTRE can be used to advantage in simulating the prime-mover characteristics of the system. The prime-mover model is converted to a suitable program and the output quantity of interest is the mechanical torque, T_m . This quantity becomes an input for the synchronous machine model through Equation (3), which is the equation for rotor angle acceleration.

Similarly, excitation control system models may be added to the machine simulation. Excitation control is generally based on monitoring the terminal voltage of the generator and changing the excitation field voltage in some fashion as the response. The control system, modeled either as a transfer function or an electronic network, is easily added to the present machine model, since in the program both the terminal voltage and the excitation voltage are accessible variables. The present work has not been concerned with modeling either the prime-mover or the excitation voltage control scheme, and the above observations are offered only to show how these models can be incorporated in the present simulation.

SECTION III

THE TRANSFORMER MODEL

3.1 OBJECTIVE

In this section various problems and options are considered which will determine the mathematical and computer program of a three phase-three leg core transformer with wye-wye or delta-wye connections. The model is to be adequate for handling unbalanced transient loads, start up transients for the system, and include saturation conditions.

The first year's work on the transformer model has involved the transformer equivalent circuit, the magnetic core characteristics, relation of circuit parameters to magnetic core characteristics and study of phenomena that may be potential problems such as initial inrush of current and ferro-resonance.

3.2 THE TRANSFORMER EQUIVALENT CIRCUIT

The equation defining the circuit relationship for each transformer winding is:

$$v_{kj} = R_{kj} i_{kj} + \frac{d\lambda_{kj}}{dt} \quad (18)$$

where

k = a, b, c for the three phases

j = 1, 2 for primary and secondary

v_{kj} = is the terminal voltage of the kj winding

i_{kj} = is the current in the kj winding

λ_{kj} = the linkages of winding kj .

The interrelationship of the currents and voltages depend on the network connections. These relationships are automatically imposed by the SCEPTRE modelling program.

The $\frac{d\lambda_{kj}}{dt}$ relates the electric network equations to the magnetic field of the three phase-three leg core of the transformer.

In general the linkages of any winding are some non-linear functions of all of the winding currents as in Equation (19)

$$\lambda_{ki} = \lambda_{kj}(i_{a1}, i_{a2}, i_{b1}, i_{b2}, i_{c1}, i_{c2}). \quad (19)$$

Due to hysteresis effects, Equation (19) is not a single valued function but the value for λ_{ki} depends not only on the particular state of the six current variables but also on whether each of the six is increasing or decreasing. A precise representation of a three phase - three leg core transformer by Equation (19) would require an unreasonable amount of data whether obtained by laboratory measurements or by calculations using magnetic core data.

Subsequent paragraphs in this section discuss some assumptions commonly made which reduce the amount of data required to model the magnetic characteristics. Some of these approximations or assumptions leave one with a reasonably accurate model because of conventional construction practices, others represent a trade-off between the amount of data required and the accuracy of the model.

The results of assuming a constant leakage inductance and constant turns ratio between windings of the same phase are illustrated in the development of Equation (20) through Equation (29).

Define mutual and leakage flux in phase "a" by Equations (20) and (21)

$$\phi_{a1} = \phi_{\ell 1} + \phi_{am} \quad (20)$$

$$\phi_{a2} = \phi_{\ell 2} + \phi_{am} \quad (21)$$

similar expressions apply to the "b" and "c" phase windings.

In terms of linkages with an effective primary turns, N_1 , Equation (18) can be rewritten for phase "a" primary and secondary

$$v_{a1} = R_{a1} i_{a1} + L_{\ell a1} \frac{di_{a1}}{dt} + \frac{d\lambda_{am}}{dt} \quad (22)$$

$$v_{a2} = R_{a2} i_{a2} + L_{\ell a2} \frac{di_{a2}}{dt} + \frac{N_2}{N_1} \frac{d\lambda_{am}}{dt} \quad (23)$$

if λ_{am} is understood to be in terms of primary turns. Thus in a three phase transformer there are three linkage variables λ_{am} , λ_{bm} and λ_{cm} .

Further implied by the constant turns ratio of a given phase is that there are three excitation variables instead of six.

$$F_a = N_{a1} i_{a1} + N_{a2} i_{a2} \quad (24)$$

$$F_b = N_{b1} i_{b1} + N_{b2} i_{b2} \quad (25)$$

$$F_c = N_{c1} i_{c1} + N_{c2} i_{c2} \quad (26)$$

Thus one has the linkages as functions of three excitations

$$\lambda_{km} = \lambda_{km}(F_a, F_b, F_c) \quad (27)$$

and the derivative term of Equation (22) becomes

$$\frac{d\lambda_{am}}{dt} = \frac{\partial \lambda_{am}}{\partial F_a} \frac{dF_a}{dt} + \frac{\partial \lambda_{am}}{\partial F_b} \frac{dF_b}{dt} + \frac{\partial \lambda_{am}}{\partial F_c} \frac{dF_c}{dt} \quad (28)$$

Thus the complete three phase magnetic field to circuit relationship can be expressed in matrix form

$$\begin{bmatrix} \frac{d\lambda_{am}}{dt} \\ \frac{d\lambda_{bm}}{dt} \\ \frac{d\lambda_{cm}}{dt} \end{bmatrix} = \begin{bmatrix} \frac{\partial \lambda_{am}}{\partial F_a} & \frac{\partial \lambda_{am}}{\partial F_b} & \frac{\partial \lambda_{am}}{\partial F_c} \\ \frac{\partial \lambda_{bm}}{\partial F_a} & \frac{\partial \lambda_{bm}}{\partial F_b} & \frac{\partial \lambda_{bm}}{\partial F_c} \\ \frac{\partial \lambda_{cm}}{\partial F_a} & \frac{\partial \lambda_{cm}}{\partial F_b} & \frac{\partial \lambda_{cm}}{\partial F_c} \end{bmatrix} \begin{bmatrix} \frac{dF_a}{dt} \\ \frac{dF_b}{dt} \\ \frac{dF_c}{dt} \end{bmatrix} \quad (29)$$

Equation (29) implies that nine magnetic characteristics are required. However, each of these are families of hysteresis loops.

Note that each term in the square matrix applies to both primary and secondary of the appropriate phase. Further, if constant leakage inductance

had not been assumed this matrix would be a 6×6 requiring 36 magnetic characteristics. Otherwise the analysis would be the same.

3.3 THE MAGNETIC CORE DATA

The major tasks in applying the circuit equations (Equation 22), are in obtaining the data required for the incremental inductances of Equation (29), storing the large amount of data in the computer in an efficient manner and developing the logic to access the data at the appropriate operating point.

The type and amount of data are discussed briefly in Nakra and Barton (Reference 10) for a somewhat simpler system. As a method of storing B-H curve data, several mathematical forms have been used. Macfadyen et al (Reference 13) discusses representation of magnetization curves by exponential series. Others use hyperbolic forms or polynomials. Manly (Reference 9) compares several methods. Somewhat less accurate but more efficient is the method given in the Air Force report AFAPL-TR-76-102 (Reference 14).

In terms of the B-H curve instead of the λ -i curve the equations are

$$B = B_s (H + KH_c) / [H_c (B_s/B_r - 1) + |H + KH_c|] - KB_0 \quad (30)$$

where

B_s is the saturation value of flux density for the major loop

B_r is the residual value of flux density for the major loop

H_c is the coercive force for the major loop

K is ± 1 to represent the lower and upper curves.

The B_0 allows representation of the minor loops (and hence the uppers and downers) where the minor loops intersect at point $(\pm H_m, \pm B_m)$ and B_0 is given by

$$B_0 = \frac{1}{2} \left[\frac{B_s(H_m + H_c)}{H_c(B_c/B_r - 1) + |H_m + H_c|} + \frac{B_s(H_m - H_c)}{H_c(B_s/B_r - 1) + |H_m - H_c|} \right] \quad (31)$$

Figure 3 shows curves computed by these formulas.

$$B_r/B_s = 0.78566$$

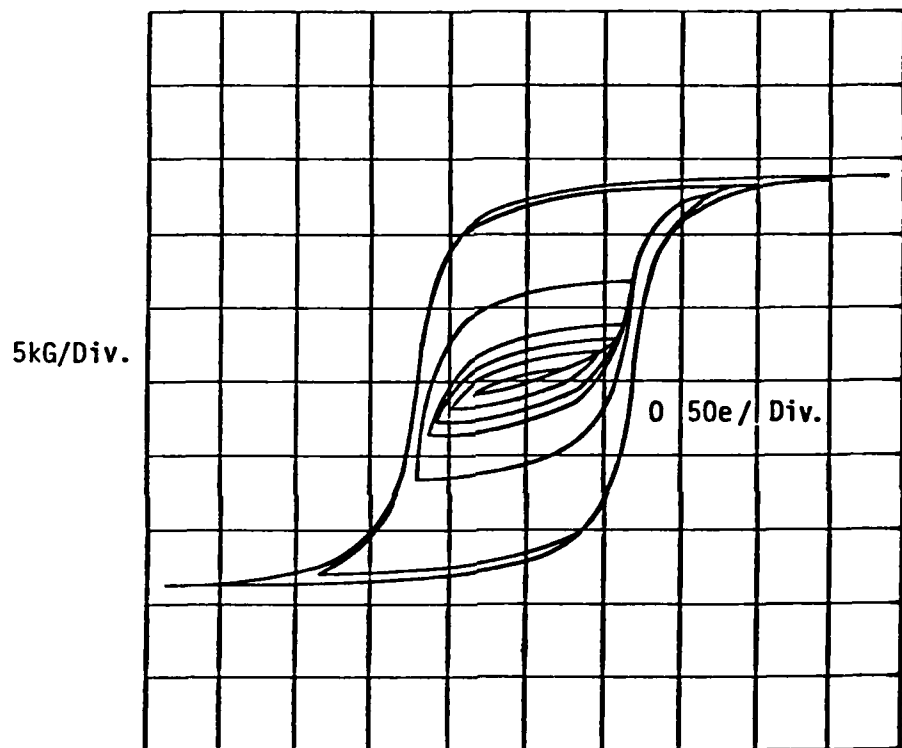


FIGURE 3. CURVES COMPUTED BY EQUATION (30)

Thus only data at several points on the major loops are required, the B_r , B_s and H_c values.

The B and H variables are common design variables but the λ and i variables are more common in measurements and are needed in network equations.

3.4 A SIMPLIFYING APPROXIMATION

Each entry in the incremental inductance matrix of Equation (29) requires the identification of an operating point in terms of the net excitation of the combined F_a , F_b and F_c . For each pair of values for F_b and F_c , F_a is varied over its range to determine a λ_{am} major or minor hysteresis loop. (For each incrementing of either F_b or F_c requires a new family of hysteresis loops.) By using Equations (30) and (31), data for major loops only are required. This still is a large amount of data to collect, store and access.

A slightly different approach will allow some approximations which will greatly reduce the amount of data required and make definition of the operating point easier.

Returning to Equation (27) and (28) let us define a net excitation of phase "a"

$$F'_a = F_a + T_{ab}F_b + T_{ac}F_c \quad (32)$$

then

$$\frac{d\lambda_{am}}{dt} = \frac{\partial \lambda_{am}}{F'_a} \left[\frac{dF_a}{dt} + T_{ab} \frac{dF_b}{dt} + T_{ac} \frac{dF_c}{dt} \right] \quad (33)$$

Equation (33) requires one incremental inductance term and one set of hysteresis loops λ_{am} vs F'_a as shown in Figure 4. However, the apparent turns ratios T_{ab} and T_{ac} will be variables depending on specific levels of F_a , F_b and F_c .

Now if one can neglect any change in shape of the λ_{am} - F'_a curves for differing levels of F_b and F_c , then F_b and F_c are accounted for by horizontal shifts in the loops of Figure 4. At each point, the shift of the vertical

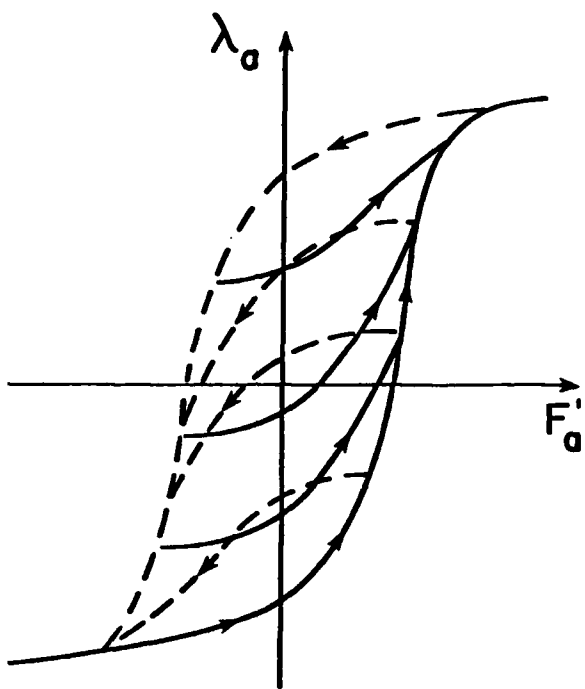


FIGURE 4. TYPE OF DATA NEEDED FOR ACCURATE MODELING OF THE CORE
 DATA FOR INCREMENTAL INDUCTANCE $\partial\lambda_a/\partial F_a'$
 $F_a' = F_a + T_{ab} F_b + T_{ac} F_c$

axis from the plot of λ_{am} as a function of F_a alone, gives a measure of T_{ab} and T_{ac} . (A set of major loops varying F_a over the full range for the set of conditions defined in Table 1 can be used with multiple regression to define $T_{ab}(F_a, F_b, F_c)$ and $T_{ac}(F_a, F_b, F_c)$.)

Thus one family of loops and equations for T_{ab} and T_{ac} would be all the data required for phase "a" magnetic characteristics. Similar data and representation would be required by phases "b" and "c" windings.

3.5 DETERMINING THE OPERATING POINT

In a computer program which performs a numerical integration to determine the system transient solution, a subroutine is required to determine the incremental inductance at each operating point. This incremental inductance is dependent on the state of each of the current variables and further the incremental inductance is dependent on whether each variable is increasing or decreasing. The use of excitation defined by Equation (32) and interpolation between curves such as those shown in Figure 4 would determine an approximate incremental inductance.

TABLE 1

REGRESSION DATA

Major $\lambda_{ma} - F_a$ Loop For Each Case Above For Determining
 T_{ab} and T_{ac} Regression Data

$$F'_a = F_a + T_{ab} \times 0 + T_{ac} \times 0 \quad \text{Over The Range of } F_a$$

$$= F_a + T_{ab} \times \Delta F_b + T_{ac} \times 0 \quad " \quad "$$

$$= F_a + T_{ab} \times k\Delta F_b + T_{ac} \times 0_c \quad " \quad "$$

$$F'_a = F_a + T_{ab} \times 0 + T_{ac} \times \Delta F_c \quad " \quad "$$

$$= F_a + T_{ab} \times \Delta F_b + T_{ac} \times \Delta F_c \quad " \quad "$$

$$= F_a + T_{ab} \times k\Delta F_b + T_{ac} \times \Delta F_c \quad " \quad "$$

$$F'_a = F_a + T_{ab} \times 0 + T_{ac} \times 2\Delta F_c$$

$$= F_a + T_{ab} \times \Delta F_b + T_{ac} \times 2\Delta F_c$$

$$= F_a + T_{ab} \times k\Delta F_b + T_{ac} \times 2\Delta F_c$$

$$F'_a = F_a + T_{ab} \times k\Delta F_b + T_{ac} \times k\Delta F_c$$

SECTION IV

THE AC RESONANT CHARGING CIRCUIT

4.1 OBJECTIVE

This part of the project was the development of the ac resonant charging circuit model which is to be the load on the generator and transformer discussed in earlier sections. The characteristics of the series RLC resonant charging circuit are well known (Reference 22) and the sequence of switching events defined by prior knowledge of the particular application. The work on this part of the project thus consists of: selection of an SCR model that will adequately represent turn-on and turn-off characteristics at the power level and with the resonating inductors of this particular application; assure that the model works when using series and/or parallel connected SCR's for higher power applications; convert the model to a form compatible with the integrated system model.

The accomplishments reported here are the selection of the SCR model with appropriate modifications for this application, testing of the model using CAD program SPICE2, the conversion of a SPICE 2 SCR model to a SCEPTRE model, and initial afforts of ac resonant charging using SCEPTRE.

4.2 SCR MODEL SELECTION

Five options were developed and considered as possible approaches to the objective of the SCR model selection. A brief summary of each option is as follows:

a. Develop a Model in House

This option was viewed as not well suited to the time frame of the project. It would be used only in the event that no suitable existing model could be found.

b. The Two Bipolar Junction Transistor (2-BJT) Model (Reference 23)

This model became the favored candidate because of the following. It was a long established model with a great deal of available supporting literature. The model had been verified by University of California-Berkeley (Reference 23) to adequately simulate the switching and operational

characteristics of an SCR. A method for determining model parameters from manufacturers specification sheet data had also been developed by University of California-Berkeley. This model had already been demonstrated using SPICE 2 and appeared readily adaptable to other advanced CAD programs such as SCEPTRE (Reference 23).

c. The Basic Three Junction (Intrinsic) Model

The intrinsic SCR model is fundamentally similar to the 2-BJT Model. No advantages over the 2-BJT Model were readily apparent. One disadvantage was apparent. That being an increased difficulty to the operator for use with SPICE 2.

d. Expanded Three Junction (J. Bowers) Model (References 24,30)

This model, developed by J. Bowers at the University of South Florida, is a complex model which is an expansion of the basic 3-Junction Model which again is fundamentally similar to the 2-BJT Model. J. Bower's Model was viewed as too complex for the application desired. In addition the complete model parameters are very difficult to obtain. On the other hand, this model could be simplified to more nearly resemble the Basic 3-Junction Model. The University of California-Berkeley method of parameter determination could then possibly be extended to this model. This model has also been extensively verified in performance using SCEPTRE. A difficulty was apparent, however, in the case of adaptation for use with another CAD program such as SPICE 2.

e. Georgia Tech Terminal Characteristics Model (Reference 25)

This option offered the possibility of a high power SCR model as called for by the research project at hand. Unfortunately, development of the model was only partially complete and therefore could not be fully evaluated. To the extent that development had proceeded, it appeared that determination of model parameters might be difficult.

There were several important considerations in selecting the model. Among these are first, the ease of obtaining numerical values for model component parameters from manufacturer's data or by measurement, second, the integrity of the model as established by the literature or by test. The

model must adequately represent features important in this particular application. Third, in this project the compatibility of the model with CAD programs such as SPICE 2 and SCEPTRE.

The 2-BJT model shown in Figure 5 was altered slightly and used in this project.

Appendix E shows the development of the BJT as it evolved from the Ebers-Moll model through the work of Ki (Reference 23) and Getreu (Reference 32). Appendix E shows the development of the SCR model from the BJT, the determination of the element values required for SPICE 2 modeling of the SCR and the determination of the element values required for the SCEPTRE modeling of the SCR. The SCEPTRE values are obtained as conversions from the more familiar SPICE 2 quantities.

4.3 SCR MODEL IN AC RESONANT CHARGING

The CAD program SCEPTRE is to be used in modeling the composite system of the ac generator, transformer, and the load consisting of ac or dc charging circuit. While it is recognized that SCEPTRE is generally slower than SPICE 2, SPICE 2 does not have the capabilities required for modeling the generator non-linear time varying parameters. However, SPICE 2 is faster and more convenient to use in electronic circuits such as the ac resonant charging circuit. In the following work the model development and testing of the SCR in ac resonant charging is done using SPICE 2, with the conversion to SCEPTRE format as a later task.

a. SPICE 2 Single Loop Analysis

A SPICE 2 program was written and ran for the circuit of Figure 6. The results of the SCR ac resonant charging circuit single loop analysis revealed an oscillation following commutation (Ref. to Fig. 7). The oscillation appears to result from the non-linear resonant behavior of the junction capacitances with the circuit inductance. This is supported by the fact that removal of the inductor from the circuit resulted in normal commutation with no oscillation after SCR cut-off. The oscillation may be suppressed by addition of a snubber to the circuit (Ref. to Fig. 8); however, investigation of the fundamental nature of the oscillation is continuing.

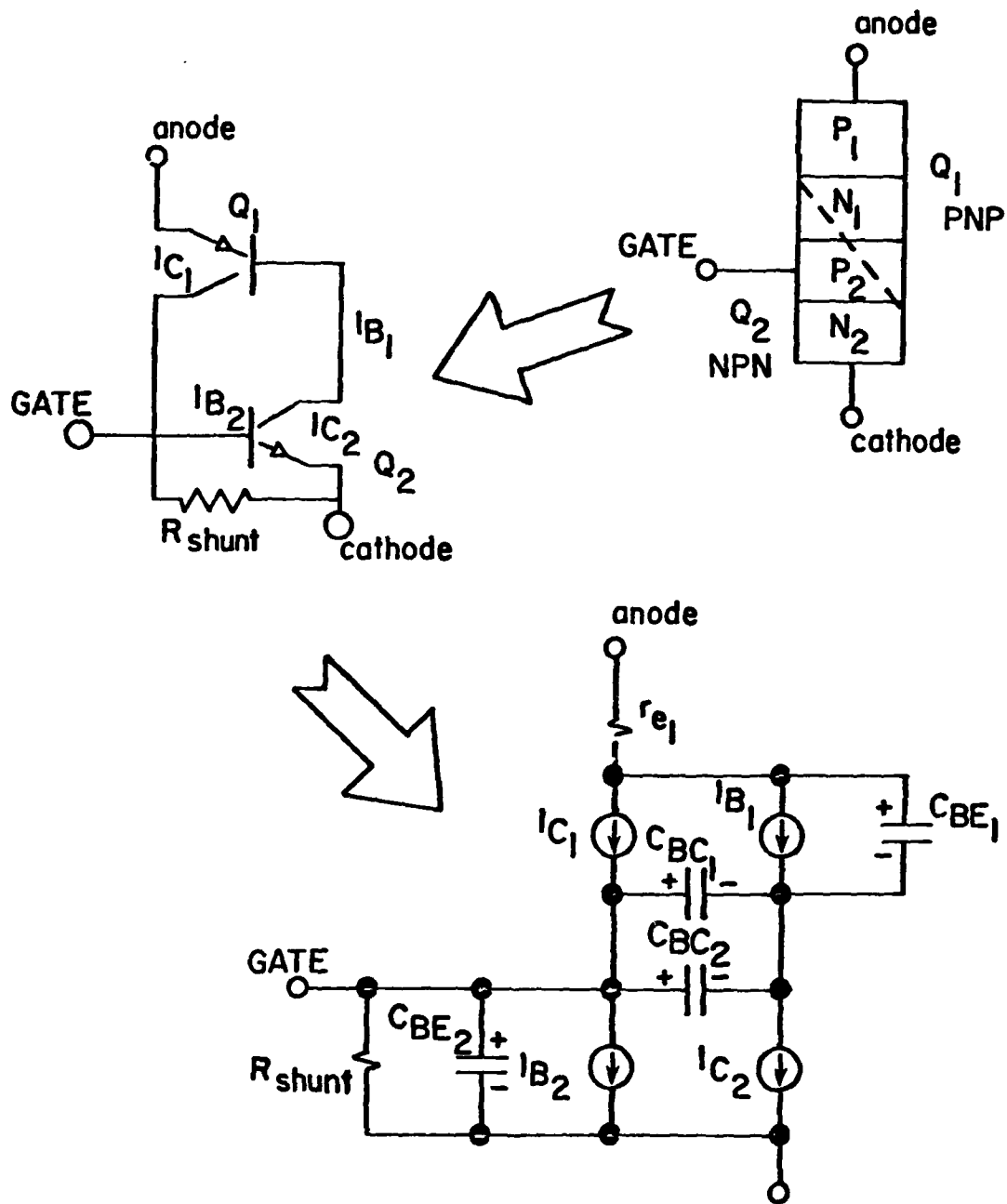
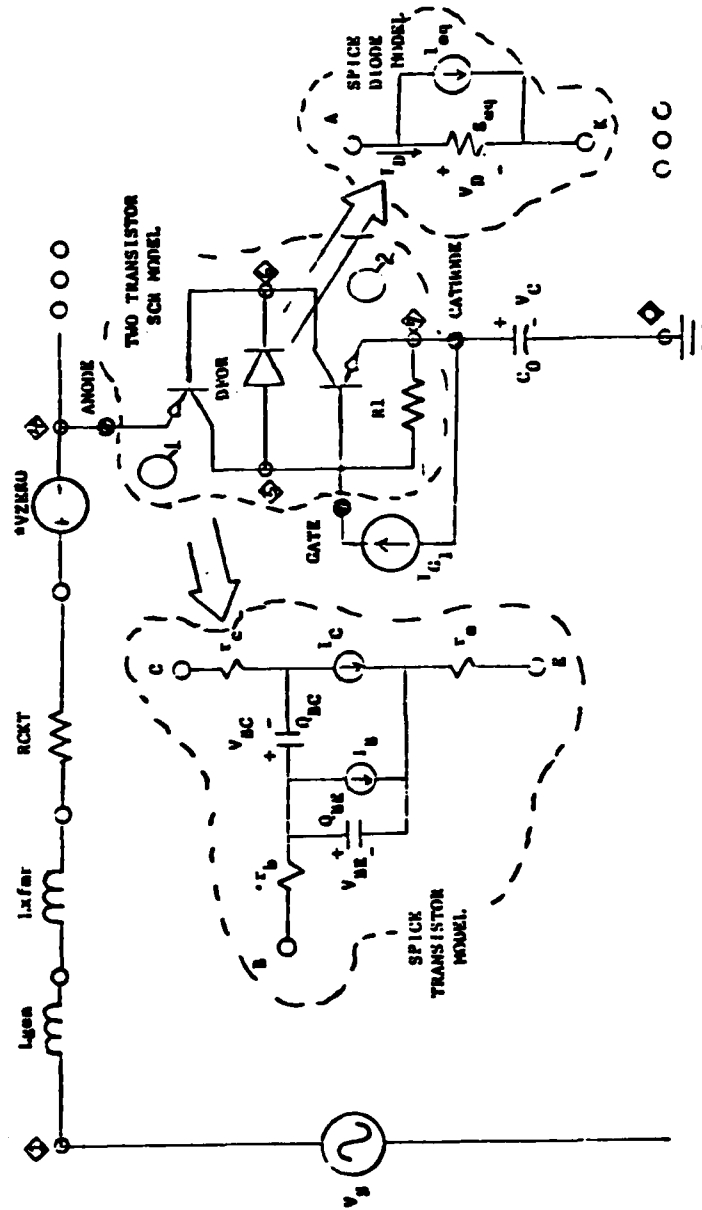


FIGURE 5. THE TWO BIPOLAR JUNCTION TRANSISTOR MODEL OF THE SCR.
A DISCUSSION OF THIS MODEL IS INCLUDED IN THE APPENDIX.



v_AZERO is a zero value voltage source which provides a method of simulating a test point in SPICE

FIGURE 6. SPICE CIRCUIT DIAGRAM FOR THE SINGLE LOOP AC RESONANT CHARGING SYSTEM

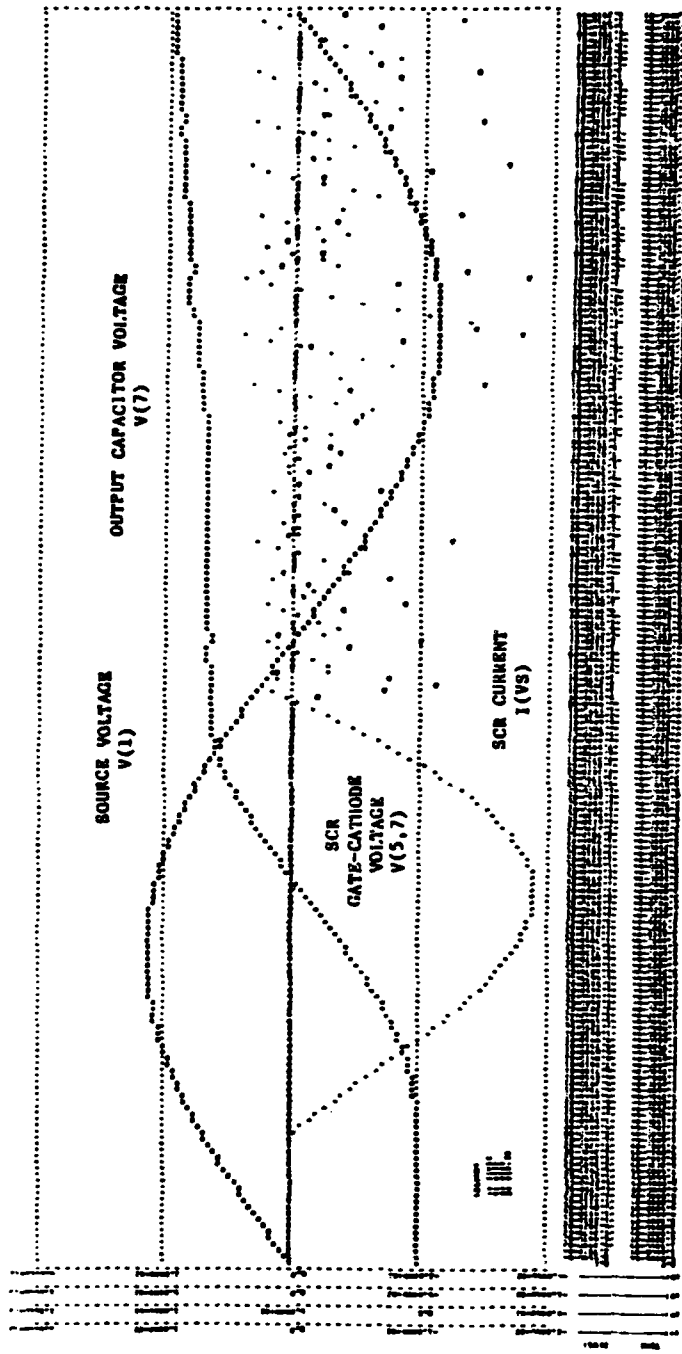


FIGURE 7. SPICE 2 SIMULATION OF THE AC RESONANT CHARGING CIRCUIT OF FIGURE 6.

FIGURE 7a. SPICE 2 PROGRAM LISTING FOR CIRCUIT OF FIGURE 6 WITH SHNUBBERS. SIMULATION RESULTS ARE SHOWN IN FIGURE 4-5.

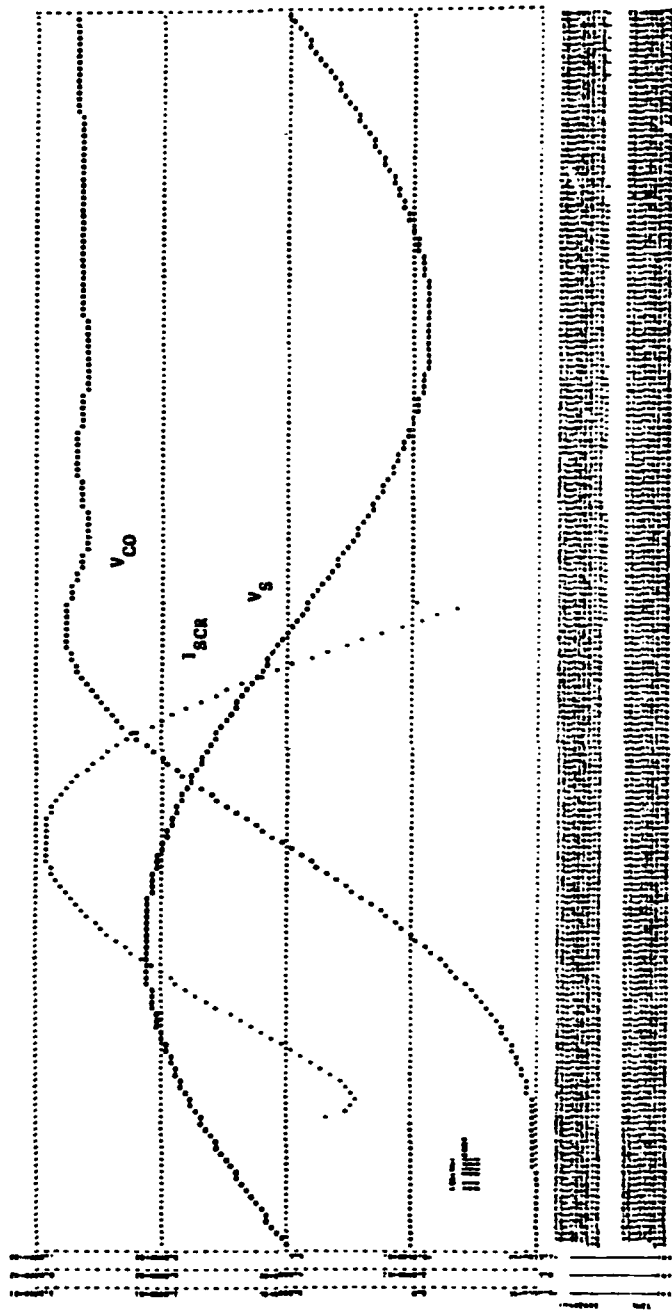


FIGURE 8. SPICE 2 SIMULATION OF SINGLE LOOP AC RESONANT CIRCUIT WITH A SNUBBER (FIGURE 9). THE "MODIFIED HU-KI MODEL" WAS USED.

THE COUSIN IN SICK - THE FRIENDS AT HIS CHURCH LIE - USELESS LIFE - WITH SICKNESS

INPUT LISTING = 27.0GL ULR C
TEMPERATURE LUMEN = 27.0GL ULR C

卷之三

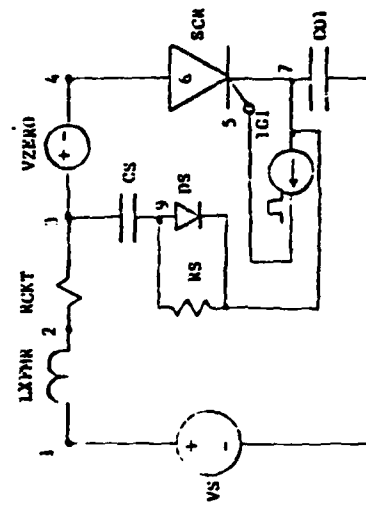


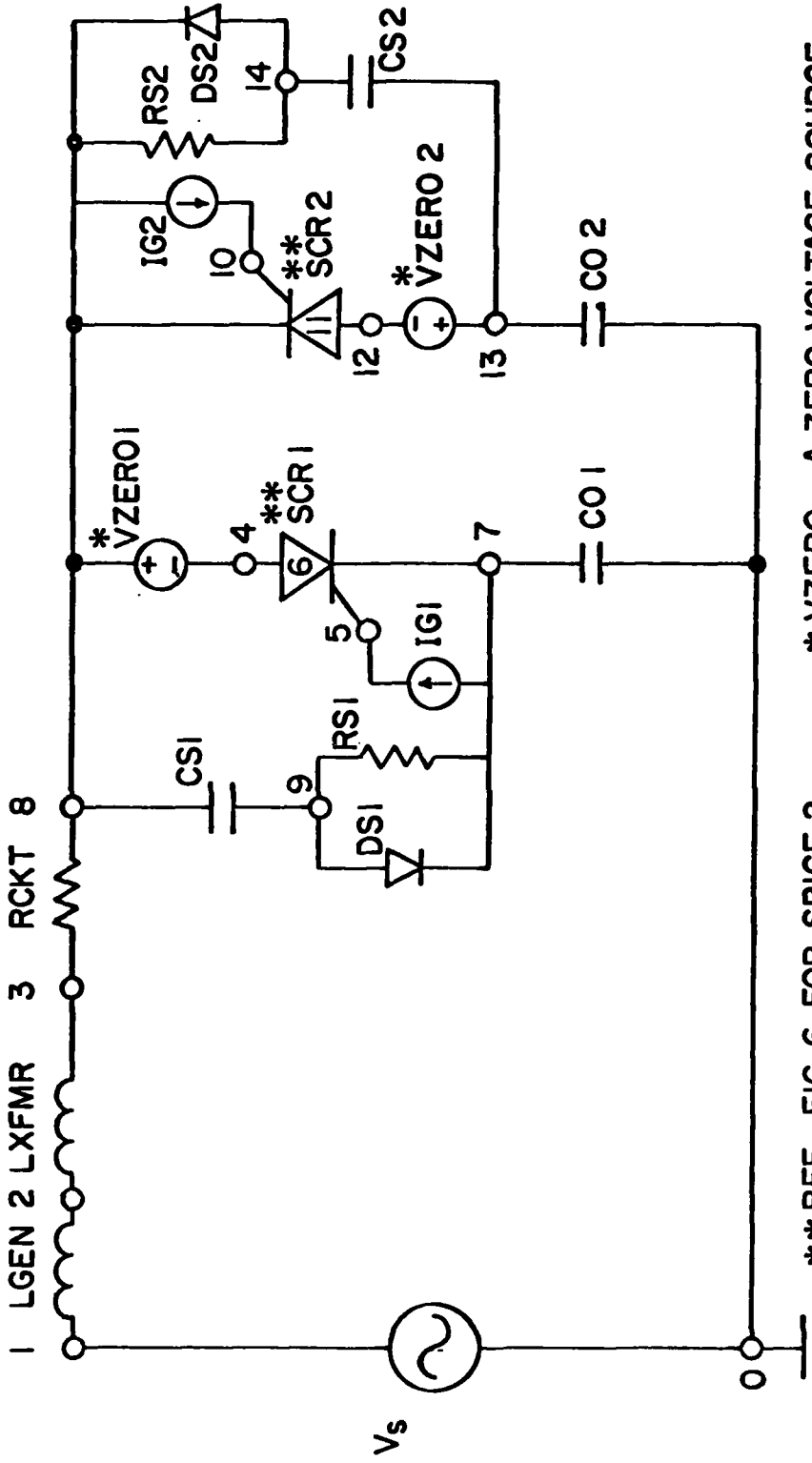
FIGURE 9. SINGLE LOOP CIRCUIT WITH SNUBBERS.

b. SPICE 2 Two Loop Analysis

A second SCR and charging capacitor loop was added to the circuit as shown in Figure 10. The associated SPICE 2 Input listing is shown in Figure 11.

The two loop analysis revealed a problem with the second branch SCR turning on prior to application of the gate₂ trigger signal. This early firing of the second branch SCR was suspected to be related to the oscillation experienced following turn-off of the first branch. Accordingly, a program was run in which all things were kept the same with the exception that no gate₁ pulse was applied to SCR₁. The circuit operated correctly in that SCR₂ did not turn-on until application of the gate₂ signal. Snubber circuits were then added in an effort to and suppress the early turn-on. This effort has not yet been successful.

In summary, the efforts were inconclusive and effort is still under way to solve problems incurred. The problems are that the circuit inductance has a resonant interaction with a SCR junction capacitance which causes unacceptable circuit oscillation following turn-off of the device. The circuit oscillation then causes uncontrolled turn-on of other SCRs in the circuit. Conventional snubber circuits have not proven successful in suppressing this problem.



** REF. FIG. 6 FOR SPICE 2
SCR MODEL CKT.
 $*VZERO$ - A ZERO VOLTAGE SOURCE
USED AS CURRENT MONITOR IN
SPICE 2 PROGRAMS.

FIGURE 10. THE SPICE 2 CIRCUIT DIAGRAM FOR THE TWO BRANCH AC RESONANT CHARGING SYSTEM WITH SNUBBERS.

*****09/02/80 ***** SPICE 2E.2 (26SEP78) *****13:49:31*****

GE C602 LM SCR - TWO BRANCH AC RES LADING CKT - DISCRETE

INPUT LISTING

TEMPERATURE = 27.000 DEG C

```
VS 1 0 SIN(0 566 1K )
IG1 7 5 PULSE(0 1.0 100US 0 0 5US )
IG2 8 10 PULSE(0 1.0 600US 0 0 5US )
VZERO1 8 4 SIN(0 0 0)
VZERO2 13 12 SIN(0 0 0)
LGEN 1 2 0.1MH
LXFMR 2 3 0.2MH
RCKT 3 8 0.5
Q1 5 6 4 QMOD1 OFF
Q2 6 5 7 QMOD2 OFF
Q3 10 11 12 QMOD1 OFF
Q4 11 10 8 QMOD2 OFF
RSHT1 5 7 9 .375
RSHT2 10 8 9 .375
C01 7 0 50UF
C02 0 13 50UF
CS1 9 8 1.0UF
RS1 7 9 100.
DS1 9 7 DMOD1
CS2 13 14 1.0UF
RS2 14 8 100
DS2 14 8 DMOD1
.MODEL DMOD1 D18V=2700
.MODEL QMOD1 PNP(BF=4,FK=4,IS=1.0E-16,RF=.005,TF=17.8US,TR=1125US)
.MODEL QMOD2 NPN(BF=9,IS=1.0E-16,CJC=4000PF,MC=0.3)
.TRAN 5US 1000US
.PRINT TRAN I(VS) V(1) V(5,7) V(7,0) V(10,8) V(0,13)
.PLOT TRAN I(VS) V(1) V(5,7) V(7,0) V(10,8) V(0,13)
.OPTIONS NOMOD NUPAGE ITL3=25 ITL4=100 ITL5=10000 LIMPTS=10000
.END
```

FIGURE 11. SPICE 2 TWO LOOP AC RESONANT CHARGING SYSTEM INPUT DECK FOR CIRCUIT SHOWN IN FIGURE 10.

SECTION V

CHOICE OF VARIABLES

5.1 OBJECTIVE

When solving systems of equations using numerical methods and in particular when the equations are non-linear, the choice of system variables may have significant effect on the computation time and on the reliability of the results. In this section the nature of these effects are examined even though the decision to use CAD programs such as SPICE 2 and SCEPTRE may preclude such considerations.

5.2 CHOICE OF VARIABLES

Chua and Lin (Reference 11) have shown that the selection of a certain set of state variables depends on the nature of the nonlinear elements. For a nonlinear capacitor characterized by a nonmonotonic voltage-controlled q-v curve, for example, the capacitor voltage must be chosen as the state-variable. Similarly, inductor current must be chosen as the state variable for a nonlinear inductor characterized by a nonmonotonic current-controlled λ-i curve. However, if the capacitor and inductor characteristic curves are strictly monotonic, then either capacitor voltage or charge may be chosen as the capacitor state variable, and for the inductor, the state variable may be chosen as either inductor flux linkage or current.

However, it is shown (Reference 12) that it is advantageous to choose capacitor charge and inductor flux linkage as the state variables when a numerical integration algorithm is used because this particular choice of state variables reduces the global error. Global error is the error accrued over the finite time interval during which the numerical integration is performed.

To see why this is so, consider a nonlinear system (Reference 12) modeled by the equations

$$\bar{\dot{x}} = \bar{f}(\bar{x}, t) \quad \bar{x}(0) = \bar{x}_0 \quad (34)$$

where the bar implies the use of vectors or matrices.

To estimate the growth of errors over some time interval, say time $t = 0$ to $t = t_f$ when solving Equation (34) numerically, consider the differential equation which results when the initial condition is perturbed so that $\underline{x}(0) \rightarrow \underline{x}_0 + \delta\underline{x}(0) = \underline{x}_0 + \underline{\delta}_0$. Then from Equation (34) the perturbed equations become

$$\frac{d}{dt} (\underline{x}(t) + \delta\underline{x}(t)) = \underline{f}(\underline{x}(t) + \delta\underline{x}(t), t) \quad (35)$$

$$\delta\underline{x}(0) = \underline{\delta}_0$$

Assuming $\delta\underline{x}(t)$ is small and expanding the right side of Equation (35) by a Taylor series gives

$$\frac{d}{dt} (\underline{x}(t) + \delta\underline{x}(t)) \approx \underline{f}(\underline{x}, t) + \frac{\partial \underline{f}}{\partial \underline{x}} \delta\underline{x}(t) \quad (36)$$

$$\delta\underline{x}(0) = \underline{\delta}_0$$

Subtracting Equation (36) from Equation (34) gives

$$\frac{d\delta\underline{x}}{dt} = \left(\frac{\partial \underline{f}}{\partial \underline{x}} \right) \delta\underline{x} \quad \delta\underline{x}(0) = \underline{\delta}_0 \quad (37)$$

where the matrix $(\partial \underline{f} / \partial \underline{x})$ as a time-varying Jacobian matrix $J_x(t)$. Equation (37) represents a linear time-varying system; thus no simple solution exists. In the case where \underline{x} and \underline{f} are scalar quantities, the solution to Equation (37) is

$$\delta\underline{x}(t) = \underline{\delta}_0 e^{\int_0^t J_x(\tau) d\tau} \quad (38)$$

Equation (38) indicates that whenever $J_x(\tau) > 0$, the error (accumulated at time t in the exact solution to the scalar version of Equation (34), due to an error $\underline{\delta}_0$ in the initial condition) actually decreases exponentially with time. Since the concern is the accrued effects of errors made at all time steps (and not just that due to an error in the initial condition), proceed to determine the accrued error E^{0,t_f} , ie., the sum of errors from time $t = 0$ to time $t = t_f$. To this end it is assumed that the error per

unit time (which is denoted by ϵ_t) is constant. Then the error made in an interval of time dt_1 , is $\epsilon_t dt_1$. From Equation (38), the growth of error for $t_1 < t$ is given by

$$\epsilon_{t_1, t} = \epsilon_t dt_1 e^{\int_{t_1}^t J_x(\tau) d\tau} \quad (39)$$

so that the accrued error E^{0, t_f} at time t_f is the sum of the error originating for all times $t_1 < t_f$, so that

$$E^{0, t_f} = \left(\begin{array}{c} t_f \\ \epsilon_t \int_0^{t_f} e^{\int_0^t J_x(\tau) d\tau} dt_1 \end{array} \right) \quad (40)$$

To demonstrate error growth, Calahan (Reference 11) used the circuit of Figure 12, where the nonlinear capacitance is strictly monotonic. If the state equation is written in terms of the capacitor voltage we have

$$(C_T + C_d^0 e^{\lambda v}) \frac{dv}{dt} = -\frac{v}{R} + \frac{v_s}{R} - I_s(e^{\lambda v} - 1); \quad \lambda = 40 \quad (41)$$

The Jacobian is given by

$$J_V = \frac{\lambda C_d^0 e^{\lambda v} \left(\frac{v-v_s}{R} \right) + I_s(e^{\lambda v} - 1)}{(C_T + C_d^0 e^{\lambda v})^2} - \frac{\left(\frac{1}{R} + \lambda I_s e^{\lambda v} \right)}{(C_T + C_d^0 e^{\lambda v})} \quad (42)$$

where $\lambda = 40$.

During switching, when $v_s < 0$ and $v > 0$, the first term shifts the eigenvalue J_V toward the right half plane. Indeed if v_s is made sufficiently negative, the eigenvalue J_V can be made as positive as desired. Thus, during this time when J_V is positive, truncation errors introduced by

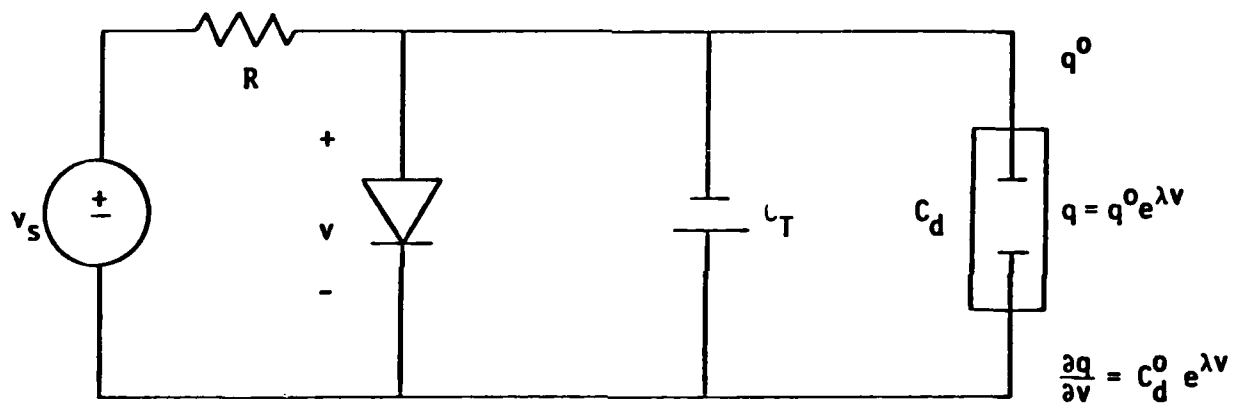


FIGURE 12. CALAHAN'S EXAMPLE CIRCUIT

the integration formula used will be amplified according to Equation (40). By choosing charge as the state variable, the resulting eigenvalue J_F can be shown to lie in the left half plane during switching, so that truncation errors will decay according to Equation (40). Finally, it should be noted that in the case of linear capacitors or inductors, either q or v for a capacitor, or λ or i for an inductor may be chosen as the state variable (Reference 11).

5.3 SCEPTRE VARIABLES

In Section VII the decision to use the CAD system called SCEPTRE is discussed. Whether SCEPTRE or the other system considered SPICE 2, is used, the system variables are capacitor voltages, inductor currents or other variables determined by the CAD system. Thus, the decision to use a CAD system represents a trade-off between ease of system formulation and some control of integration error by judicious choice of system variables.

The state-variables used in SCEPTRE are capacitor voltage and inductor current. Both nonlinear capacitors and nonlinear inductors are present in the integrated system. The nonlinear inductors arise naturally in the generator and transformer models, the nonlinear capacitors in the SCR model. Further, the nonlinear capacitors in the SCR model are strictly monotonic so that computationally the choice of capacitor voltage as the state variable is desirable. Also, the nonlinear inductors in the transformer and generator model are strictly monotonic so that inductor flux linkages are the preferred state variables.

While it has been rigorously proven that for nonlinear dynamic networks containing passive elements and independent sources it is desirable to choose capacitor charges and inductor flux linkages as state variables, no one has been yet able to prove that the same criterion applies for networks containing active elements and controlled sources, although it would seem to apply (Reference 11). In a system as complex as the one in this project it is not clear what the trade-off may have cost in terms of integration error.

SECTION VI

NUMERICAL METHODS FOR STIFF DIFFERENTIAL EQUATIONS

6.1 INTRODUCTION

In this section suitable numerical methods for solving stiff differential equations are investigated. Stiff means that the magnitude of the largest eigenvalue to the smallest eigenvalue of the system differs by many orders of magnitude. Most standard methods, such as the Runge Kutta method, or the forward Euler method, are not well suited for solving stiff differential equations (Reference 15). This is because the step size in the forward Euler method, for example, is determined by the smallest time constant, but the number of iterations required to reach the steady state is determined by the largest time constant. Thus, if the time constants are widely separated a small step size would necessarily be employed and a great deal of computer time would be spent on determining the steady-state solution (Reference 16).

6.2 INTEGRATION METHODS

It has been shown (Reference 16) that the widely separated time constant problem can be eased by using implicit integration algorithms, such as the backward Euler and trapezoidal algorithms. Typically, the use of the trapezoidal algorithm is avoided because of the "ringing behavior" it exhibits when implemented with a large step size. This is undesirable since it may erroneously lead the designer to conclude the solution to the system is oscillatory (Reference 16).

Gear (Reference 17) has proposed a family of methods of order $p+1$ which have been shown to be extremely useful for solving stiff differential equations. These methods are based on the implicit formula

$$y_{n+1} = \sum_{i=0}^p c_i y_{n-1} + d \dot{y}_{n+1}$$

For $p = 0$ the backward Euler method is obtained. The Gear methods possess the property that $\text{Re}\{h\lambda\} < -a$ for some small positive a ; that is, the

method is stable where stability is the prime consideration. In addition, when $\text{Re}\{h\lambda\} > a$ they are accurate (Reference 17, 18). In general there is a tradeoff between accuracy and stability for any numerical integration method. Choosing a high-order Gear method, for example, increases the accuracy (ie, reduces truncation error) at the expense of decreasing the stability (Reference 17). The maximum order must be limited to $p+1=5$ because of stability considerations (Reference 17).

Gear's methods can be implemented in a fixed or variable step size mode, or in a variable step size and variable-order mode. While the latter is difficult to implement there are several reasons why it is well worth the effort. First of all, since the computation is started with a low-order rule and small step size the method is self-starting. The order and the step size are adaptive in the sense that they are modified at each time step so that the optimal order and step size are chosen, subject to certain constraints. This leads to a very efficient and accurate solution over the integration interval of interest. At the present time, stability theory in variable step size, variable-order methods is not fully comprehended so that decisions for determining step size are based on experimental evidence (Reference 18).

Another advantage of using Gear's method is that it has an outstanding error control feature (Reference 19). Calahan was the first to discuss how to implement Gear's method in a nodal-based analysis program (Reference 20).

Gear's method is a vast improvement over previous techniques because it is not troubled by the minimum time constant problem. However, if step size is changed very rapidly, Gear's method could become numerically unstable. To overcome this deficiency in Gear's method, Brayton, Gustafson and Hachtel (Reference 21) have proposed yet another method which is less likely to become unstable when the step-size changes rapidly, as demonstrated by numerical experiments. In the case where the step size is fixed, the method of Brayton et al. can be shown to be equivalent to Gear's method (Reference 21).

6.3 INTEGRATION METHODS OF SCEPTRE

SCEPTRE offers several options for integration methods including Gear's (Reference 17) method in variable step size. SCEPTRE should be appropriate for this project. The generator, transformer and SCR models in a composite system with its stiff differential equations require the implicit integration capability. The program also allows specification of maximum and minimum step size and error limits can be specified control the variable step size feature.

However, even though implicit integration allows larger step size than non-implicit methods there is no doubt that a step size appropriate for the short time constants of the SCR model will still require long computer times for the representation of the periodic swings of the electromechanical equations of the generator.

SECTION VII

SYSTEM INTEGRATION

The system integration parts of this project did not have any specific effort scheduled for the period of this report. However, in making the decision to use SCEPTRE as a modeling and simulation program, system integration became involved.

The original plan was to model the system by components and form the system by integrating the components. This is in contrast to modeling the system by elements (R, L, C and sources) and integration of the system with network equation formulation.

As work began in the study of methods for solving "stiff" differential equations several problems became apparent. First, small step sizes and long computation times would be required to account for the effects of both long and short time constants. Secondly, while implicit integration methods for "stiff" differential equations allow larger step sizes, iteration is required for convergence to a solution at each step. Finally, any further iterations that may be required to find the equilibrium point for the component interface variables make the component approach less attractive.

Three alternatives were considered.

1. write a network solving program
2. use CAD program SPICE 2
3. use CAD program SCEPTRE

The first alternative has the advantages of a much simpler and smaller program than SPICE 2 or SCEPTRE since they were written to do much more than a simple transient network analysis. Also, system variables could be used which would enhance the accuracy of the nonlinear systems. (Note Section V) SPICE 2 and SCEPTRE normally use voltage and current as variables.

The disadvantage is an unpredictable amount of time in writing and debugging such a program.

While SPICE 2 is well recognized as a good computer aided design program for electronic components, it has limited capability in representing nonlinear

time varying coefficients such as the inductance of the generator model. SCEPTRE allows definition of such elements through functions and FORTRAN function subprograms.

SPICE 2 has the capability of defining dependent sources as polynomial functions of current variables, thus, some nonlinearities can be represented. Possibly the time varying nonlinear generator inductances could be represented in SPICE 2 but SCEPTRE is preferred since such manipulation is not required.

Both SPICE 2 and SCEPTRE have implicit integration options for "stiff" differential equations. Both have variable step size with some external control through error limit specifications. Also, both have the capability of storing electronic component models.

In SPICE 2 the system elements are supplied to the program and the programs integrates the elements into a system using a nodal formulation. In SCEPTRE the system elements are supplied to the program in much the same format as for the SPICE 2 program. SCEPTRE then integrates the elements into a system by formulating state equations. It is well known that the nodal formulation is generally more efficient.

The overriding features that resulted in the selection of SCEPTRE over SPICE 2 was the limited capability of SPICE 2 in representing nonlinear elements. Both generator and transformer model components not only have nonlinear elements but these elements are subject to saturation effects. SCEPTRE's ability to define elements in more general terms and to use FORTRAN function subprograms for further flexibility were necessary in the generator and transformer model.

SECTION VIII

GENERATOR MODEL RESULTS

8.1 INTRODUCTION

The results illustrated in this section represent the culmination of many experimental computer solutions. At each step in the development of the generator model two types of runs were made. First, runs were made to determine appropriate initial conditions so that subsequent runs would display results due to faults and not due to mismatch of initial conditions. These initial conditions are not obvious in nonlinear systems. Secondly, runs were made under severe fault conditions to assure that the model would properly represent severe transients expected in later simulations.

The steps in developing the model included: allow the speed to vary; add torque equations; formulate linear model; account for saturation in terms of Equation (13).

In accounting for saturation for the first step the A_a and similar terms were taken as zero and the C_{aa} and similar terms were taken as unity. This gives a run for the unsaturated linear model.

The next run was made where the A_a and similar terms were taken as zero but the C_{aa} and similar terms were computed as described in Appendix B. This gives a run including the change of the inductance due to saturation.

The final run includes the variation of the A_a and similar terms. This will include the effect of the rate of change of inductance with current. These terms are many and complex and a successful run has not been completed.

8.2 DISCUSSION OF RESULTS

Figure 13 and 14 show C_{aa} and C_{FF} curves as examples of the saturation coefficients used in the example of the subsequent figures. Data for the other saturation coefficients are included in Appendix C.

Figures 15 through 19 show some systems variables for the conditions:

1. one cycle of steady state operation

2. a symmetric three phase short circuit is applied at the stator terminals for one cycle
3. the short is removed and system load is restored.

The above sequence has no significance except that it represent a severe transient under load and the model responds as expected in all circuits.

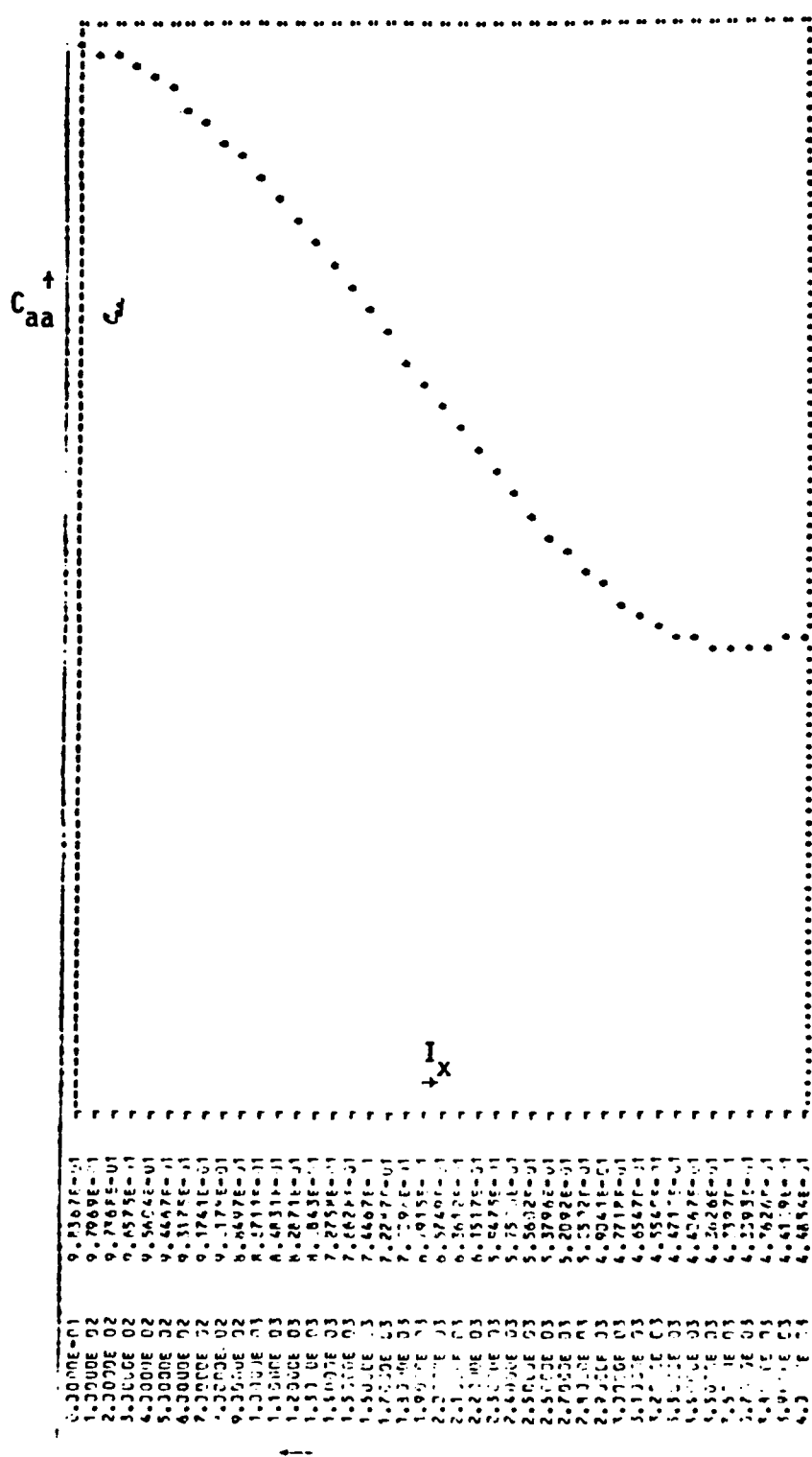
Figure 15 shows phase "a" current.

Figure 16 shows the main field current.

Figure 17 shows the direct axis damper circuit current.

Figure 18 shows the quadrature axis damper circuit current.

Figure 19 shows the rotor speed.



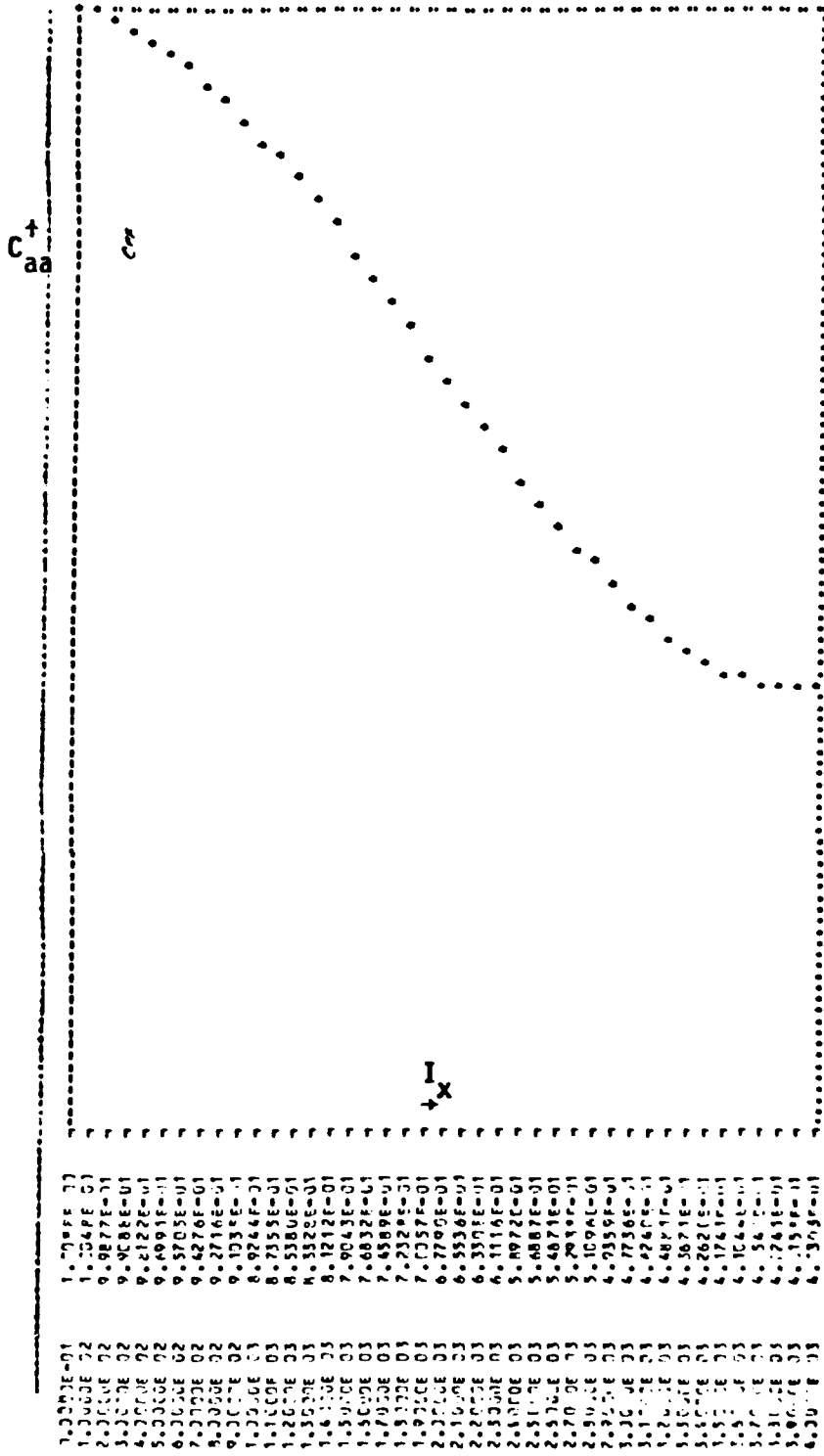


FIGURE 14. SATURATION MULTIPLIER, C_{FF} VERSUS I_x

2. Implement the specific AC charging configuration to be used in comparing modeling and simulation results with Air Force hardware test results. It is expected that this will involve series and parallel combinations of SCR's to accomodate the required voltage and current volves.

Before the Phase III simulations can be carried out the specific devices, the number in series and the number in parallel and the exact charging circuit voltages, currents and configuration must be supplied by the Air Force.

The conversion of SPICE 2 models to SCEPTRE models can be construed to be part of Phase II task 3, System Integration.

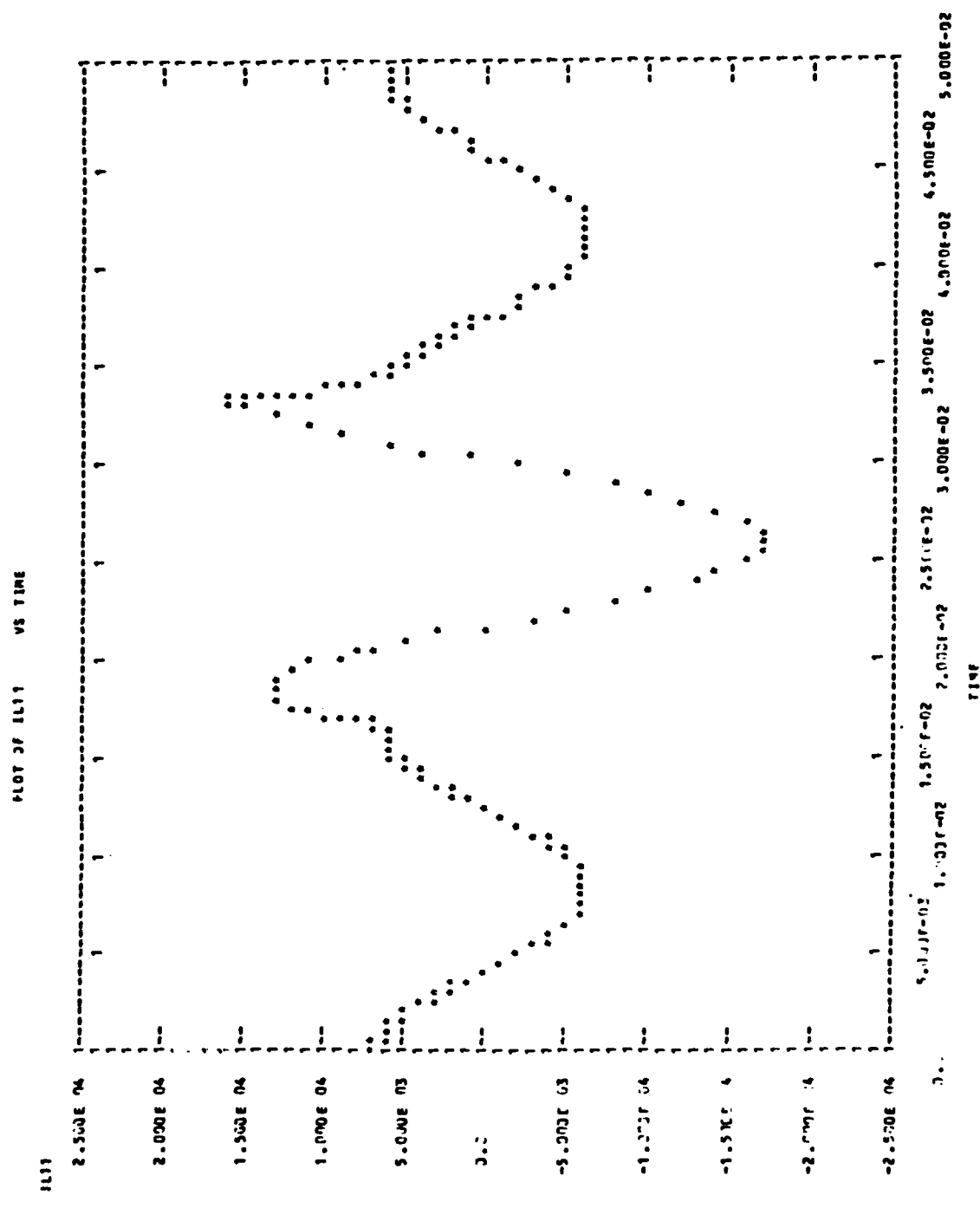


FIGURE 15. PHASE "a" CURRENT 3 PHASE SHORT AT T = 0.0166 SEC FAULT REMOVED AT T = 0.0333 SEC.

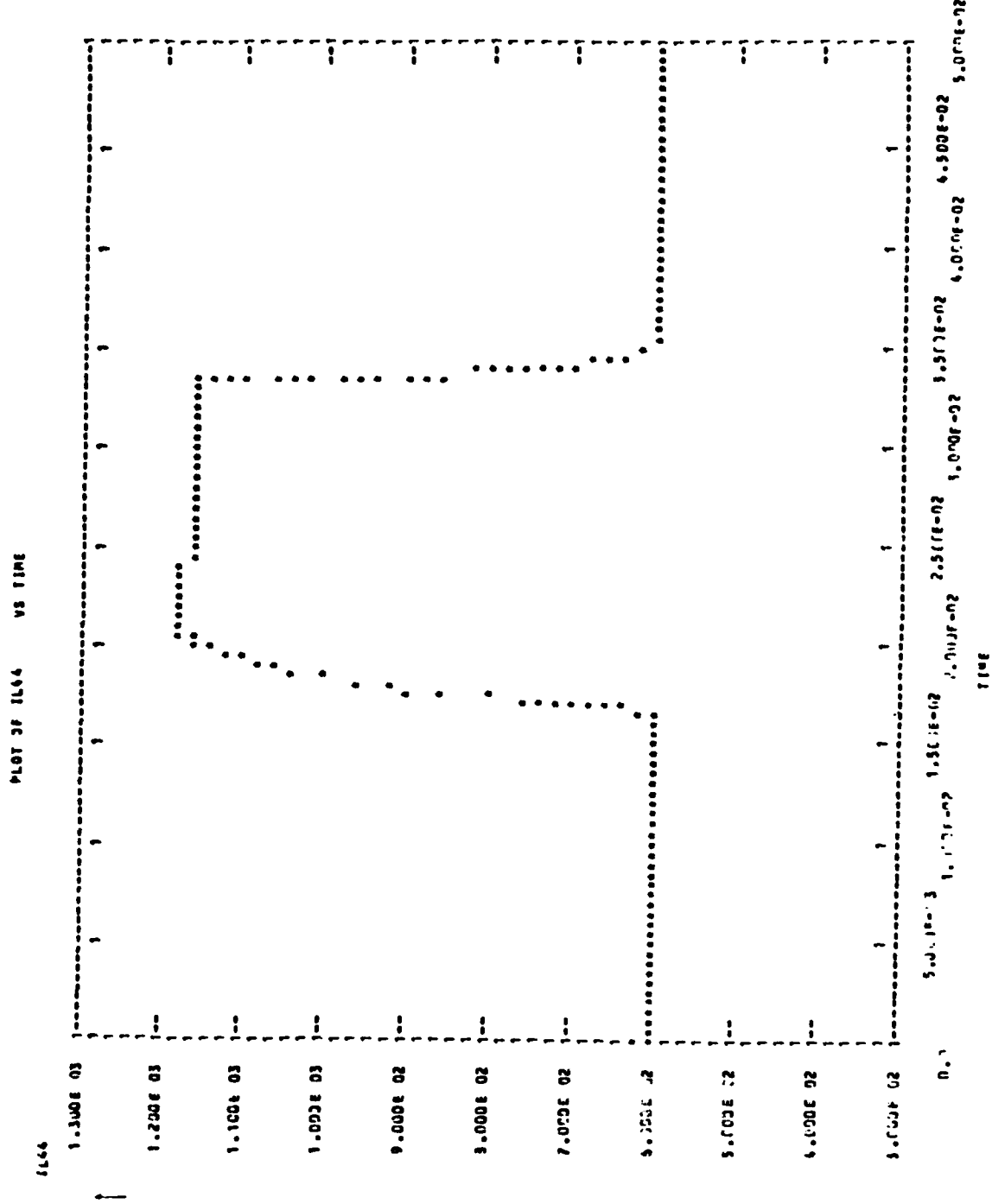


FIGURE 16. FIELD CURRENT I_f FAULT CONDITIONS AS IN FIGURE 15.

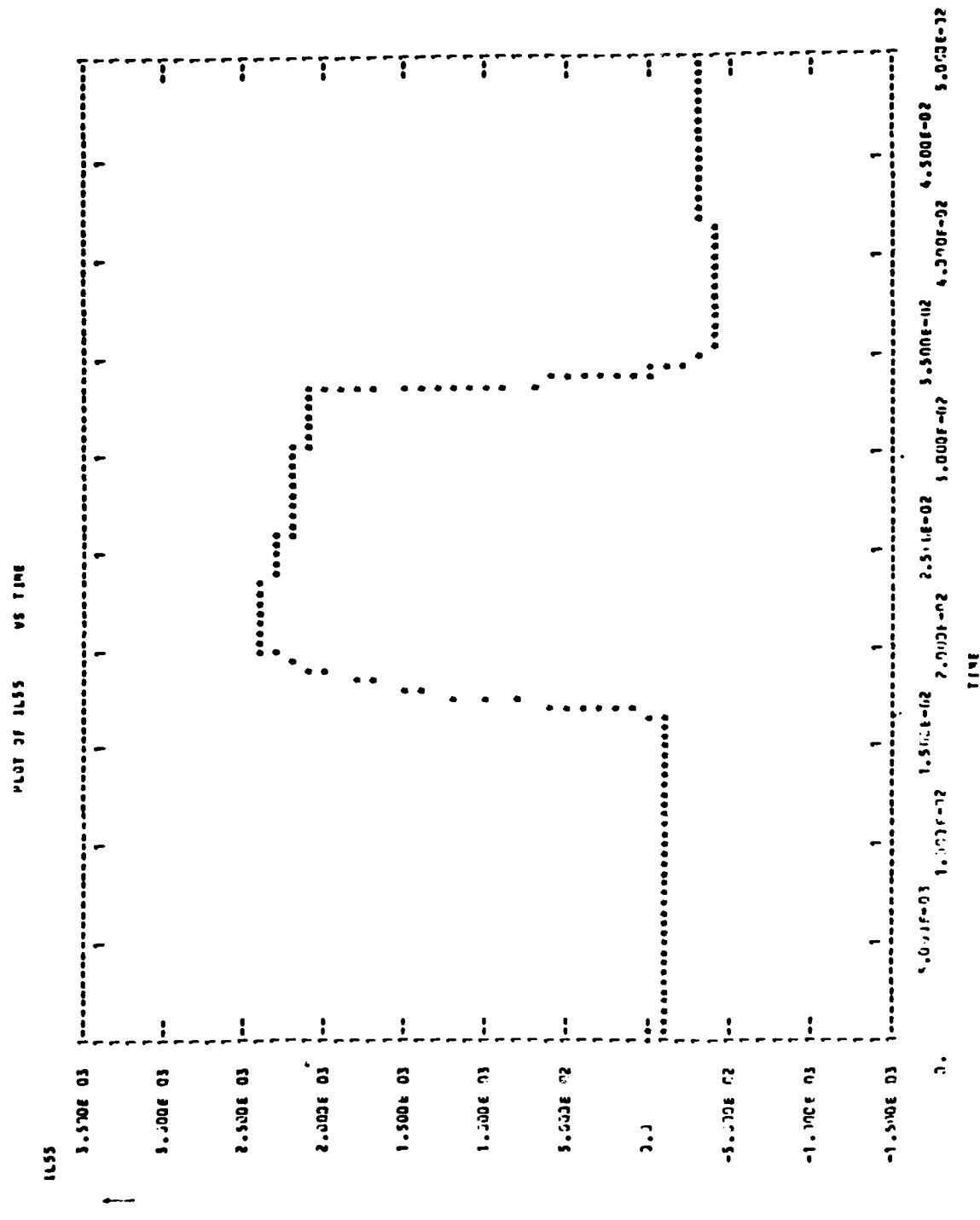


FIGURE 17. DIRECT AXIS DAMPER CURRENT FAULT CONDITIONS AS IN FIGURE 15.

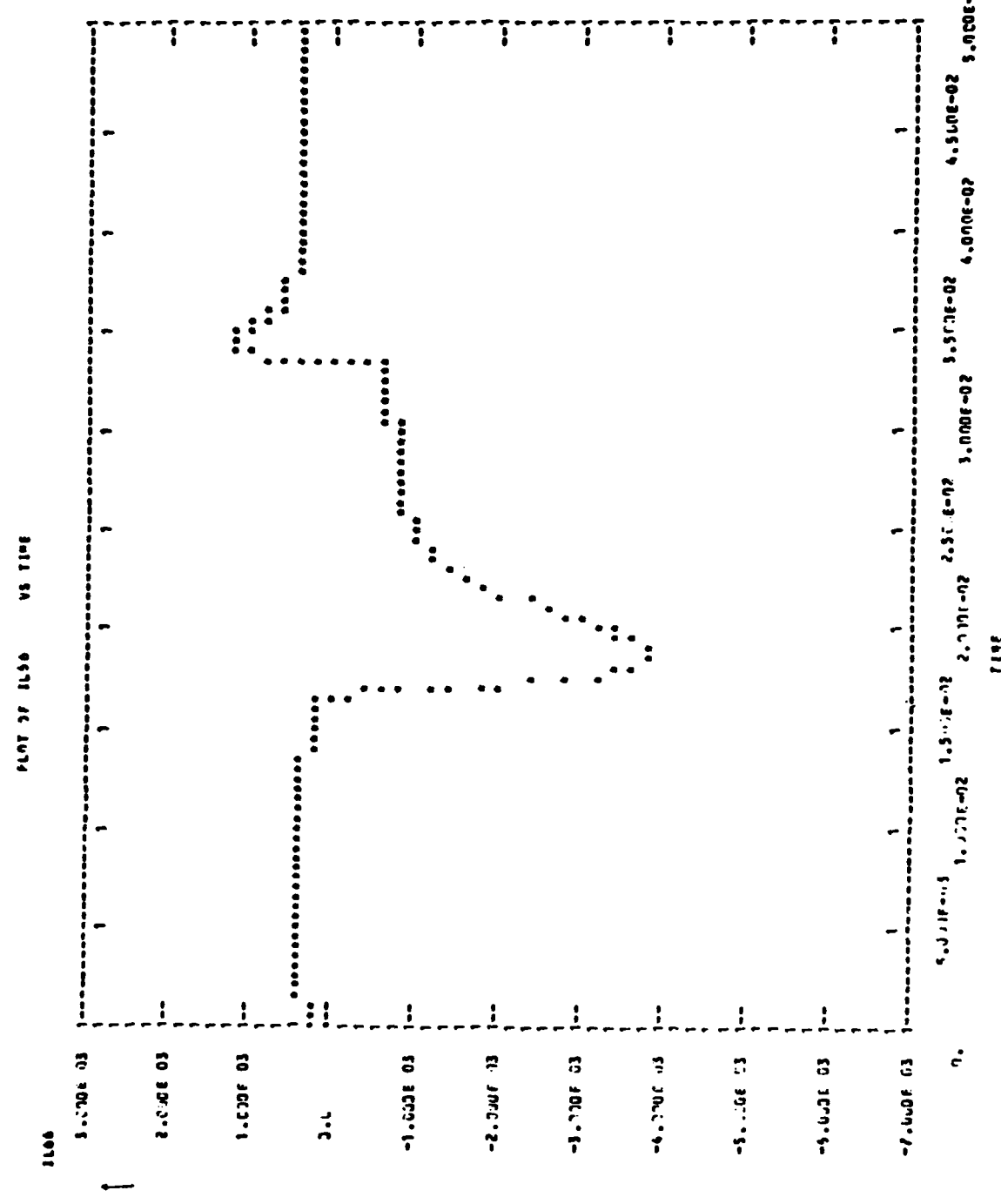


FIGURE 18. QUADRATURE AXIS DAMPER CURRENT FAULT CONDITIONS AS IN FIGURE 15.

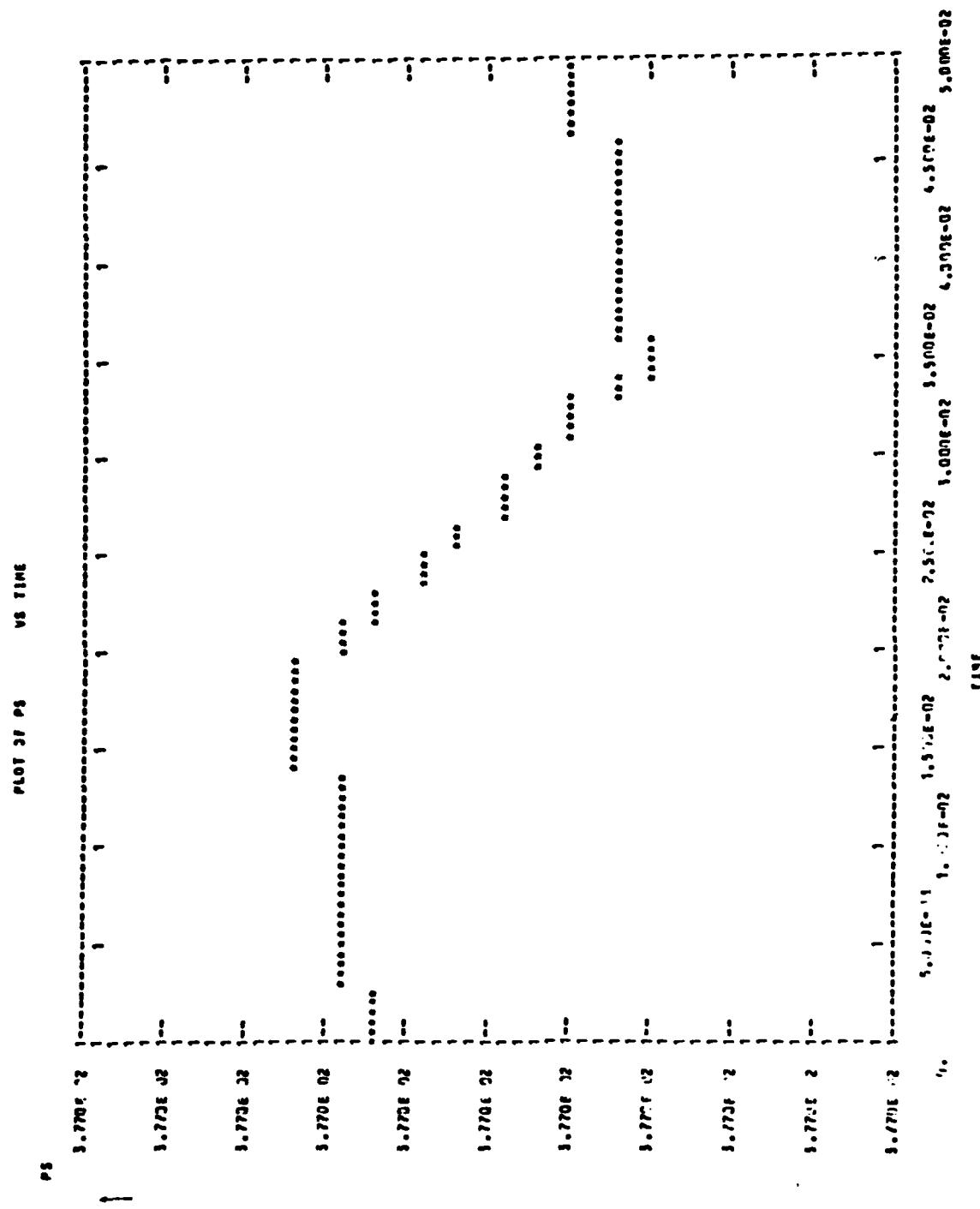


FIGURE 19. ROTOR SPEED FAULT CONDITIONS AS IN FIGURE 15.

APPENDIX A

THE GENERATOR MODEL

The purpose of this appendix is to establish the notation and address the approximations and assumptions in the generator model.

A.1 EQUIVALENT CIRCUIT EQUATIONS

Figure 20 shows the three phase generator equivalent circuit. The vector circuit equations are

$$V = RI + \frac{d\lambda}{dt} \quad (43)$$

where

$$V = [v_a, v_b, v_c, v_F, v_D, v_Q]^T \quad (44)$$

$$I = [i_a, i_b, i_c, i_F, i_D, i_Q]^T \quad (45)$$

$$\lambda = [\lambda_a, \lambda_b, \lambda_c, \lambda_F, \lambda_D, \lambda_Q]^T \quad (46)$$

$$R = \begin{bmatrix} r_a & & & & & \\ & r_b & & & & \\ & & r_c & & & \\ & & & r_F & & \\ & & & & r_D & \\ & & & & & r_Q \end{bmatrix} \quad (47)$$

and

v_a, v_b, v_c are the stator phase terminal voltages

v_F is the rotor field terminal voltage

v_D and v_Q are the damper winding terminal voltages

i_a, i_b, i_c are the stator phase currents

i_F is the rotor field current

i_D and i_Q are the direct and quadrature damper field currents

$\lambda_a, \lambda_b, \lambda_c, \lambda_F, \lambda_D, \lambda_Q$ are the circuit flux linkages with the subscripts referring to the same circuits as for V and I .

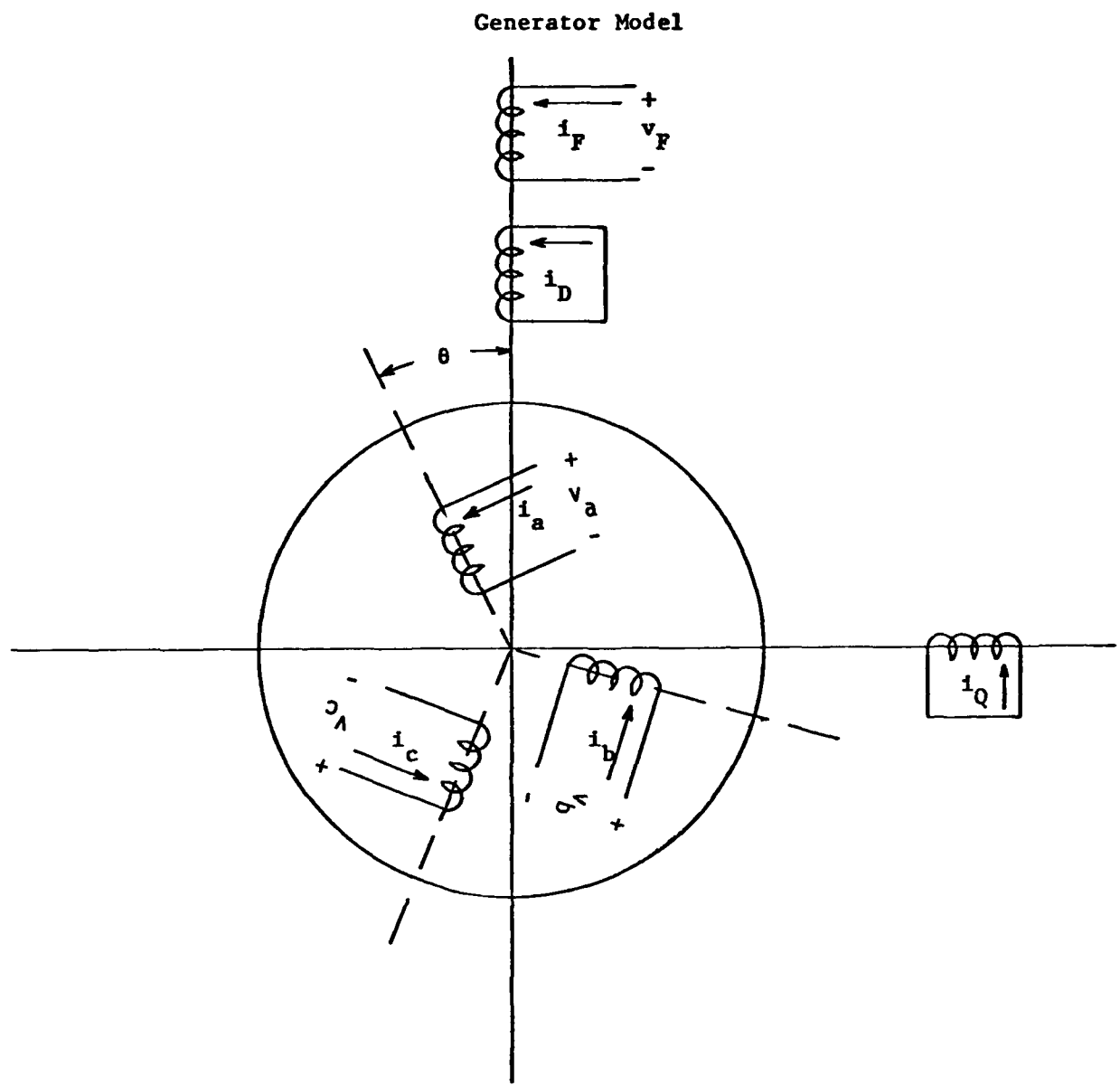


FIGURE 20. IDEALIZED CIRCUIT MODEL OF A THREE-PHASE GENERATOR

In terms of inductances Equation (43) can be written

$$V = RI + \frac{d}{dt} (LI) \quad (48)$$

with the flux linkages defined by

$$\begin{bmatrix} \lambda_a \\ \lambda_b \\ \lambda_c \\ \lambda_F \\ \lambda_D \\ \lambda_Q \end{bmatrix} = \begin{bmatrix} L_{aa} & L_{ab} & L_{ac} & L_{aF} & L_{aD} & L_{aQ} \\ L_{ba} & L_{bb} & L_{bc} & L_{bF} & L_{bD} & L_{bQ} \\ L_{ca} & L_{cb} & L_{cc} & L_{cF} & L_{cD} & L_{cQ} \\ L_{Fa} & L_{Fb} & L_{Fc} & L_{FF} & L_{FD} & L_{FQ} \\ L_{Da} & L_{Db} & L_{Dc} & L_{DF} & L_{DD} & L_{DQ} \\ L_{Qa} & L_{Qb} & L_{Qc} & L_{QF} & L_{QD} & L_{QQ} \end{bmatrix} \begin{bmatrix} i_a \\ i_b \\ i_c \\ i_F \\ i_D \\ i_Q \end{bmatrix} \quad (49)$$

Some approximations and assumptions are implied in the choice of the inductance terms used. These involve the space distribution of the air gap flux and the resulting variation of inductance with rotor position. The inductances are given by the following:

$$L_{aa} = L_s + L_m \cos(2\theta)$$

$$L_{bb} = L_s + L_m \cos 2(\theta - \frac{2\pi}{3})$$

$$L_{cc} = L_s + L_m \cos 2(\theta + \frac{2\pi}{3})$$

$$L_{ab} = -M_s - L_m \cos 2(\theta + \frac{\pi}{3}) = L_{ba}$$

$$L_{bc} = -M_s - L_m \cos 2(\theta - \frac{\pi}{3}) = L_{cb}$$

$$L_{ca} = -M_s - L_m \cos 2(\theta + \frac{5\pi}{3}) = L_{ca}$$

$$\begin{aligned}
L_{aF} &= M_F \cos(\theta) & = L_{Fa} \\
L_{bF} &= M_F \cos(\theta - \frac{2\pi}{3}) & = L_{Fb} \\
L_{cF} &= M_F \cos(\theta + \frac{2\pi}{3}) & = L_{Fc} \\
L_{aD} &= M_D \cos(\theta) & = L_{Da} \\
L_{bD} &= M_D \cos(\theta - \frac{2\pi}{3}) & = L_{Db} \\
L_{cD} &= M_D \cos(\theta + \frac{2\pi}{3}) & = L_{Dc} \\
L_{aQ} &= M_Q \sin(\theta) & = L_{Qa} \\
L_{bQ} &= M_Q \sin(\theta - \frac{2\pi}{3}) & = L_{Qb} \\
L_{cQ} &= M_Q \sin(\theta + \frac{2\pi}{3}) & = L_{Qc} \\
L_{FF} &= L_F \\
L_{DD} &= L_D \\
L_{QQ} &= L_Q \\
L_{FD} &= M_R = L_{DF} \\
L_{FQ} &= 0 = L_{QF} \\
L_{DQ} &= 0 = L_{QD} \tag{50}
\end{aligned}$$

Figure 21 defines the rotor angle, θ used in the inductance expressions

$$\theta(t) = \omega t \tag{51}$$

A.2 SATURATION EFFECTS

References 3, 5, 6 show curves of the inductance variation with rotor position, θ , similar to the curves of Figure 22. Kimbark (Reference 5) and Anderson (Reference 6) use the same equation form as used here in Equation (50). Smith (Reference 3) uses an L_{aa} of the form

$$L_{aa} = L_s + L_{m2} \cos(2\theta) + C_{m4} \cos(4\theta) \tag{52}$$

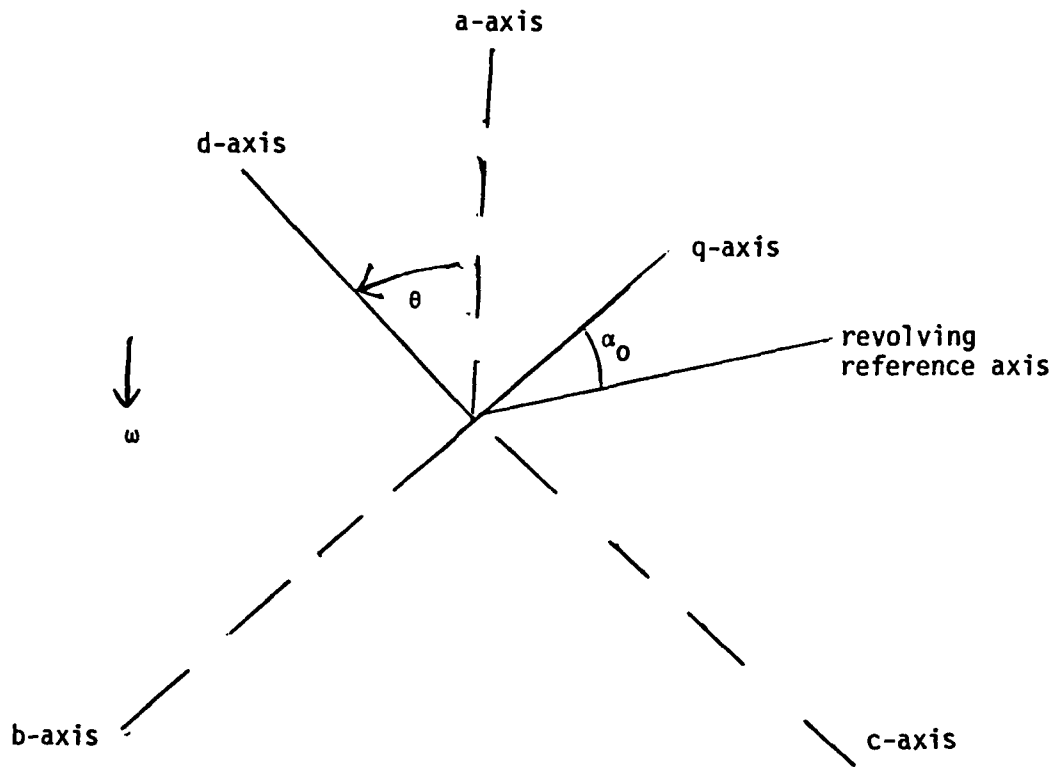


FIGURE 21. CONVENTION FOR DEFINING ROTOR POSITION

the fourth harmonic being due to a third harmonic in the space distribution of the air gap flux. Smith further states that this fourth harmonic is the highest significant harmonic observed over many tests.

The simpler model of Equations (50) was used here for various reasons. First, the inductance model of Equations (50) is a generally accepted model and it is simpler than Smith (Reference 4). This becomes significant when the non-linear terms of $\frac{\partial L}{\partial i}$ are expanded.

Secondly, it is clear that the third harmonic in the flux space distribution is evidence of the peaks of the wave being flattened. This effect is due to saturation effects or is at least analogous to saturation effects and saturation effects in our model are being accounted for by direct measurements.

In this work saturation is taken into account by assuming the shape of the curve of inductance variation with θ will not change but the inductance coefficients in the equation change. For example the saturated L_{aa} becomes L_{aas}

$$\begin{aligned} L_{aas} &= C_{aa} L_{aa} = \\ &= C_{aa} L_s + C_{aa} L_m \cos(2\theta) \end{aligned} \quad (53)$$

Where the C_{aa} is obtained from a measured curve showing the variation of L_{aa} as a function of a net excitation, i_x , of the magnetic circuit.

It is clear that more saturation gives a larger third harmonic in the flux space distribution and hence also changes the shape of the inductance curves of Figure 22. According to Smith (Reference 4) this changes the relative amplitude of the fourth harmonic compared to the second. Smith computes his saturated L_{aas} as follows.

$$L_{aas} = L_{s1} + (1 + \frac{K}{3}) \frac{L_d C_{aa} - L_q}{2} \cos(2\theta) + \frac{K}{3} \frac{L_d C_{aa} + L_q}{2} \cos(4\theta) \quad (54)$$

where

L_d is the direct axis inductance

L_q is the quadrature axis inductance

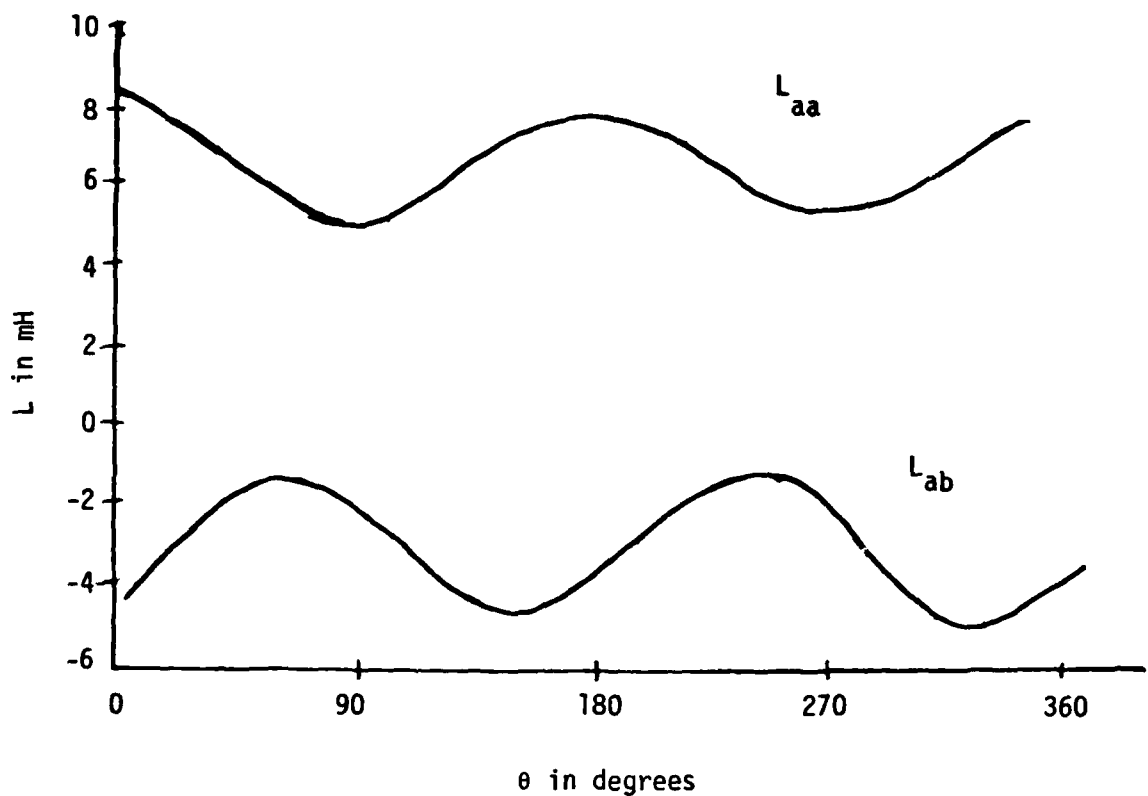


Figure 22. VARIATION OF INDUCTANCE WITH θ

K is the decimal fraction of third harmonic to fundamental flux

$$L_{s1} = \frac{L_d C_{aa} + L_q}{2}$$

The Equation (54) formula assumes saturation effects on the direct axis and no saturative effects on the quadrature axis which seems reasonable for a salient pole machine. Smith does not refer to the fact that K is a function of saturation.

While the Smith formulation Equation (54) does address the fact that saturation would affect the shape of the $L_{aa}(\theta)$ curve it is quite complex and it is not clear that it would give better results than Equation (53) with measured C_{aa} since it does include several assumptions and approximations.

This is an area that may be worthy of further investigation if the computer simulation results do not match observations adequately.

A.3 THE TORQUE EQUATION

The equation relating electrical circuit quantities to mechanical rotation quantities is

$$\frac{d^2\theta}{dt^2} = \frac{1}{J} [T_m - T_e - B \frac{d\theta}{dt}] \quad (55)$$

where

J is the polar moment of inertia of the rotating parts

B represents rotational losses and may include viscous damping and possibly core losses related to rotational speed.

T_m is the mechanical torque input at the shaft

T_e is the so called electric torque developed.

The electrical torque developed is given by the expression

$$T_e = \frac{1}{2} [I] T \left[\frac{\partial L}{\partial \theta} \right] [I] \quad (56)$$

The circuit model and Equations (55) and (56) do not include any eddy current or hysteresis loss effects.

These losses are sometimes considered as rotational losses and the B in Equation (55) is adjusted to include them. It is quite common to neglect both the core losses and the viscous damping and omit the B term.

APPENDIX B
SATURATED GENERATOR MODEL

B.1 SATURATED GENERATOR EQUATIONS

Section II of this report discusses the effects of saturation on the network model. Equations (12) and (13) illustrate the phase "a" equation development. This section shows more detail in the phase "a" equation and also lists the equations for the other phases.

This development is based on the expansion of Equation (43) and (48) of Appendix A. From these we write

$$\frac{d\lambda}{dt} = \frac{d}{dt} (LI) \quad (57)$$

or

$$\frac{d\lambda}{dt} = L \frac{dI}{dt} + \left(\frac{dL}{dt} \right) I \quad (58)$$

The expansion of the matrix products gives as the first row of Equation (58)

$$\begin{aligned} \frac{d\lambda_a}{dt} &= L_{aa} \frac{di_a}{dt} + L_{ab} \frac{di_b}{dt} + L_{ac} \frac{di_c}{dt} + L_{aF} \frac{di_D}{dt} \\ &+ L_{aQ} \frac{di_Q}{dt} + \frac{dL_{aa}}{dt} i_a + \frac{dL_{ab}}{dt} i_b + \frac{dL_{ac}}{dt} i_c + \frac{dL_{aF}}{dt} i_F \\ &+ \frac{dL_{aD}}{dt} i_D + \frac{dL_{aQ}}{dt} i_Q \end{aligned} \quad (59)$$

Saturation effects on the first six terms on the right hand side of Equation (59) are as shown in Appendix A Equation (53).

The development of the one derivative term $\frac{dL_{aa}}{dt}$ is shown in Equation (12). The complete set of terms for $\frac{d\lambda_a}{dt}$ is now listed

$$\begin{aligned} \frac{d\lambda_a}{dt} &= \left[N_{Fa} \cos(\theta) i_a \frac{\partial L_{aa}}{\partial i_x} \right] \frac{\partial i_a}{\partial t} + \left[N_{Fa} \cos(\theta - \frac{2\pi}{3}) i_a \frac{\partial L_{aa}}{\partial i_x} \right] \frac{\partial i_b}{\partial t} \\ &+ \left[N_{Fa} \cos(\theta + \frac{2\pi}{3}) i_a \frac{\partial L_{aa}}{\partial i_x} \right] \frac{\partial i_c}{\partial t} + \left[i_a \frac{\partial L_{aa}}{\partial i_x} \right] \frac{\partial i_F}{\partial t} + \left[N_{FD} i_a \frac{\partial L_{aa}}{\partial i_x} \right] \frac{\partial i_D}{\partial t} \end{aligned}$$

$$- \left[N_{Fa} i_a \frac{\partial L_{aa}}{\partial i_x} (i_a \sin(\theta) + i_b \sin(\theta - \frac{2\pi}{3}) + i_c \sin(\theta + \frac{2\pi}{3})) + i_a 2C_{aa} L_m \sin 2\theta \right] \frac{\partial \theta}{\partial t}$$

$$+ \left[N_{Fa} \cos(\theta) i_b \frac{\partial L_{ab}}{\partial i_x} \right] \frac{\partial i_a}{\partial t} + \left[N_{Fa} \cos(\theta - \frac{2\pi}{3}) i_b \frac{\partial L_{ab}}{\partial i_x} \right] \frac{\partial i_b}{\partial t}$$

$$+ \left[N_{Fa} \cos(\theta + \frac{2\pi}{3}) i_b \frac{\partial L_{ab}}{\partial i_x} \right] \frac{\partial i_c}{\partial t} + \left[i_b \frac{\partial L_{ab}}{\partial i_x} \right] \frac{\partial i_F}{\partial t} + \left[N_{FD} i_b \frac{\partial L_{ab}}{\partial i_x} \right] \frac{\partial i_D}{\partial t}$$

$$- \left[N_{Fa} i_b \frac{\partial L_{ab}}{\partial i_x} (i_a \sin(\theta) + i_b \sin(\theta - \frac{2\pi}{3}) + i_c \sin(\theta + \frac{2\pi}{3})) + i_b 2C_{aa} L_m \sin(2\theta - \frac{2\pi}{3}) \right] \frac{\partial \theta}{\partial t}$$

$$+ \left[N_{Fa} \cos(\theta) i_c \frac{\partial L_{ac}}{\partial i_x} \right] \frac{\partial i_a}{\partial t} + \left[N_{Fa} \cos(\theta - \frac{2\pi}{3}) i_c \frac{\partial L_{ac}}{\partial i_x} \right] \frac{\partial i_b}{\partial t}$$

$$+ \left[N_{Fa} \cos(\theta + \frac{2\pi}{3}) i_c \frac{\partial L_{ac}}{\partial i_x} \right] \frac{\partial i_c}{\partial t} + \left[i_c \frac{\partial L_{ac}}{\partial i_x} \right] \frac{\partial i_F}{\partial t} + \left[N_{FD} i_c \frac{\partial L_{ac}}{\partial i_x} \right] \frac{\partial i_D}{\partial t}$$

$$- \left[N_{Fa} i_c \frac{\partial L_{ac}}{\partial i_x} (i_a \sin(\theta) + i_b \sin(\theta - \frac{2\pi}{3}) + i_c \sin(\theta + \frac{2\pi}{3})) + i_c 2C_{aa} L_m \sin(2\theta - \frac{2\pi}{3}) \right] \frac{\partial \theta}{\partial t}$$

$$+ \left[N_{Fa} \cos(\theta) i_F \frac{\partial L_{aF}}{\partial i_x} \right] \frac{\partial i_a}{\partial t} + \left[N_{Fa} \cos(\theta - \frac{2\pi}{3}) i_F \frac{\partial L_{aF}}{\partial i_x} \right] \frac{\partial i_b}{\partial t}$$

$$+ \left[N_{Fa} \cos(\theta + \frac{2\pi}{3}) i_F \frac{\partial L_{aF}}{\partial i_x} \right] \frac{\partial i_c}{\partial t} + \left[i_F \frac{\partial L_{aF}}{\partial i_x} \right] \frac{\partial i_F}{\partial t} + \left[N_{FD} i_F \frac{\partial L_{aF}}{\partial i_x} \right] \frac{\partial i_D}{\partial t}$$

$$- \left[N_{Fa} i_F \frac{\partial L_{aF}}{\partial i_x} (i_a \sin(\theta) + i_b \sin(\theta - \frac{2\pi}{3}) + i_c \sin(\theta + \frac{2\pi}{3})) + i_F C_{aF} M_{aF} \sin(\theta) \right] \frac{\partial \theta}{\partial t}$$

$$\begin{aligned}
& + \left[N_{Fa} \cos(\theta) i_D \frac{\partial L_{aD}}{\partial i_x} \right] \frac{\partial i_a}{\partial t} + \left[N_{Fa} (\cos \theta - \frac{2\pi}{3}) i_D \frac{\partial L_{aD}}{\partial i_x} \right] \frac{\partial i_b}{\partial t} \\
& + \left[N_{Fa} \cos(\theta + \frac{2\pi}{3}) i_D \frac{\partial L_{aD}}{\partial i_x} \right] \frac{\partial i_c}{\partial t} + \left[i_D \frac{\partial L_{aD}}{\partial i_x} \right] \frac{\partial i_F}{\partial t} + \left[N_{FD} i_D \frac{\partial L_{aD}}{\partial i_x} \right] \frac{\partial i_D}{\partial t} \\
& - \left[N_{Fa} i_D \frac{\partial L_{aD}}{\partial i_x} (i_a \sin(\theta) + i_b \sin(\theta - \frac{2\pi}{3}) + i_c \sin(\theta + \frac{2\pi}{3})) \right. \\
& \quad \left. + i_D C_{aD} M_{aD} \sin \theta \right] \frac{\partial \theta}{\partial t} \\
& + \left[N_{Fa} \cos(\theta) i_Q \frac{\partial L_{aQ}}{\partial i_x} \right] \frac{\partial i_a}{\partial t} + \left[N_{Fa} \cos(\theta - \frac{2\pi}{3}) i_Q \frac{\partial L_{aQ}}{\partial i_x} \right] \frac{\partial i_b}{\partial t} \\
& + \left[N_{Fa} (\cos \theta + \frac{2\pi}{3}) i_Q \frac{\partial L_{aQ}}{\partial i_x} \right] \frac{\partial i_c}{\partial t} + \left[i_Q \frac{\partial L_{aQ}}{\partial i_x} \right] \frac{\partial i_F}{\partial t} + \left[N_{FD} i_Q \frac{\partial L_{aQ}}{\partial i_x} \right] \frac{\partial i_D}{\partial t} \\
& - \left[N_{Fa} i_Q \frac{\partial L_{aQ}}{\partial i_x} (i_a \sin(\theta) + i_b \sin(\theta - \frac{2\pi}{3}) + i_c \sin(\theta + \frac{2\pi}{3})) \right. \\
& \quad \left. - i_Q C_{aQ} M_{aQ} \cos(\theta) \right] \frac{\partial \theta}{\partial t} \\
& + L_{aa} \frac{di_a}{dt} + L_{ab} \frac{di_b}{dt} + L_{ac} \frac{di_c}{dt} + L_{aF} \frac{di_F}{dt} + L_{aD} \frac{di_D}{dt} + L_{aQ} \frac{di_Q}{dt} \quad (60)
\end{aligned}$$

To make the expression appear less formidable the following terms are defined,

$$A_a = i_a \frac{\partial L_{aa}}{\partial i_x} + i_b \frac{\partial L_{ab}}{\partial i_x} + i_c \frac{\partial L_{ac}}{\partial i_x} + i_F \frac{\partial L_{aF}}{\partial i_x} + i_D \frac{\partial L_{aD}}{\partial i_x} + i_Q \frac{\partial L_{aQ}}{\partial i_x} \quad (61)$$

$$B_a = N_{Fa} \left[i_a \sin(\theta) + i_b \sin(\theta - \frac{2\pi}{3}) + i_c \sin(\theta + \frac{2\pi}{3}) \right], \quad (62)$$

$$\text{and } C_a = 2C_{aa} L_m \left[i_a \sin(2\theta) + i_b \sin(2\theta - \frac{2\pi}{3}) + i_c \sin(\theta + \frac{2\pi}{3}) \right] \quad (63)$$

The voltage generated in phase "a" can now be written more compactly as

$$\begin{aligned}
 \frac{d\lambda_a}{dt} = & \left[A_a N_{Fa} \cos(\theta) + C_{aa}(L_s + L_m \cos(2\theta)) \right] \frac{di_a}{dt} \\
 & + \left[A_a N_{Fa} \cos(\theta - \frac{2\pi}{3}) + C_{aa}(-M_s + L_m \cos(2\theta - \frac{2\pi}{3})) \right] \frac{di_b}{dt} \\
 & + \left[A_a N_{Fa} \cos(\theta + \frac{2\pi}{3}) + C_{aa}(-M_s + L_m \cos(2\theta + \frac{2\pi}{3})) \right] \frac{di_c}{dt} \\
 & + \left[A_a + C_{aF} M_{aF} \cos(\theta) \right] \frac{di_F}{dt} - \left[A_a N_{FD} + C_{aD} M_{aD} \cos(\theta) \right] \frac{di_D}{dt} \\
 & - C_{aQ} M_{aQ} \sin(\theta) \frac{di_Q}{dt} \\
 & - \left[B_a A_a + C_a + (i_F C_{aF} M_{aF} + i_D C_{aD} M_{aD}) \sin(\theta) - i_Q C_{aQ} M_{aQ} \cos(\theta) \right] \frac{d\theta}{dt} \quad (64)
 \end{aligned}$$

For the other generator circuits the results are now listed

$$\begin{aligned}
 \frac{d\lambda_b}{dt} = & \left[A_b N_{Fa} \cos(\theta) - C_{aa} M_s + C_{aa} L_m \cos(2\theta - \frac{2\pi}{3}) \right] \frac{di_a}{dt} \\
 & + \left[A_b N_{Fa} \cos(\theta - \frac{2\pi}{3}) + C_{aa} L_s + C_{aa} L_m \cos(2\theta + \frac{2\pi}{3}) \right] \frac{di_b}{dt} \\
 & + \left[A_b N_{Fa} \cos(\theta + \frac{2\pi}{3}) - C_{aa} M_s - C_{aa} L_m \cos(2\theta) \right] \frac{di_c}{dt} \\
 & + \left[A_b + C_{aF} M_{aF} \cos(\theta - \frac{2\pi}{3}) \right] \frac{di_F}{dt} \\
 & + \left[A_b N_{FD} + C_{aD} M_{aD} \cos(\theta - \frac{2\pi}{3}) \right] \frac{di_D}{dt} \\
 & + \left[C_{aQ} M_{aQ} \sin(\theta - \frac{2\pi}{3}) \right] \frac{di_Q}{dt} \\
 & - \left[A_b B + 2C_b C_{aa} L_m + (C_{aF} M_{aF} i_F + C_{aD} M_{aD} i_D) \sin(\theta - \frac{2\pi}{3}) \right. \\
 & \quad \left. - C_{aQ} M_{aQ} i_Q \cos(\theta - \frac{2\pi}{3}) \right] \frac{d\theta}{dt} \quad (65)
 \end{aligned}$$

where

$$A_b = i_a \frac{\partial L_{ba}}{\partial i_x} + i_b \frac{\partial L_{bb}}{\partial i_x} + i_c \frac{\partial L_{bc}}{\partial i_x} + i_F \frac{\partial L_{bF}}{\partial i_x} + i_D \frac{\partial L_{bD}}{\partial i_x} + i_Q \frac{\partial L_{bQ}}{\partial i_x} \quad (66)$$

$$C_b = i_a \sin(2\theta - \frac{2\pi}{3}) + i_b \sin(2\theta + \frac{2\pi}{3}) + i_c \sin(2\theta) \quad (67)$$

$$\begin{aligned} \frac{d\lambda_c}{dt} = & \left[A_c N_{Fa} \cos(\theta) - C_{aa} M_s + C_{aa} L_m \cos(2\theta + 120) \right] \frac{di_a}{dt} \\ & + \left[A_c N_{Fa} \cos(\theta - 120) - C_{aa} M_s + C_{aa} L_m \cos(2\theta) \right] \frac{di_b}{dt} \\ & + \left[A_c N_{Fa} \cos(\theta + 120) - C_{aa} L_s + C_{aa} L_m \cos(2\theta - 120) \right] \frac{di_c}{dt} \\ & + \left[A_c + C_{aF} M_{aF} \cos(\theta + 120) \right] \frac{di_F}{dt} \\ & + \left[A_c N_{FD} + C_{aD} M_{aD} \cos(\theta + 120) \right] \frac{di_D}{dt} \\ & + \left[C_{aQ} M_{aQ} + \sin(\theta + 120) \right] \frac{di_Q}{dt} \\ & - \left[A_c B + 2 C_c C_{aa} L_m + (C_{aF} M_{aF} i_F + C_{aD} M_{aD} i_D) \sin(\theta + 120) \right. \\ & \quad \left. - M_{aQ} i_Q \cos(\theta + 120) \right] \frac{d\theta}{dt} \quad (68) \end{aligned}$$

Where $A_c = i_a \frac{\partial L_{ca}}{\partial i_x} + i_b \frac{\partial L_{cb}}{\partial i_x} + i_c \frac{\partial L_{cc}}{\partial i_x} + i_F \frac{\partial L_{cF}}{\partial i_x} + i_D \frac{\partial L_{cD}}{\partial i_x} + L_Q \frac{\partial L_{cQ}}{\partial i_x} \quad (69)$

$$C_c = i_a \sin(2\theta + 120) + i_b \sin(2\theta) + i_c \sin(2\theta - 120) \quad (70)$$

$$\begin{aligned} \frac{d\lambda_F}{dt} = & \left[A_F N_{Fa} \cos(\theta) + C_{aF} M_{aF} \cos(\theta) \right] \frac{di_a}{dt} \\ & + \left[A_F N_{Fa} \cos(\theta - 120) + C_{aF} M_{aF} \cos(\theta - 120) \right] \frac{di_b}{dt} \end{aligned}$$

$$\begin{aligned}
& + \left[A_F N_{Fa} \cos(\theta + 120) + C_{aF} M_{aF} \cos(\theta + 120) \right] \frac{\partial i_c}{\partial t} \\
& + \left[A_F + C_{FF} L_F \right] \frac{\partial i_F}{\partial t} \\
& + \left[A_F N_{FD} + C_{FD} M_R \right] \frac{\partial i_D}{\partial t} \\
& - \left[B A_F - C_F C_{aF} M_{aF} \right] \frac{\partial \theta}{\partial t}
\end{aligned} \tag{71}$$

where $A_F = i_a \frac{\partial L_{Fa}}{\partial i_x} + i_b \frac{\partial L_{Fb}}{\partial i_x} + i_c \frac{\partial L_{Fc}}{\partial i_x} + i_F \frac{\partial L_{FF}}{\partial i_x} + i_D \frac{\partial L_{FD}}{\partial i_x}$ (72)

$$C_F = i_a \sin(\theta) + i_b \sin(\theta - 120) + i_c \sin(\theta + 120) \tag{73}$$

$$\begin{aligned}
\frac{d\lambda_D}{dt} = & \left[A_D N_{Fa} \cos \theta + C_{aD} M_{aD} \cos(\theta) \right] \frac{di_a}{dt} \\
& + \left[A_D N_{Fa} \cos(\theta - 120) + C_{aD} M_{aD} \cos(\theta - 120) \right] \frac{di_b}{dt} \\
& + \left[A_D N_{Fa} \cos(\theta + 120) + C_{aD} M_{aD} \cos(\theta + 120) \right] \frac{di_c}{dt} \\
& + \left[A_D + C_{FD} M_R \right] \frac{di_F}{dt} \\
& + \left[N_{FD} A_D + C_{DD} L_D \right] \frac{di_D}{dt} \\
& - \left[B A_D + C_{aD} M_{aD} C_D \right] \frac{d\theta}{dt}
\end{aligned} \tag{74}$$

where $A_D = i_a \frac{\partial L_{Da}}{\partial i_x} + i_b \frac{\partial L_{Db}}{\partial i_x} + i_c \frac{\partial L_{Dc}}{\partial i_x} + i_F \frac{\partial L_{DF}}{\partial i_x} + i_D \frac{\partial L_{DD}}{\partial i_x}$ (75)

$$C_D = i_a \sin(\theta) + i_b \sin(\theta - 120) + i_c \sin(\theta + 120) \tag{76}$$

$$\begin{aligned}
 \frac{d\lambda_Q}{dt} = & \left[C_{aQ} M_{aQ} \sin(\theta) \right] \frac{\partial i_a}{\partial t} \\
 & + \left[C_{aQ} M_{aQ} \sin(\theta - 120) \right] \frac{\partial i_b}{\partial t} \\
 & + \left[C_{aQ} M_{aQ} \sin(\theta + 120) \right] \frac{\partial i_c}{\partial t} \\
 & + \left[L_Q \right] \frac{\partial i_Q}{\partial t} \\
 & + \left[C_Q M_{aQ} \right] \frac{\partial \theta}{\partial t}
 \end{aligned} \tag{77}$$

where $C_Q = i_a \cos(\theta) + i_b \cos(\theta - 120) + i_c \cos(\theta + 120)$ (78)

APPENDIX C

GENERATOR DATA USED

Considerable difficulty was encountered in obtaining data for machine model. Data were needed to test the model performance. Some data were supplied by the Air Force through technical publications AFAPL-TR-75-87 and AFAPL-TR-77-31. In both publications the data were incomplete even for a fairly standard model. In one of the publications the data purported to have been used was inconsistent in the sense that it gave mutual inductance with coefficients of coupling that were greater than unity. This problem was identified after spending considerable time and effort and having several unsuccessful computer runs. Further, neither of the above reports contained any useful saturation data. The needed data is not available currently.

C.1 UNSATURATED GENERATOR DATA

In order to have data for a real machine and move forward with the simulation, data were taken for a machine from Reference 6. No usable saturation data were available from this reference. Saturation conditions were simulated using trend curves from Reference 3.

The machine data used are listed below. These are unsaturated values.

Balanced three phase 60 Hz Generator

$$L_s = 4.152 \text{ mH}$$

$$L_m = 0.074 \text{ mH}$$

$$L_F = 2.189 \text{ H}$$

$$L_D = 5.989 \text{ mH}$$

$$L_Q = 1.423 \text{ mH}$$

$$M_s = 2.076 \text{ mH}$$

$$M_F = 89.006 \text{ mH}$$

$$M_D = 4.721 \text{ mH}$$

$$M_Q = 2.269 \text{ mH}$$

$$M_R = 0.108994 \text{ H}$$

Rated Power 160 MVA

Rated Voltage 15 KV (line to line)

Inertia Constant H = 2.37 sec.

$$R_a = 0.001542 \Omega$$

$$R_F = 0.371 \Omega$$

$$R_D = 0.018421 \Omega$$

$$R_Q = 0.018969 \Omega$$

rated field excitation voltage = 375 volts

C.2 SATURATION DATA

The additional data required for the model are saturation data. It will be necessary to measure or determine in some other manner this saturation data for the specific machine being modeled. Measurement methods are discussed briefly in subsequent paragraphs.

For the purpose of obtaining numbers for the machine model used to test the computer model, curve data were used from Smith and Snider (Reference 3,4). These curves were normalized and applied to the above machine data. The premise in measurement of this saturation data is that saturation is dependent on some net equivalent field excitation

$$i_x = i_F + N_{FD} i_D + N_{Fa} \left[i_a \cos(\theta) + i_b \cos(\theta - \frac{2\pi}{3}) + i_c \cos(\theta + \frac{2\pi}{3}) \right] \quad (79)$$

The excitation level can be obtained by varying only i_F . The incremental inductances are obtained by perturbing the various other currents, say Δi_a , for incremental L_{aa} . Integrated incremental inductances give saturated inductances. Thus a plot of L_{aa} versus i_F with $\theta = 0$ gives appropriate saturation data for the "a" phase self inductance. Data for the plot of L_{aa} vs i_F is normalized and put into an algebraic equation form using a least square regression analysis. The following form is obtained from the L_{aa} versus i_F data

$$C_{aa} = a_{10} + a_{11} i_x + a_{12} i_x^2 + a_{13} i_x^3 \quad (80)$$

Saturation data must be determined for L_{aa} , L_{aF} , L_{DD} , L_{aD} , L_{FD} . From these the regression coefficients for the C's are found: C_{aa} , C_{FF} , C_{DD} , C_{aF} , C_{AD} , C_{aQ} , C_{FD} .

Table 2 lists the coefficients used in the simulation. These were obtained by reading data from curves given by Smith and Snider (Reference 3) and are not necessarily correct or typical for the machine used here. The ballistic method described in Snider and Smith (Reference 3,4) permits the measurement of saturated incremental inductances. These are integrated into the saturated inductance curves.

C.3 MEASUREMENT OF THE UNSATURATED INDUCTANCES

1. L_s and L_m

With the rotor locked into position ($\theta = 0^\circ$), measure the inductance of phase A of the stator. The measured inductance is $L_s + L_m$. Rotate the rotor and lock into position ($\theta = 45^\circ$). Measure the inductance of phase A of the stator. The measured inductance is L_s .

Rotate the rotor and lock into position ($\theta = 90^\circ$). Measure the inductance of phase A of the stator. The measured value is $L_s - L_m$. Compare all measured values.

TABLE 2. SATURATION COEFFICIENTS

	a_{j0}	a_{j1}	a_{j2}	a_{j3}
aa	0.98367	-2.9246×10^{-5}	-1.0771×10^{-7}	2.0394×10^{-11}
FF	1.0088	-2.9867×10^{-5}	-1.0519×10^{-7}	1.8699×10^{-11}
DD	0.97827	-2.1569×10^{-5}	-7.9586×10^{-8}	1.5930×10^{-11}
AF	1.0000	-6.9202×10^{-5}	-8.4819×10^{-8}	1.6303×10^{-11}
AD	0.9886	-8.0120×10^{-5}	-6.1443×10^{-8}	1.2983×10^{-11}
AQ	0.99419	-2.6322×10^{-5}	-5.5511×10^{-8}	1.0182×10^{-11}
DF	1.0007	-6.9355×10^{-5}	-6.6663×10^{-8}	1.3054×10^{-11}

$$C_{xx} = a_{j0} + a_{j1} i_x + a_{j2} i_x^2 + a_{j3} i_x^3$$

2. L_s and M_s

With the rotor locked into position ($\theta = 105^\circ$), connect a sinusoidal voltage source between phase A and neutral of the stator. Measure the RMS current flow in phase A. Measure the resultant RMS voltage induced between phase B and neutral. The mutual inductance between phase A and Phase B is computed as

$$-M_s = \frac{V_{b-N}(\text{RMS})}{\omega I_a(\text{RMS})} .$$

where ω is the radian frequency of the phase A current. The quantity M_s should be positive and should be smaller than L_s .

With the rotor locked into position ($\theta = 60^\circ$), measure V_{b-N} and I_a as before. The result yields $L_m - M_s$. With the rotor locked into position ($\theta = 150^\circ$), measure V_{b-N} and I_a as before. Calculation results in $-M_s - L_m$. Compare values of M_s .

3. L_F

Measure the field coil inductance directly.

4. M_{aF}

With the rotor locked into position ($\theta = 0^\circ$), connect a sinusoidal voltage source between the field terminal connections. Measure the RMS current flow in the field coil. Measure the RMS voltage induced between phase A and neutral of the stator. Calculate M_{aF} .

$$M_{aF} = \frac{V_{a-N}(\text{RMS})}{\omega I_F(\text{RMS})} .$$

5. L_D , M_R , R_F , R_D

As measured from the field coil terminals,

$$Z_F = \frac{V_F(\text{RMS})}{I_F(\text{RMS})} = R + j\omega L$$

$$\begin{aligned}
 Z_F &= R_F + J\omega L_F + \frac{\omega^2 M_{DF}^2}{R_D + J\omega L_D} \\
 &= \left(R_F + \frac{\omega^2 R_D M_{DF}^2}{R_D^2 + \omega^2 L_D^2} \right) - J \left(\frac{\omega^3 M_{DF}^2 L_D}{R_D^2 + \omega^2 L_D^2} \right) \\
 &= R_F + R_e + J\omega(L_F + L_e)
 \end{aligned}$$

Measure the field coil resistance directly.

$$R_e = R - R_F$$

$$L_e = L - L_F$$

Assume a value of damper resistance R_D

$$M_{DF}^2 = \frac{R_e(R_D^2 + \omega^2 L_D^2)}{\omega^2 R_D^2}$$

$$L_D = -\frac{L_e R_D}{R_e}$$

Note that M_R and M_{FD} are the same parameter.

6. M_{aQ} , L_Q , R_A

As measured from phase A terminals,

$$Z_a = \frac{V_a(\text{RMS})}{I_a(\text{RMS})} = R + J\omega L, \quad Z_a = R_a + J\omega L_a + \frac{\omega^2 M_{aQ}^2}{R_Q + J\omega L_Q},$$

All measurements are taken with the rotor locked into position ($\theta = 90^\circ$)

$$\begin{aligned}
 Z_a &= \left(R_a + \frac{\omega^2 R_Q M_{aQ}^2}{R_Q^2 + \omega^2 L_Q^2} \right) - J \left(\frac{\omega^3 M_{aQ}^2 L_Q}{R_Q^2 + \omega^2 L_Q^2} \right) \\
 &= R_a + R_e + J\omega(L_a + L_e)
 \end{aligned}$$

Measure the phase A resistance directly.

$$R_e = R - R_a$$

$$L_e = L - L_a$$

Assume a value of quadrature damper resistance R_Q

$$L_Q = -\frac{L_e R_Q}{R_e}$$

$$M_{aQ}^2 = \frac{R_e (R_Q^2 + \omega^2 L_Q^2)}{\omega^2 R_Q^2}$$

7. M_{aD}

With the rotor locked into position ($\theta = 0^\circ$) and the field coil open,

$$Z_a = \frac{V_a (\text{RMS})}{I_a (\text{RMS})} = R + j\omega L$$

$$Z_a = R_a + j\omega L_a + \frac{\omega^2 M_{aD}^2}{R_D + j\omega L_D}$$

$$Z_a = \left(R_a + \frac{\omega^2 R_D M_{aD}^2}{R_D^2 + \omega^2 L_D^2} \right) - j \left(\frac{\omega M_{aD}^2 L_D}{R_D^2 + \omega^2 L_D^2} \right)$$

$$= R_a + R_e + j\omega(L_a + L_e)$$

$$R_e = R - R_a$$

$$R_e = L - L_a$$

$$L_D = -\frac{L_e R_D}{R_e} \quad (\text{compare values})$$

$$M_{aD}^2 = \frac{R_e (R_D^2 + \omega^2 L_D^2)}{\omega^2 L_D^2} .$$

APPENDIX D

THE SCEPTRE GENERATOR PROGRAM

D.1 INTRODUCTION

The following pages contain the listing of the SCEPTRE program for the generator model. The program is an implementation of the equations of Appendix B. The circuit diagram of phase "a" is shown in Figure 1.

It should be emphasized that this is a working program and not a finished product. Somewhat more efficient use of defined parameters will be necessary in a final program. Also, the particular outputs used are for program analysis purposes and not necessarily important in system simulation.

The first four pages contain the circuit model and the run controls. The last two pages contain FORTRAN subroutines used to compute the torque relationships and the nonlinear saturation effects.

D.2 Circuit Model

CIRCUIT DESCRIPTION

ELEMENTS

EF1, 134-0=PFV

RAL, 131-0=T1

RRL, 132-0=T1

RCL, 133-0=T1

RA, 1-11=PRP

RB, 2-12=PRP

RC, 3-13=PRP

P33, 13-23= EQUATION 3 (-1.,PLM,PM2P3,PCAA)

R22, 12-22= EQUATION 3 (-1.,PLM,P2P3,PCAA)

R11, 11-21= EQUATION 3 (-1.,PLM,0.0D0,PCAA)

RF, 4-14= PRF

RD, 5-15= PRD

RQ, 6-16= PRQ

E12, 21-31=EQUATION 3 (IL22,PLM,PM2P3,PCAA)

E13, 31-41=EQUATION 3 (IL33,PLM,P2P3,PCAA)

E14, 41-51=EQUATION 4 (IL44,PMAF,0.0D0,PCAF)

E15, 51-61=EQUATION 4 (IL55,PMAD,0.0D0,PCAD)

E16, 61-71=EQUATION 5 (IL66,PMAG,0.0D0,-1.0D,PCAQ)

E18, 71-91=EQUATION 11 (PC)FAA,PNFA,DL22,FM2P3)

E19, 91-101=EQUATION 11 (PCOFAA,PNFA,DL33,P2P3)

E101, 101-111=EQUATION 12 (-1.0D0,PCOFAA,1.0D0,DL44)

E111, 111-121=EQUATION 12 (-1.0D0,PCOFAA,PNFD,DL55)

E121, 121-131=EQUATION 12 (1.0D0,PCOFAA,PCOFBA,PS)

E21, 22-32=EQUATION 3 (IL11,PLM,PM2P3,PCAA)

E23, 32-42=EQUATION 3 (IL33,PLM,0.0D0,PCAA)

E24, 42-52=EQUATION 4 (IL44,PMAF,P42P3,PCAF)

E25, 52-62=EQUATION 4 (IL55,PMAD,P42P3,PCAD)

E26, 62-72=EQUATION 5 (IL66,PMAG,PM2P3,-1.0D,PCAQ)

E28, 72-92=EQUATION 11 (PC)FAE,PNFA,DL11,0.0D0)

E29, 92-102=EQUATION 11 (PCOFAB,PNFA,DL33,P2P3)

E102, 102-112=EQUATION 12 (-1.0D0,PCOFAB,1.0D0,DL44)

E112, 112-122=EQUATION 12 (-1.0D0,PCOFAB,PNFD,DL55)

E122, 122-132=EQUATION 12 (1.0D0,PCOFAB,PCOFBA,PS)

E31, 23-33=EQUATION 3 (IL11,PLM,P2P3,PCAA)

E32, 33-43=EQUATION 3 (IL22,PLM,0.0D0,PCAA)

E34, 43-53=EQUATION 4 (IL44,PMAF,P2F3,PCAF)

E35, 53-63=EQUATION 4 (IL55,PMAD,P2P3,PCAD)

E36, 63-73=EQUATION 5 (IL66,PMAG,P2F3,-1.0D,PCAQ)

E38, 73-93=EQUATION 11 (PCOFAC,FNFA,DL11,0.0D0)

E39, 93-103=EQUATION 11 (PCOFAC,PNFA,DL22,PM2P3)

E103, 103-113=EQUATION 12 (-1.0D0,PCOFAC,1.0D0,DL44)

E113, 113-123=EQUATION 12 (-1.0D0,PCOFAC,FNFD,DL55)

E123, 123-133=EQUATION 12 (1.0D0,PCOFAC,PCOFBA,PS)

E41, 14-24=EQUATION 4 (IL11,PMAF,0.0D0,PCAF)

E42, 24-34=EQUATION 4 (IL22,PMAF,P42P3,PCAF)

E43, 34-44=EQUATION 4 (IL33,PMAF,P2P3,PCAF)

E48, 44-94=EQUATION 11 (PCOFAF,FNFA,DL11,0.0D0)

E49, 94-104=EQUATION 11 (PCOFAF,PNFA,DL22,PM2P3)

E104, 104-114=EQUATION 11 (PCOFAF,PNFA,DL33,P2P3)

E114, 114-124=EQUATION 12 (-1.0D0,PCOFAF,PNFD,DL55)

E124, 124-134=EQUATION 12 (1.0D0,PCOFAF,PCOFBA,PS)

E51, 15-25=EQUATION 4 (IL11,PMAD,0.,PCAD)

E52, 25-35=EQUATION 4 (IL22,PMAD,P42P3,PCAD)

E53, 35-45=EQUATION 4 (IL33,PMAD,P2P3,PCAD)

E56, 45-95=EQUATION 11 (PCOFAD,FNFA,DL11,0.0D0)

E59, 95-105=EQUATION 11 (PCOFAD,PNFA,DL22,FM2P3)

E105, 105-115=EQUATION 11 (PCOFAD,PNFA,DL33,P2P3)

E115, 115-125=EQUATION 12 (-1.0D0,PCOFAD,1.0D0,DL44)

D.2 Circuit Model (Continued)

```

E125,125-C=EQUATION 12 (1.0D0,PCOFAD,PCOFBA,PS)
E61,16-26=EQUATION 5 (IL11,PMAQ,0.0,-1.0D0,PCAQ)
E62,26-36=EQUATION 5 (JL72,PM10,PM2P3,-1.0D0,PCAQ)
E63,36-0 =EQUATION 5 (IL33,PMAG,P2P3,-1.0D0,PCAQ)
RAD,131-0 = 1.0D4
RBD,132-0 = 1.0D4
RCD,133-0 = 1.0D4
M12,L11-L22=PM12
M13,L11-L33=PM13
M14,L11-L44=PM14
M15,L11-L55=PM15
M16,L11-L66=PM16
M23,L22-L33=PM23
M24,L22-L44=PM24
M25,L22-L55=PM25
M26,L22-L66=PM26
M34,L33-L44=PM34
M35,L33-L55=PM35
M36,L33-L66=PM36
M45,L44-L55=PM45
L11,0-1 =PL11
L22,0-2 =PL22
L33,0-3 =PL33
L44,0-4 =PL44
L55,0-5 =PL55
L66,0-6 =PL66
DEFINED PARAMETERS
P2P3=2.0943951024DC
PM2P3=-2.0943951024DD
PRQ=18.969D-3
PRD=18.421D-3
PRP=1.542D-3
PRF=0.61D0
PLS=4.47005D-3
PLM=0.07433D-3
PLFF=2.189D0
PLDD=5.989D-3
PLQQ=1.423D-3
PMS=1.75945D-3
PMR=0.09901383D0
PMAF=89.006D-3
PMAQ=1.96904D-3
PMAD=4.22098D-3
PRL=1.75781D0
PFV=375.0D0
PCNA A=0.98367D0
PA11=-2.9246D-5
PA12=-1.0771D-7
PA13= 2.0394D-11
PA14= 0.0D0
PCNA F=1.00000D0
PA21=-6.9272D-5
PA22=-8.4719D-8
PA23= 1.6303D-11
PA24= 0.0D0
PCNA D=0.9886D0
PA31=-8.0120D-5
PA32=-6.1443D-8
PA33= 1.2983D-11
PA34= 0.0D0

```

D.2 Circuit Model (Continued)

```

PCNFD=1.00
PA41=-6.9355D-5
PA42=-6.6663D-8
PA43=1.3054D-11
PA44= 0.00
PCNDD=0.97E27D5
PA51=-2.1569D-5
PA52=-7.9586D-8
PA53= 1.5930D-11
PA54= 0.00
PCNFF=1.0098D0
PA61=-2.9867D-5
PA62=-1.0519D-7
PA63=1.8699D-11
PA64=0.00
PCNAQ=0.99419D0
PA71=-2.6322D-5
PA72=-5.5511D-8
PA73=1.0182D-11
PA74=0.00
PNFA=4.066D-4
PNFD=4.98007E-2
PCE2=FIEG(IL11,IL22,IL33,IL44,IL55,PNFA,FNFD,PT)
PCAA= FPOLY(PA11,PA12,PA13,PA14,PCEQ,3.03,PCNAA)
PCFF= FPOLY(PA61,PA62,PA63,PA64,PCEQ,3.03,PCNFF)
PCDD= FPOLY(PA51,PA52,PA53,PA54,PCEQ,3.03,PCNDD)
PCAF= FPOLY(PA21,PA22,PA23,PA24,PCEQ,3.03,PCNAF)
PCAD= FPOLY(PA31,PA32,PA33,PA34,PCEQ,3.03,PCNAD)
PCAQ= FPOLY(PA71,PA72,PA73,PA74,PCEQ,3.03,PCNFQ)
PCFD= FPOLY(PA41,PA42,PA43,PA44,PCEQ,3.03,PCNFD)
PDAA= FPOLY1(PA11,PA12,PA13,PA14,PCEQ,3.03)
PDFF= FPOLY1(PA61,PA62,PA63,PA64,PCEQ,3.03)
PDDD= FPOLY1(PA51,PA52,PA53,PA54,PCEQ,3.03)
PDAF= FPOLY1(PA21,PA22,PA23,PA24,PCEQ,3.03)
PDAD= FPOLY1(PA31,PA32,PA33,PA34,PCEQ,3.03)
PDAQ= FPOLY1(PA71,PA72,PA73,PA74,PCEQ,3.03)
PDFD= FPOLY1(PA41,PA42,PA43,PA44,PCEQ,3.03)
PCOFRA= FSIMP(PNFA,IL11,IL22,IL33,PT)
PCOFAA= FMESS1(IL11,IL22,IL33,IL44,IL55,IL66,PDAA,PDAF,PDAD,PDAQ,
          FLS,PLM,PMS,PT,0.0DC,PMAF,PMAD,PMAQ,1)
PCOFAB= FMESS1(IL11,IL22,IL33,IL44,IL55,IL66,PDAB,PDAF,PDAD,PDAQ,
          FLS,PLM,PMS,PT,PM2P3,PMAF,PMAD,PMRQ,2)
PCOFAC= FMESS1(IL11,IL22,IL33,IL44,IL55,IL66,PDAA,PDAF,PDAD,FDAR,
          FLS,PLM,PMS,PT,P2P3,PMAF,PMAD,PMAQ,3)
PCOFAF= FMESS2(IL11,IL22,IL33,IL44,IL55,PDAF,PDAD,PDFD,
          PT,PMAF,PLFF,PMR)
PCOFAD= FMESS2(IL11,IL22,IL33,IL44,IL55,PDAD,PDFD,PDDD,
          PT,PMAD,PMR,PLDD)
PM12=EQUATION 2 (PMS,FLM,PCAA,PM2P3)
PM13=EQUATION 2 (PMS,PLM,PCAA,P2P3)
PM14=EQUATION 9 (1.000,PMAF,PCAF,0.000)
PM15=EQUATION 9 (1.0DC,PMAD,PCAD,0.000)
PM15=EQUATION 8 (1.0DC,PMAQ,0.0,PCAQ)
PM23=EQUATION 2 (FMS,FLM,PCAA,0.000)
PM24=EQUATION 9 (1.0DC,PMAF,PCAF,PM2P3)
PM25=EQUATION 9 (1.0DC,PMAD,PCAD,PM2P3)
PM26=EQUATION 8 (1.000,PMAQ,PM2P3,PCAO)
PM34=EQUATION 9 (1.0DC,PMAF,PCAF,P2P3)
PM35=EQUATION 9 (1.0DC,PMAD,FCAD,P2P3)
PM36=EQUATION 8 (1.0DC,PMAQ,P2P3,PCAQ)

```

D.2 Circuit Model (Continued)

```

PM45=X13(PMR*FCFD)
PL11=EQUATION 1 (PLS,PLM,7.0DC,PCAA,PCOFAB,PNFA)
PL22=EQUATION 1 (PLS,PLM,P2P3,PCAA,PCOFAB,PNFA)
PL33=EQUATION 1 (PLS,PLM,PM2P3,PCAA,PCOFAC,PNFA)
PL44= X11(PLFF*PCFF+PCOFAC)
PL55= X12(PLDD*PCDD + PCOFAD*FNFD)
PL65 = PLQ0
DPS=X1(FD2THT(IL11,IL22,IL33,VRAD,VRED,VRC0,PRP,PS))
DPT=X2(PS)
PS=376.99800
PT=2.4894900
FUNCTIONS
EQUATION 1 (A,B,C,D,E,F)=(D*(A+B*D*COS(2.*D*D*PT+C))+ F*E*D*COS(PT-C))
EQUATION 2 (A,B,C,D)=(C*(-A + B*D*COS(2.*D*D*PT+D)))
EQUATION 3 (A,B,C,D)=(?-D)*A*B*D*PS*D*SIN(2.*D*D*PT+C))
EQUATION 4 (A,B,C,D)=(A*B*D*PS*D*SIN(PT+C))
EQUATION 5 (A,B,C,D,E)=(E*D*A*B*PS*D*COS(PT+C))
EQUATION 7 (A,B,C)=(?-A*B*D*SIN(2.*PT+C))
EQUATION 8 (A,B,C,D)=(A*B*D*D*SIN(PT+C))
EQUATION 9 (A,B,C,D)=(A*B+C*D*COS(PT+D))
EQUATION 11 (A,B,C,D)=(-1.0D0*A*B*C*D*COS(PT+D))
EQUATION 12 (A,B,C,D)=(A*B*C*D)
TABLE 1
0.000,1.7578100,0.01666600,1.7578100,0.01666700,0.500,0.0333300,0.500,
0.0333400,1.7578100,0.100,1.7578100
OUTPUTS
IL11,IL44,IL55,IL66,PS
PLOT INTERVAL =1.0-8
INITIAL CONDITIONS
IL11=6967.4400
IL22=-3483.7200
IL33=-3483.7200
IL44=616.3100
IL55=0.000
IL65=0.000
RUN CONTROLS
INTEGRATION ROUTINE=IMPLICIT
MINIMUM ABSOLUTE ERROR=1.0-4
MINIMUM STEP SIZE =1.0-24
STOP TIME=0.0500
END
/*

```

D.3 Fortran Subroutines

```

//FORT.FORTSRC DD *
      DOUBLE PRECISION FUNCTION FD2THT(IL11,IL22,IL33,VRAD,VRBD,
1           VRCD,PRP,PS)
      IMPLICIT REAL*8(A-H,I-O-Z)
      REAL*8 IL11,IL22,IL33
C THIS SUBPROGRAM COMPUTES ROTOR ANGLE ACCELERATION. THE MECHANICAL AND
C ELECTRICAL POWERS ARE CALCULATED IN P.U.
      DATA SB3,PM,HCON,OMEGAR/160.0D6,0.8D0,2.37D0,376.998D0/
      PE1=IL11*VRAD + IL22*VRBD + IL33*VRCD
      PE = PE1 + PRP*(IL11*IL11 + IL22*IL22 + IL33*IL33)
      PEPU = PE/SB3
      OMEGAU = PS/OMEGAR
      DENOM = 2.0D0*HCON*OMEGAU
      DIFF=PM-PEPU
      FD2THT = DIFF/DENOM
      RETURN
      END
      DOUBLE PRECISION FUNCTION FIEQ(IL11,IL22,IL33,IL44,IL55,
1           PNFA,PNFD,PT)
      IMPLICIT REAL*8(A-H,I-O-Z)
C THIS SUBPROGRAM COMPUTES THE EQUIVALENT CURRENT ALONG THE ROTOR AXIS.
C REFER TO PAPER BY SMITH AND SNIDER FOR THEORECTICAL FORMULATION.
      A = DCOS(PT)
      B = DCOS(PT-2.0943951D2393D0)
      C = DCOS(PT+2.0943951D2393D0)
      STEP1 = (IL11*A + IL22*B + IL33*C)*2.0D0/3.0D0
      STEP2 = PNFD*IL55 + PNFA*STEP1
      FIEQ= IL44 + STEP2
      FIEQ= DAHS(FIEQ)
      RETURN
      END

      DOUBLE PRECISION FUNCTION FPOLY(A1,A2,A3,A4,CEQ,PLIM,CONS)
      IMPLICIT REAL*8(A-Z)
      IF(CEQ .GT. PLIM)CEQ=PLIM
      CEQ2=CEQ*CEQ
      CEQ3=CEQ*CEQ2
      CEQ4=CEQ*CEQ3
      FPOLY=CONS + A1*CEQ + A2*CEQ2 + A3*CEQ3 + A4*CEQ4
      RETURN
      END
      DOUBLE PRECISION FUNCTION FPOLY1(A1,A2,A3,A4,CEQ,PLIM)
      IMPLICIT REAL*8(A-Z)
      CEQ2=CEQ*CEQ
      CEQ3=CEQ*CEQ2
      CEQ4=CEQ*CEQ3
      FPOLY1= A1 + 2.0D0*A2*CEQ + 3.0D0*A3*CEQ2 + 4.0D0*A4*CEQ3
      IF(CEQ .GT. PLIM)FPOLY1=0.0D0
      RETURN
      END
/*
*/

```

D.3 Fortran Subroutines (Continued)

```

DOUBLE PRECISION FUNCTION FMESS1(IL11,IL22,IL33,IL44,IL55,IL66,
1      XLAA,XLAF,XLAD,XLAQ
2      PLS,PLM,PMS,THT,PHASE,PMAF,PMAD,PMAQ,NFLAG)
IMPLICIT REAL*8(A-H,I,O-Z)
C THIS SUBPROGRAM COMPUTES COEFFICIENTS OF VOLTAGES SOURCES PUT IN TO
C TAKE INTO ACCOUNT THE EFFECTS OF SATURATION.
GO TO (10,20,30),NFLAG
10 X1=PLS
X2=-PMS
X3=-PMS
GO TO 40
20 X1=-PMS
X2= PLS
X3=-PMS
GO TO 40
30 X1=-PMS
X2=-PMS
X3=PLS
40 DLAA= XLAA*(X1 + PL1*DCOS(2.0D0*THT+PHASE))
DLBB= XLAA*(X2 + PL1*DCOS(2.0D0*THT-2.0943951D2393D0+PHASE))
DLCC= XLAA*(X3 + PL1*DCOS(2.0D0*THT + 2.0943951D2393D0+PHASE))
DLAF= XLAF*PMAF*DCOS(THT+PHASE)
DLAD= XLAD*PMAD*DCOS(THT+PHASE)
DLAQ= XLAQ*PMAQ*DSIN(THT+PHASE)
FMESS1= IL11*DLAA + IL22*DLBB + IL33*DLCC + IL44*DLAF + IL55*DLAD
& + IL66*DLAQ
FMESS1= 0.0D0
RETURN
END
DOUBLE PRECISION FUNCTION FSIMP(PNFA,CA,CB,CC,THT)
IMPLICIT REAL*8(A-H,O-Z)
C THIS SUBPROGRAM COMPUTES THE NONLINEAR SPEED VOLTAGE ARISING
C FORM CONSIDERATIONS OF SATURATION.
X1 = DSIN(THT)
X2 = DSIN(THT-2.0943951D2393D0)
X3 = DSIN(THT+2.0943951D2393D0)
FSIMP=PNFA*(CA*X1 + CB*X2 + CC*X3)
RETURN
END
DOUBLE PRECISION FUNCTION FMESS2(IL11,IL22,IL33,IL44,IL55,
1      XLAA,XLAF,XLAD,
2      THT,PL1,PL2,PL3)
IMPLICIT REAL*8(A-H,I,O-Z)
C THIS SUBPROGRAM COMPUTES COEFFICIENTS OF VOLTAGES SOURCES PUT IN TO
C TAKE INTO ACCOUNT THE EFFECTS OF SATURATION.
DLAA= XLAA*PL1*DCOS(THT)
DLBB= XLAA*PL1*DCOS(THT - 2.0943951D2393D0)
DLCC= XLAA*PL1*DCOS(THT + 2.0943951D2393D0)
DLAF= XLAF*PL2
DLAD= XLAD*PL3
FMESS2= IL11*DLAA + IL22*DLBB + IL33*DLCC + IL44*DLAF + IL55*DLAD
FMESS2= 0.0D0
RETURN
END

```

APPENDIX E
SCR MODELS FOR SPICE 2, AND SCEPTRE

E.1 THE BIPOLAR JUNCTION TRANSISTOR MODEL

Development of the SCR models begins with the bipolar junction transistor model. This BJT model is a variation of the Ebers-Moll one dimensional model in which junction capacitances are added to account for charge storage in the depletion region and charge storage in the base regions due to diffusion time across the base region.

$$C_{BC} = \frac{\tau_R \alpha_R I_{CS}}{\theta} e^{\frac{V_{BC}}{\theta}} + C_{jCo} \left[\frac{1}{\sqrt{1 - V_{BC}/\phi_C}} \right] \quad (81)$$

$$C_{BE} = \frac{\tau_R \alpha_R I_{CS}}{\theta} e^{\frac{V_{BE}}{\theta}} + C_{jEo} \left[\frac{1}{\sqrt{1 - V_{BC}/\phi_E}} \right] \quad (82)$$

The equations describing the components in the above model are:

$$\begin{aligned} I_C &= \alpha_F I_F - I_R \\ &= \alpha_F I_{ES} (e^{\frac{V_{BE}}{\theta}} - 1) - I_{CS} (e^{\frac{V_{BE}}{\theta}} - 1) \\ I_E &= \alpha_R I_R - I_F \\ &= \alpha_R I_{CS} (e^{\frac{V_{BC}}{\theta}} - 1) - I_{ES} (e^{\frac{V_{BC}}{\theta}} - 1) \end{aligned} \quad (84)$$

E.2 LIST OF PARAMETERS

α_F = proportion of current injected from emitter into the base that diffuses to the base-collector junction.

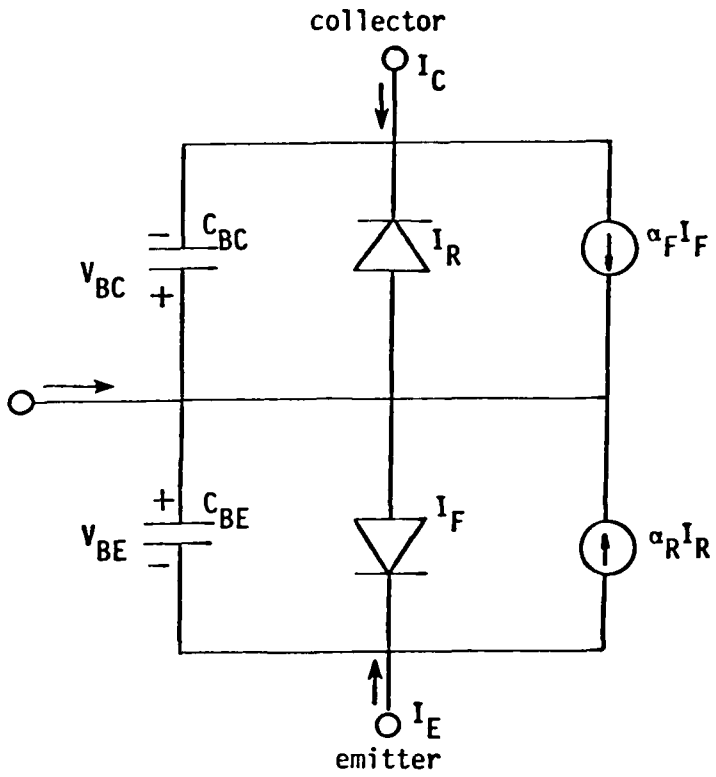


FIGURE 23. MODIFIED EBERS-MOLL BIPOLAR JUNCTION TRANSISTOR MODEL (INJECTION MODEL).

τ_F = transit time for carriers injected by the emitter into the base-collector depletion layer.

I_{ES} = base-emitter saturation current for reverse biased base-emitter junction.

C_{jE0} = zero bias base-emitter depletion layer capacitance.

θ = physical constant (at a fixed temperature) = 0.025 v^{-1} .

ϕ_E = emitter junction potential ($0.6 - 0.8 \text{ v}$) - a physical property.

α_R = proportion of current injected from the collector into the base that diffuses to the base-emitter junction.

τ_R = transit time for carriers injected by the collector into the base to reach the base-emitter depletion layer boundary.

I_{CS} = base collector saturation current for reverse biased base-collector junction.

C_{jCo} = zero bias base-collector depletion layer capacitance.

ϕ_C = collector junction potential ($0.6 - 0.8 \text{ v}$) - a physical property.

m = the junction capacitance gradient factor. For heavily doped semiconductors $m \approx 0.5$. For lightly doped semiconductors $m \approx 0.33$.

The modified Ebers-Moll model as given is the basic model as applied to SCEPTR. it is referred to as the injection model, because the reference currents I_R and I_F are the currents injected into the base region from the collector and emitter respectively.

SPICE 2 incorporates a mathematically identical model, but, the SPICE 2 MODEL is referenced to the proportion of the injected currents (I_R, I_F) which actually arrive at their respective collecting junctions ($\alpha_R I_R \Rightarrow$ called I_{EC} , $\alpha_F I_F \Rightarrow$ called I_{CC}). For this reason, it is referred to as the charge transport model (meaning that the reference currents are those actually transported across the base region).

Utilizing the reciprocity relationship:

$$\alpha_F I_{ES} = \alpha_R I_{CS} \triangleq I_S .$$

AD-A101 316 CLEMSON UNIV S C DEPT OF ELECTRICAL AND COMPUTER EN--ETC F/6 10/2
DYNAMIC SIMULATION OF AIRBORNE HIGH POWER SYSTEMS.(U)
MAR 81 R W GILCHRIST, H ALMAULA F33615-79-C-2047

AFWAL-TR-80-2115

NL

UNCLASSIFIED

2nd 2
41-310

END
DATE
FILED
8-81
DTIC

E.3 CIRCUIT SIMPLIFICATION

The BJT model equations are then rewritten utilizing this relationship

$$I_C = I_S(e^{\frac{V_{BE}}{\theta}} - 1) - I_S/\alpha_R(e^{\frac{V_{BC}}{\theta}} - 1) \quad (85)$$

$$= I_{CC} - I_{EC}/\alpha_R$$

$$I_E = I_S(e^{\frac{V_{BC}}{\theta}} - 1) - I_S/\alpha_F(e^{\frac{V_{BE}}{\theta}} - 1) \quad (86)$$

$$= I_{EC} - I_{CC}/\alpha_F$$

$$C_{BC} = \frac{\tau_R I_S}{\theta} e^{\frac{V_{BC}}{\theta}} + C_{jCo} \left[\frac{1}{1 - V_{BC}/\phi_C} \right]^m \quad (87)$$

$$C_{BE} = \frac{\tau_F I_S}{\theta} e^{\frac{V_{BE}}{\theta}} + C_{jEo} \left[\frac{1}{1 - V_{BE}/\phi_E} \right]^m \quad (88)$$

This modification is advantageous in that one less parameter determination is required and that numerical methods are simplified due to an increase in the range of linearity of logarithmic calculations based on the reference current I_S (Reference 33).

Note. There is no physical or mathematical modification, only a notation modification.

Still further modification in form is made for the SPICE 2 model while keeping the model mathematically identical. The two reference currents (current collected at the emitter I_{EC} and current collected at the collector I_{CC}) are combined to form a single reference current (current collected total I_{CT}). This I_{CT} is defined by

$$I_{CT} = I_{CC} - I_{EC} = I_S(e^{\frac{V_{BE}}{\theta}} - e^{\frac{V_{BC}}{\theta}})$$

The combining of the transport current into a single term requires that the diodes have only base connections at their anode points (NPN model) and therefore an expression for base current must be formed so that the diode currents may be expressed correctly. Referring to Figure 24.

$$I_B = -I_C - I_E \quad (89)$$

$$I_B = (1/\alpha_F - 1)I_{CC} + (1/\alpha_R - 1)I_{EC} \quad (90)$$

$$I_B = I_{CC}/\beta_F + I_{EC}/\beta_R \quad (91)$$

The model now appears as Figure 25, the model terminal equations are now

$$\begin{aligned} I_C &= I_{CT} - I_{EC}/\beta_R \\ &= I_S(e^{V_{BE}/\theta} - e^{V_{BC}/\theta}) - I_S/\beta_R (e^{V_{BC}/\theta} - 1) \end{aligned} \quad (92)$$

$$\begin{aligned} I_E &= -I_{CT} - I_{CC}/\beta_F \\ &= I_S(e^{V_{BC}/\theta} - e^{V_{BE}/\theta}) - I_S/\beta_F (e^{V_{BE}/\theta} - 1) \end{aligned} \quad (93)$$

$$\begin{aligned} I_B &= I_{CC}/\beta_F + I_{EC}/\beta_R \\ &= I_S/\beta_F (e^{V_{BE}/\theta} - 1) + I_S/\beta_R (e^{V_{BC}/\theta} - 1) \end{aligned} \quad (94)$$

The terminal characteristic model used in SPICE 2 is then given in terms of I_B and I_C . This model is shown in Figure 26, with contact resistances r_b , r_c and r_e added.

E.4 THE SCR MODEL IN SPICE 2

The SCR model is developed in SPICE 2 by connecting TWO BJT models (a PNP and a NPN) as shown in Figure 27. In addition to the two transistors, a resistor R_{shunt} is added to the model. Since the Spice BJT model has no capability to simulate the reverse breakdown of the p-n junctions, then a

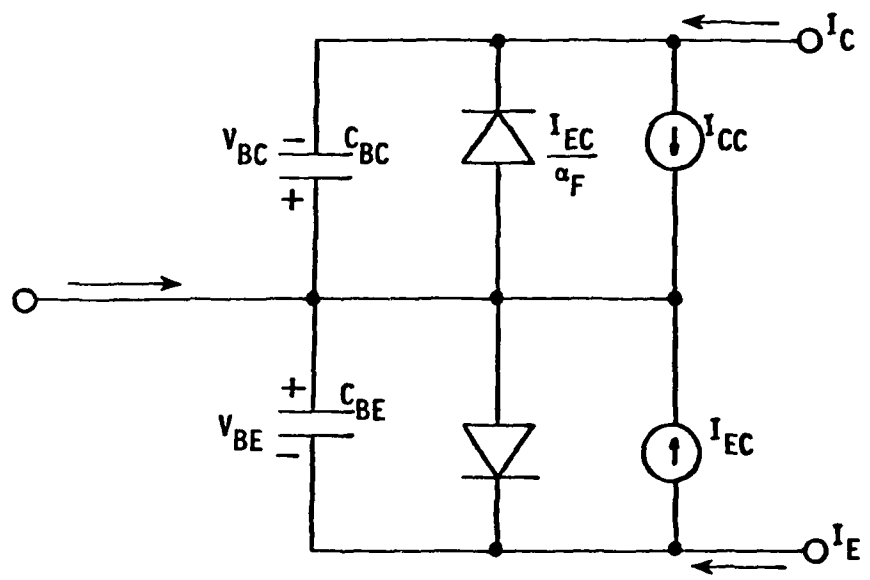


FIGURE 24. MODIFIED EBERS-MOLL BJT MODEL (TRANSPORT MODEL).

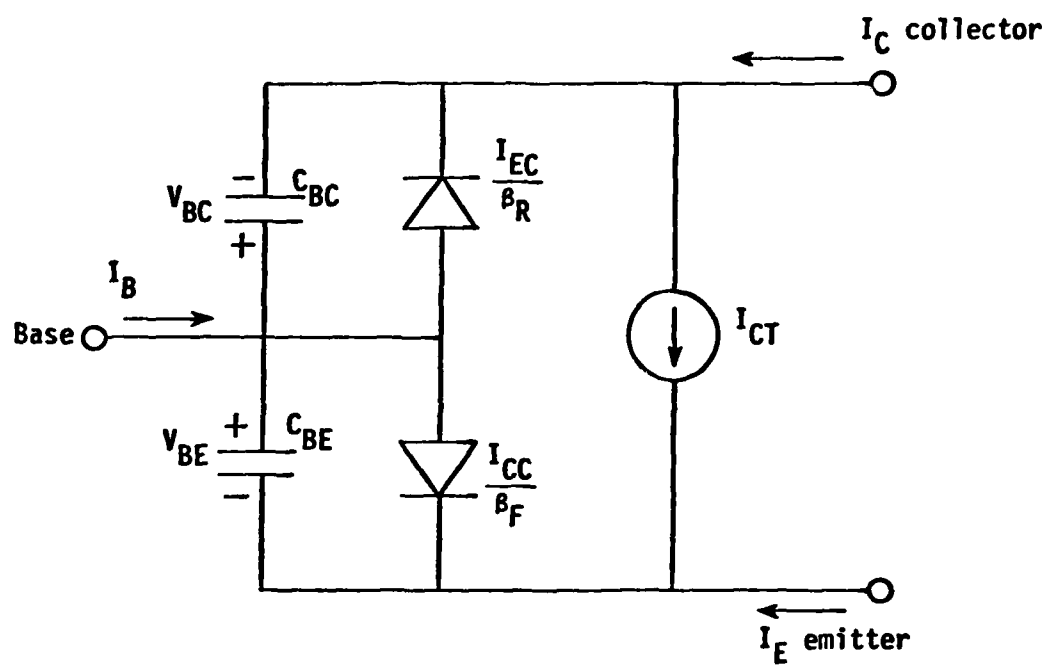


FIGURE 25. MODIFIED EBERS-MOLL BJT MODEL

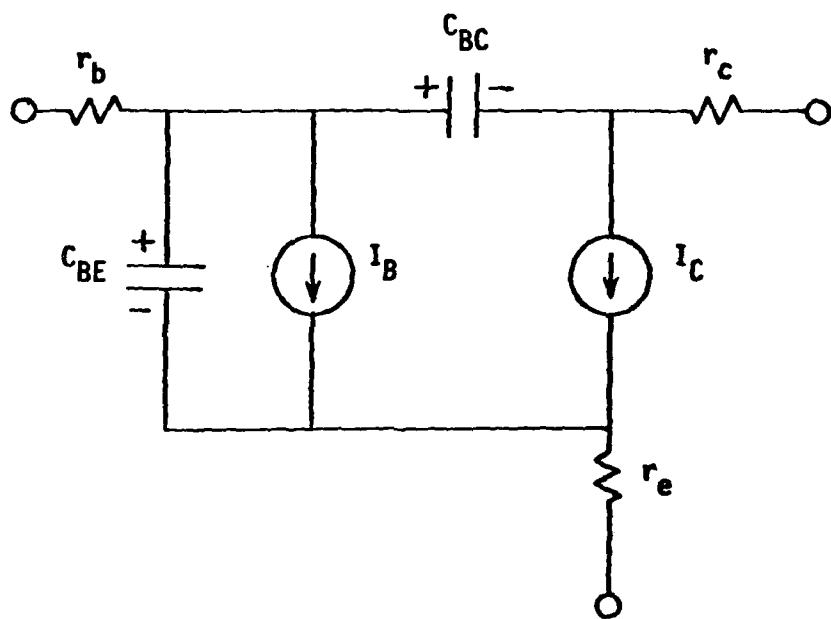


FIGURE 26. SPICE 2 MODIFIED EBERS-MOLL BJT MODEL.

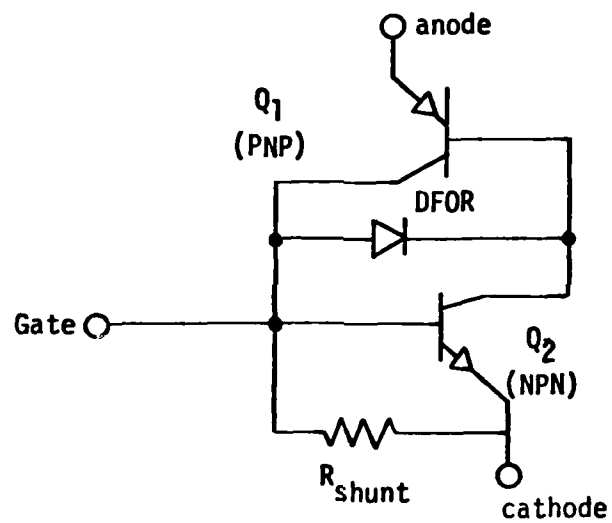


FIGURE 27. A SPICE 2 SCR MODEL BASED ON THE TWO BJT MODEL.

diode DFOR must be added to simulate the forward breakdown voltage of the SCR. In addition DFOR provides a means of controlling the amount of forward bias of the center p-n junction of the SCR as well as a path of discharge of the junction capacitance during that portion of the SCR turn-off transient in which the center junction is relieved if excess carriers in the depletion region by recombination.

When using the SPICE 2 BJT AND DIODE MODELS, there are a large number of parameters that may be specified (28 for the BJT, 14 for the Diodes). If these parameters are not supplied via the input deck, then SPICE 2 has built in default values to use in order to satisfy the model equations. The SPICE 2 SCR MODEL equivalent circuit is shown in Figure 28 with applicable default values applied to circuit elements.

The 10 circuit components of Figure 28 are described by the following equations in which any SPICE 2 default values used in the model have been applied to the equations.

$$r_{e_1} = r_{e_1} \quad (95)$$

$$I_{C_1} = I_{S_1} (e^{40V_{EB_1}} - e^{-40V_{CB_1}}) - \frac{I_{S_1}}{\beta_{R_1}} (e^{40V_{CB_1}} - 1) \quad (96)$$

$$I_{B_1} = \frac{I_{S_1}}{\beta_{f_1}} (e^{40V_{EB_1}} - 1) + \frac{I_{S_1}}{\beta_{R_1}} (e^{40V_{CB_1}} - 1) \quad (97)$$

$$C_{BE_1} = \frac{\tau_{f_1} I_{S_1}}{40} e^{40V_{EB_1}} \quad (98)$$

$$C_{BC_1} = \frac{\tau_{R_1} I_{S_1}}{40} e^{40V_{CB_1}} \quad (99)$$

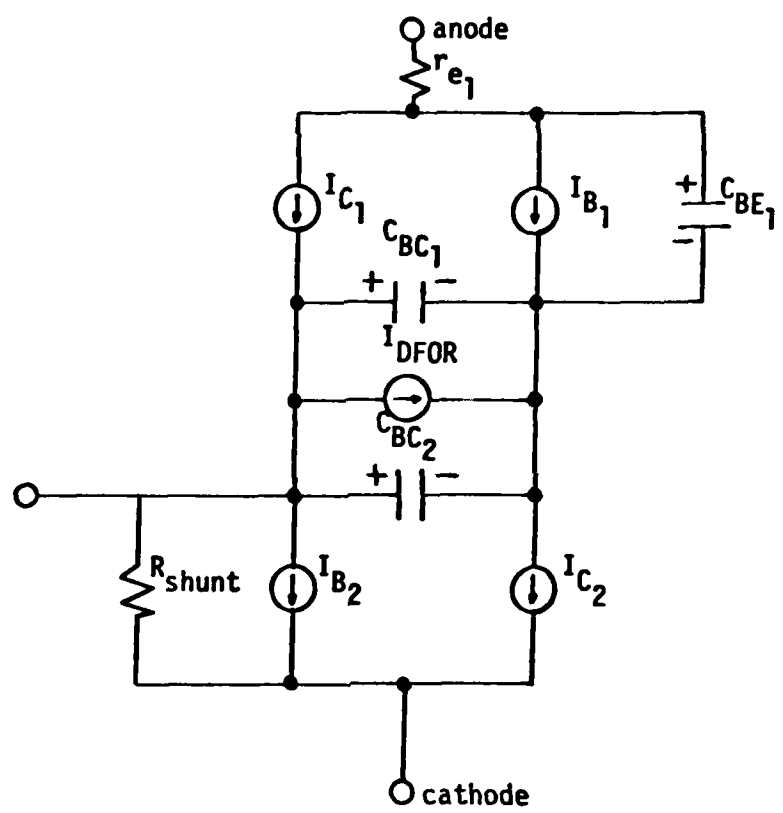


FIGURE 28. THE SPICE 2 SCR MODEL EQUIVALENT CKT.

$$I_{DFOR} = \frac{I_{S_{diode}} (e^{\frac{40V_{CB_1}}{V_{BO}}} - 1)}{1 + [V_{CB_1}/V_{BO}]^6} = \frac{I_{S_{diode}} (e^{\frac{40V_{BC_2}}{V_{BO}}} - 1)}{1 + [V_{BC_2}/V_{BO}]^6} \quad (100)$$

$$I_{C_2} = I_{S_2} (e^{\frac{40V_{BE_2}}{V_{BO}}} + 1) \quad (101)$$

$$I_{B_2} = \frac{I_{S_2}}{\beta_{f_2}} (e^{\frac{40V_{BE_2}}{V_{BO}}} - 1) + I_{S_2} (e^{\frac{40V_{BC_2}}{V_{BO}}} - 1) \quad (102)$$

$$C_{BC_2} = C_{jC_2} (1 - V_{BC_2})^{-0.5} \quad (103)$$

$$R_{shunt} = R_{shunt} \quad (104)$$

From these 10 equations, one develops the following list of parameters that must be provided in order for the model to function.

1. r_{e_1}
2. I_{S_1}
3. β_{f_1}
4. β_{R_1}
5. τ_{f_1}
6. τ_{R_1}
7. $I_{S_{diode}}$

8. V_{B0}

9. I_{S2}

10. β_{f2}

11. C_{jc2}

The method of determining these parameter values is given in Reference 24.

E.5 THE SCR MODEL IN SCEPTRE

The SCR model is developed in SCEPTRE by connecting a PNP transistor and NPN transistor in the same regenerative feedback arrangement as was used in the SPICE 2 model (Figure 27). In the case of SCEPTRE, however, the BJT model has the form shown in Figure 23. Applying similar procedures as used in developing the SPICE 2 SCR model leads to the equivalent circuit shown in Figure 29. One advantage of SCEPTRE is that the ability to model the dependent exponential current sources in the input deck (thereby not relying on a fixed internal model for the BJT) allows elimination of the diode used in SPICE 2 to model the SCR forward break-over voltage. This SCR characteristic is modeled by including reverse breakdown in the mathematical expression for the base-collector junction of the transistors.

It is notable that a minor rearrangement of the form of this model [combine diodes I_{R1} and I_{R2} , combine capacitors C_{BC1} and C_{BC2} , and include the junction capacitor (defaulted to zero) of the gate to cathode junction] results in the intrinsic 3-junction model of the SCR.

The SCEPTRE SCR model of Figure 29 has 13 elements, but, since the current sources are defined as a constant, α , times the corresponding diode current, then only the equations for diode currents are given.

$$r_{e_1} = r_{e_1} \quad (105)$$

$$I_{F1} = I_{ES1} (e^{40V_{EB1}} - 1) \quad (106)$$

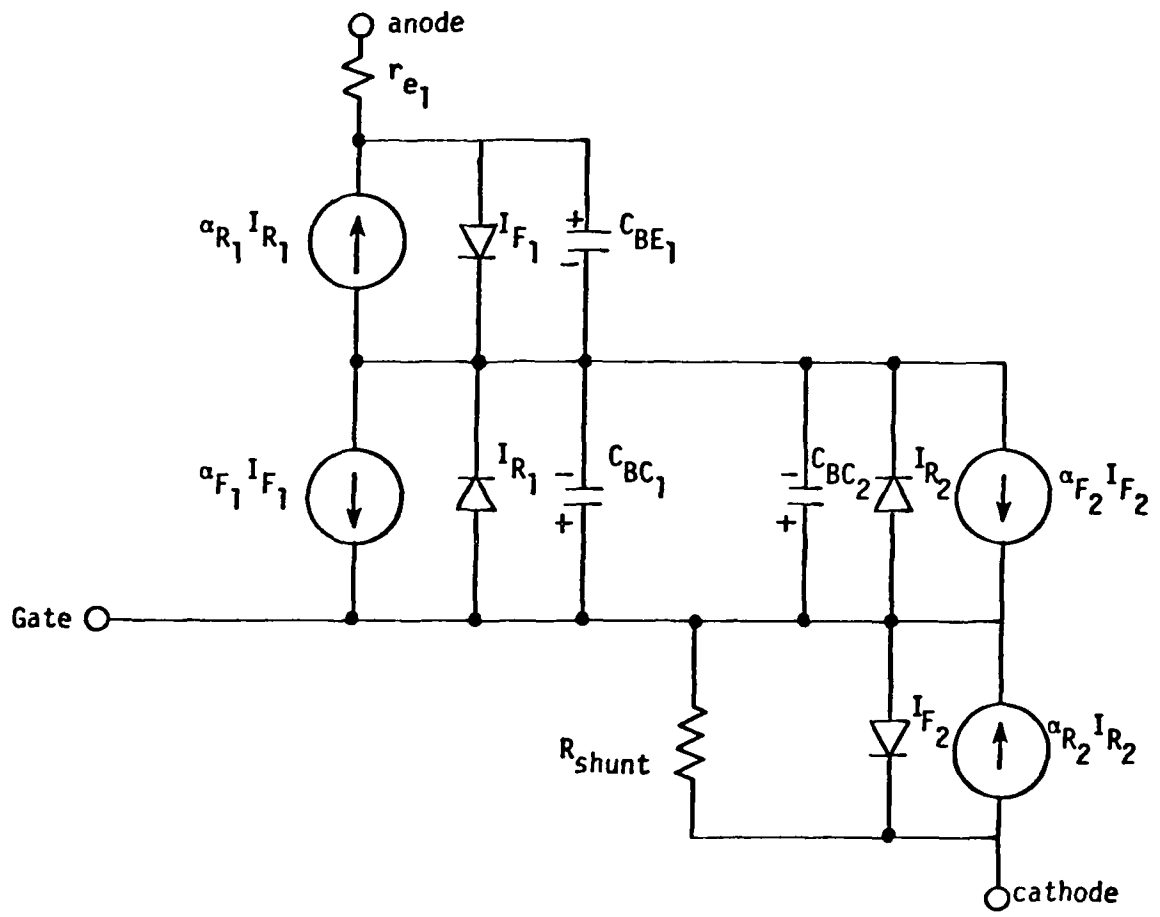


FIGURE 29. SCEPTRE TWO BJT SCR MODEL.

$$C_{BE_1} = \frac{\tau_f \alpha_f I_{ES_1}}{40} e^{40V_{EB_1}} \quad (107)$$

$$I_{R_1} = \frac{I_{CS_1} (e^{40V_{CB_1}} - 1)}{1 + [V_{CB_1}/V_{BO}]^6} \quad (108)$$

$$C_{BC_1} = \frac{\tau_R \alpha_R I_{CS_1}}{40} e^{40V_{CB_1}} \quad (109)$$

$$C_{BC_2} = C_j C_2 (1 - V_{BC_2})^{-0.5} \quad (110)$$

$$I_{R_2} = I_{CS_2} (e^{40V_{BC_2}} - 1) \quad (111)$$

$$I_{F_2} = I_{ES_2} (e^{40V_{BE_2}} - 1) \quad (112)$$

$$R_{shunt} = R_{shunt} \quad (113)$$

The parameters required to implement the above model are obtained from the SPICE 2 parameters as follows:

TABLE 3
CONVERSION OF SPICE 2 TO SCEPTRE

1.	r_{e_1}	=	r_{e_1}
2.	I_{ES_1}	=	I_{S_1}/α_{f_1}
3.	α_{f_1}	=	α_{f_1}
4.	τ_{f_1}	=	τ_{f_1}
5.	α_{R_1}	=	α_{R_1}
6.	I_{CS_1}	=	I_{S_1}/α_{R_1}
7.	τ_{R_1}	=	τ_{R_1}
8.	$C_j C_2$	=	$C_j C_2$
9.	I_{CS_2}	=	I_{S_2}/α_{R_2}
10.	I_{ES_2}	=	I_{S_2}/α_{f_2}
11.	α_{R_2}	=	α_{R_2}
12.	α_{f_2}	=	α_{f_2}
13.	R_{shunt}	=	R_{shunt}
14.	V_{B0}	=	V_{B0}

REFERENCES

1. R. H. Park and B. L. Robertson, "The Reactances of Synchronous Machines," Trans. AIEE, Vol. 471, No. 21, pp. 514-536.
2. S. R. Sedore and J. Bowers, "SCEPTRE: A Computer Program for Circuits and Systems Analysis," Prentice-Hall, Inc., Englewood Cliffs, N.Y., 1971.
3. I. R. Smith and L. A. Snider, "Prediction of Transient Performance of Isolated Saturated Synchronous Generators," Proc. IEE (London), Vol. 119, No. 9, pp. 1309-1318, September, 1972.
4. L. A. Snider and I. R. Smith, "Measurement of Inductance Machines," Proc. IEE, Vol. 119, No. 5, May 1972.
5. E. W. Kimbark, "Power System Stability," (Vol. III, Synchronous Machines) 1956, Wiley.
6. P. M. Anderson and A. A. Fouad, "Power Systems Control and Stability," Iowa State University Press, 1977.
7. Charles Concordia, "Synchronous Machines - Theory and Performance," Wiley 1951.
8. H. L. Nakra and T. H. Barton, "Three Phase Transformer Transient," IEEE Winter Power Meeting, New York, N.Y. 1973.
9. W. A. Manly Jr., "An Appraisal of Several Nonlinear Hysteresis Loop Models," IEEE Trans. on Magnetics, Vol. No.3, May 9, Sept. 1973.
10. H. L. Nakra and J. H. Barton, "The Dynamics of Coupled Circuits with Ferromagnetic Non-Linearity. IEEE Winter Power Meeting, New York, N.Y., 1971.
11. Leon O. Chua and Pen-Min Lin, "Computer-Analysis of Electronic Circuits," Englewood Cliffs, New Jersey, Prentice Hall, 1975.

12. D. A. Calahan, "Computer-Aided Analysis of Electronic Circuits." Englewood Cliffs, New Jersey: Prentice Hall, 1975.
13. W. K. Macfadyen, R. R. S. Simpson, R. D. Slater, W. S. Wood, "Representation of Magnetization Curves by Exponential Series." PROC. IEE, Vol. 120, No. 8, August 73.
14. AFAPL-TR-76-102 "Development of Lightweight Transformers for Air-borne High Power Supplies." Thermal Technology Laboratories, Inc., December, 1976.
15. G. E. Forsythe, M. A. Malcom and C. B. Moler, Computer Methods for Mathematical Computations - Englewood Cliffs, New Jersey: Prentice Hall, 1977.
16. L. O. Chua and P. M. Lin, Computer-Aided Analysis of Electronic Circuits: Algorithms and Computational Techniques. Englewood Cliffs, New Jersey: Prentice Hall, 1975.
17. C. W. Gear, Numerical Initial Value Problems in Ordinary Differential Equations. Englewood Cliffs, New Jersey: Prentice Hall, 1971.
18. A. Ralston and P. Rabinowitz, A First Course in Numerical Analysis. 2nd ed. New York: McGraw-Hill, 1978, 1965, Chap. 5.
19. S. W. Director, Computer-Aided Circuit Design: Simulation and Optimization. Stroudsburg, Pennsylvania: Dowden, Hutchinson and Ross, 1974.
20. D. A. Calahan, "Numerical Considerations for Implementation of a Nonlinear Transient Circuit Analysis Program," IEEE Trans. Circuit Theory, CT-18, pp. 66-73, Jan. 1971.
21. R. K. Brayton, F. G. Gustafson and G. D. Hachtel, "A New Efficient Algorithm for Solving Differential-Algebraic Systems Using Implicit Backward Differentiation Formulas," PROC. IEEE, 60, pp. 98-108, Jan. 1972.
22. F. H. Branin, Jr., G. R. Hogsett, R. L. Lunde, and L. E. Kugal, "ECAP II A New Electronic Circuit Analysis Program," IEEE J. Solid-State Circuits, SC-6, pp. 146-166, Aug. 1971.

23. G. N. Glasoe, J. V. Lebacqz, "Pulse Generators" Radiation Laboratory Series, McGraw-Hill, 1948.
24. F. Ki. Waiman, "A SPICE Model for the SCR," Master Thesis, Department of Electrical and Computer Science, University of California-Berkeley, Dec. 1979.
25. "A Computer Model for a High Power SCR," Final Report, AFAPL-TR-75-106, Dec. 1975.
26. "Silicon Controlled Rectifier Large Signal Model," Report No. AFAPL-TR-75-89, Oct. 1975.
27. W. W. Nagel, "SPICE 2: A Computer Program to Simulate Semiconductor Circuits," Electronic Research Laboratory, College of Engineering, University of California, Berkeley, CA, Memo No. ERL-M520.
28. James Bowers, et al., "A Survey of Computer Aided-Design and Analysis Programs," Technical Report, AFAPL-TR-76-33, USAF Aero Propulsion Laboratory, AFAPL/POD, Wright-Patterson Air Force Base, Ohio, April 1976.
29. James C. Bowers and Stephen R. Sedore, "SCEPTRE: A Computer Program for Circuit and Systems Analysis, Prentice-Hall, Inc., Englewood Cliffs, New Jersey, 1971.
30. James C. Bowers, et al., "User's Manual for SUPER-SCEPTRE," Final Report on Contract No. DAAA-21-73-C-0655, Fuse Development and Engineering Division, Picatinny Arsenal, Dover, New Jersey, May 1975.
31. H. A. Nienhus and J. C. Bowers, "A General Purpose Computer Model for a High Power SCR," Technical Report AFAPL-TR-76-82, USAF Aero Propulsion Laboratory, AFAPL/POD, Wright-Patterson Air Base.
32. M. Dougherty, "A Series Resonant Inverter Simulation Aging SUPER-SCEPTRE," Proceedings of the IEEE 1979 National Aerospace and Electronics Conference, NAECON 1979.
33. I. E. Getreu, "Modeling the Bipolar Transistor," Elsevier Scientific Publishing Company, New York, 1978.